BMI1 AND HEDGEHOG SIGNALING IN MEDULLOBLASTOMA PATHOGENESIS

by

Lowell Evan Michael

A dissertation submitted in partial fulfillment
of the requirements for the degree of
Doctor of Philosophy
(Cellular and Molecular Biology)
in The University of Michigan
2008

Doctoral Committee:

Professor Andrzej A. Dlugosz, Chair
Professor Deborah L. Gumucio
Associate Professor Gary D. Hammer
Associate Professor John V. Moran
Associate Professor Sean J. Morrison
Associate Professor Theodora S. Ross

2008

Acknowledgements

I owe a great many people a great deal of thanks for their help and support during the course of my thesis work. First and foremost, to my thesis advisor, Dr. Andrzej Dlugosz. Throughout the course of my graduate education, I benefited immensely from his tireless assistance. Anj gave me the autonomy to pursue my research in the ways in which I saw fit, sometimes against his better judgment, while still providing a guiding hand and a tremendous amount of welcome advice, scientific and otherwise. His passion for science, good food and life in general translates into an indefatigable optimism that I have come to believe is critical to his success in science, and which I now actively try to cultivate in my own life.

I am also very grateful to the members of my thesis committee, Drs. Deb Gumucio, Gary Hammer, John Moran, Sean Morrison, and Theo Ross. They provided excellent assistance with my project, including a very wide range of expertise and perspectives. Particular thanks go to Sean Morrison and Theo Ross for critical manuscript review along the way. I am also hugely indebted to the others in my lab who have helped my with my thesis work, in particular Jenny Ferris, Jianhong Liu, Anna Wang, Marina Grachtchouk and Jim Diener. Many, many thanks go to Karen Myers and Penny Morris for always making sure that I was taken care of, and for making problems magically disappear. Thanks also to Professor Kathy Jacobson, my undergraduate research advisor, and Drs. Craig Woodworth and Stuart Yuspa, my PIs during my post-baccalaureate NIH research fellowship, for inspiring me to pursue my graduate education.

While at UM, I've been tremendously lucky to make many truly wonderful friends who have helped shape my graduate experience. There are too many people to thank them all, but I would like to specifically acknowledge Ben Bassin, Alex Bondoc, Tim Egan, Mike Fatt, Jason "T." Kurzer, Mike Charles and Travis Maures for their friendship and support throughout the whole graduate experience, good and bad. Thanks to Kevin Leeser and Lauren Miller for playing matchmaker. Also many thanks are due to my cousin Mike Madill, who plays the dual role of friend and family, and who has introduced me to many wonderful people.

I would be nowhere without the love and support of my parents. To my father, Greg Michael, my mother, Mary Jane Joyal, and my stepfather, George Joyal – thank you. Thank you for challenging me, for encouraging me, and for supporting me, unconditionally, every step of the way. I have learned so much from all of you. Each of you is an inspiration to me.

And lastly, but most importantly, thank you to my wonderful partner, Lisa Locke. Lisa, you were my greatest discovery during grad school. You are my best friend and the light of my life, and are amazingly generous with your time and energy. I cannot imagine how I would have been able to finish this thesis without your unwavering love, support, and truly remarkable skill in the kitchen. Thank you. I love you.

Table of Contents

List of Figures

List of Tables

Abstract

Medulloblastoma is the most common malignant brain tumor in children, and occurs in up to 5% of patients with Gorlin syndrome, a familial cancer susceptibility disorder characterized by inappropriate activation of the Hedgehog (Hh) signaling pathway. Activation of Hh signaling is also seen in a significant fraction of sporadic medulloblastomas, many of which are believed to arise from the external granular layer (EGL) of the cerebellum, a transient, highly proliferative pool of Hh-responsive neural progenitors that disappears within the first several weeks of life, in mice. I investigated where and when medulloblastomas arise using a novel mouse model expressing SmoA1, a constitutively activated allele of the proximal Hh effector Smo, in the brain in a temporally restricted manner. SmoA1 induction in the developing cerebellum induced 100% penetrant medulloblastoma as early as two weeks old. Once the EGL had disappeared, however, mice were completely refractory to induction of *de novo* medulloblastomas, providing strong evidence that the EGL represents a bona fide pool of cells with the potential to become medulloblastoma, and that other SmoA1-expressing cells in adult mice are not competent to form medulloblastomas.

To test whether SmoA1-induced medulloblastomas remain dependent on continued Hh signaling, I repressed transgene expression in established tumors. I observed that even relatively brief 3-week inhibition of SmoA1 resulted in complete and durable elimination of tumors. Tumors did not recur following resumption of transgene expression, suggesting that no dormant tumor cells remain. This is a timely finding, as a

Hh antagonist is currently in Phase II clinical trials for antitumor therapy. Lastly, I examined the dependence of tumor formation on the stem cell maintenance gene *Bmi1*, which is required for physiologic cerebellar development and is expressed in Hh-active human medulloblastomas. Breeding SmoA1 mice onto a *Bmi1*-null background revealed that in the absence of *Bmi1*, tumor initiation occurs, but lesions do not progress to frank medulloblastomas. This implicates *Bmi1* as a key downstream target of Hh in a pathologic setting. The work presented herein provides several important insights into the pathogenesis of Hh-driven medulloblastoma, and may suggest a more general role for *Bmi1* in Hh-mediated cancer.

Chapter 1

A Role for Hedgehog and Bmi1 in Maintenance and Disease of the Epithelium and Cerebellum

Introduction

The Hedgehog signaling pathway is a key morphogenic and mitogenic pathway in mammalian development. Originally identified in *Drosophila*, this pathway has come to be recognized as a critical factor in either embryogenesis or postnatal tissue maintenance in virtually every organ system in mammals. Mounting evidence also links dysregulation of the Hh pathway to the development of multiple types of tumors, including basal cell carcinomas in the skin and medulloblastomas in the cerebellum. In some settings, such as postnatal cerebellar development, the Hh pathway regulates expression of the polycomb protein Bmi1. Bmi1 plays an important role in the development of the cerebellum, and expression of Bmi1 is frequently seen in medulloblastomas in which the Hh pathway is activated.

In this thesis, I address several aspects of medulloblastoma development, expansion, and maintenance, using a novel doxycycline-regulated mouse model that I have generated for pathologic activation of the Hh pathway. The model described herein is based on an oncogenic mutant form of the Hedgehog effector protein smoothened (Smo) designated SmoA1. To develop our model, we placed *SmoA1* under transcriptional control of the tetracycline response element, allowing us to restrict its expression spatially and temporally by choosing appropriate driver mice and modulating

doxycycline treatment. We utilized this model, in conjunction with previously developed Hh pathway activation models, to demonstrate that activation of the Hh pathway at the level of Smo is sufficient to drive tumorigenesis in the cerebellum, but not elsewhere in the central nervous system. We also took advantage of the doxycycline-inducible nature of our model to define the developmental window for medulloblastoma susceptibility, helping define the precursor cell for these tumors, and examined whether Hh-driven medulloblastomas remain dependent on continued Hh signaling. I also describe the use of *Bmi1*-null mice to investigate the role of *Bmi1* in epithelial maintenance and medulloblastoma development, demonstrating the importance of *Bmi1* both in skin maintenance and Hh-driven medulloblastoma expansion, perhaps suggesting a role for Bmi1 in epithelial and medulloblastoma stem cells. The work described in this thesis presents a powerful new tool in the study of medulloblastoma, suggests a place for anti-Hh therapy in treatment of medulloblastomas, and provides the first evidence that *Bmi1* is required for *de novo* formation of a solid tumor.

Sonic Hedgehog Signaling

Sonic Hedgehog, one of three members of the Hedgehog (Hh) family, is a secreted morphogen that plays a critical role in embryologic development of many tissues. During embryogenesis, appropriate localization of Shh ligand within the embryo controls limb polarity, left-right asymmetry, and dorsal-ventral patterning of somites (Casey *et al.*, 2000, Chuang *et al.*, 2000). Homozygous null mutation of Shh ($Shh^{-/-}$) is incompatible with life and results in severe defects including cyclopia, holoprosencephaly and lack of distal limb structures (Chiang *et al.*, 1996). Additionally, signaling via the Hh pathway impacts tissue maintenance in adult tissues such as hair and the central nervous system

(CNS) (Dlugosz, 1999, Ahn *et al.*, 2005). Although all three members of the mammalian Hh family, Sonic, Indian and Desert Hedgehog, play important and often non-redundant roles, Shh is the best characterized of the three.

Shh functions as an extracellular signaling peptide that can exert its effects in an autocrine or paracrine, dose-dependent manner (Chuang *et al.*, 2000). In its active form, its N-terminus is palmitoylated, and its C-terminus contains a cholesterol modification, which facilitates extracellular diffusion (Miura *et al.*, 2006). Upon reaching its target cell, Shh binds to the 12-span transmembrane protein Patched1 (Ptch). In the absence of Hh ligands, Ptch represses the function of Smoothened (Smo), a 7-span transmembrane protein with structural homology to the G protein-coupled receptor proteins (Kasai *et al.*, 2004). Upon binding of Shh to Ptch, Ptch function is inhibited and Smo is de-repressed, leading to Hh pathway activation. Pathway activation occurs via a series of intracellular intermediates, ultimately resulting in activation of the Gli family of transcription factors (Ruiz i Altaba *et al.*, 2007) (Fig. 1-1).

The manner in which Ptch represses the function of Smo in a resting cell is not entirely understood. Despite an initial report using highly overexpressed proteins that suggested the contrary (Stone *et al.*, 1996), Taipale et al. (Taipale *et al.*, 2002) demonstrated that there is no direct interaction between Ptch and Smo. They also showed that the impact of ligand-free Ptch on repression of Smo function was sub-stoichiometric, as a 1:45 ratio of Ptch:Smo reduced total Smo function by approximately 80%. These data are most consistent with a model in which Ptch functions catalytically to repress Smo. A potential mechanism for the catalytic action of Ptch was proposed by Corcoran and Scott (Corcoran *et al.*, 2006). They demonstrated that oxysterols stimulate activity of

the Shh signaling pathway, and suggest that Ptch, which is structurally related to several bacterial transmembrane pump proteins, may pump sterols out of the cell, thereby keeping them from interacting with and activating Smo.

Following Shh ligand binding to Ptch, the next step in the canonical Shh signaling pathway is de-repression of Smo. The mechanism by which Smo signals through to the Gli transcription factors is an active area of research. Several studies have shown that following Hh stimulation in *Drosophila*, Smo is extensively phosphorylated by protein kinase A and casein kinase I (Zhang *et al.*, 2004, Apionishev *et al.*, 2005). Furthermore, it has been demonstrated that this PKA and CKI-mediated phosphorylation of Smo is necessary for Hh-dependent Smo cell surface accumulation and activation in *Drosophila* (Jia *et al.*, 2004, Zhou *et al.*, 2006). The situation is different in mammalian cells, however, as the cytoplasmic tails of mammalian Smo orthologs diverge significantly from that of *Drosophila*. Activation of Smo is coupled to its translocation to the primary cilium (Corbit *et al.*, 2005).

Smo itself has structural similarities to members of the seven-pass membrane spanning G protein-coupled receptor (GPCR) family, but as yet no endogenous ligand for Smo has been directly identified (Frank-Kamenetsky *et al.*, 2002). In mammalian cells, it appears that G protein-coupled receptor kinase 2 (GRK2) associates with and phosphorylates Smo when the Hh pathway is activated, and that this association is required for Smo signal transduction (Chen *et al.*, 2004, Meloni *et al.*, 2006). This phosphorylation leads to localization of β-Arrestin 2 to activated Smo. Recruitment of β-Arrestin 2 appears to be involved in the clathrin-dependent internalization of activated Smo, although functional relevance of this internalization has yet to be demonstrated

(Chen *et al.*, 2004). Independent confirmation of the internalization of activated Smo in vertebrate cells was presented by Masdeu et al., who demonstrated a 74% reduction in cell-surface localization of oncogenic, constitutively active SmoA1 when compared to unstimulated Smo (Masdeu *et al.*, 2006). It has been suggested that the G protein $G_{\alpha 12}$ and the small GTPase RhoA mediate Shh pathway signaling, as constitutively active $G_{\alpha 12}$ increases Gli1 reporter activity, whereas a dominant-negative form of RhoA decreases signaling from a Gli1 reporter (Kasai *et al.*, 2004).

In vertebrate Shh signaling, the downstream protein suppressor of fused (Sufu) is a key player in the transduction of signal at a level between Smo and the Gli transcription factors. It appears that Sufu inhibits Shh signaling pathway activity, a hypothesis borne out by the fact that *Sufu*$^{-/-}$ mice have a phenotype similar to that of *Ptch*$^{-/-}$ mice (Cooper *et al.*, 2005, Svärd *et al.*, 2006). It has been postulated that Sufu achieves this by disrupting Gli activity either by sequestering Gli proteins in the cytoplasm and preventing their translocation to the nucleus or by binding, along with members of a histone deacetylase complex, to promoters containing the Gli binding element, thereby repressing transcription from these promoters (Cheng *et al.*, 2002, Merchant *et al.*, 2004). Although the mechanism is unclear, activated Smo has been proposed to inhibit Sufu (Varjosalo *et al.*, 2006).

Once inhibition is released, the activator forms of the Gli transcription factors are able bind to their promoter recognition sites and activate transcription of target genes. In mammalian cells, the Gli family comprises three zinc finger transcription factors, Gli1, Gli2 and Gli3. Although Gli1 is a transcriptional activator and is upregulated in response to Hh signaling, it appears to be largely dispensable in the context of normal Gli2

expression, as *Gli1* mutant mice develop essentially normally (Park *et al.*, 2000, Bai *et al.*, 2002). These data suggest that both Gli1 and Gli2 function as transcriptional activators, with at least partially redundant function. Gli3, conversely, appears to function primarily as a transcriptional repressor, despite containing both activation and repression domains. Loss of *Gli3* expression, for example, is able to partially or completely rescue neural and limb development defects of $Shh^{-/-}$ mice (Litingtung *et al.*, 2000, Rallu *et al.*, 2002, te Welscher *et al.*, 2002, Wang *et al.*, 2007). Gli3 is believed to act primarily as a transcriptional repressor because the majority of full-length Gli3 protein is proteolytically processed (Wang *et al.*, 2000, Pan *et al.*, 2006).

Of the three members of the vertebrate Gli family, Gli2 is the primary activating effector of the Shh pathway. Mice lacking *Gli2* have significant defects in the development of multiple organs, including the hair follicles, skeletal system and central nervous system (Mo *et al.*, 1997, Matise *et al.*, 1998, Mill *et al.*, 2003). Recently, several groups have demonstrated a molecular mechanism by which Gli2 transcriptional activity can be directly regulated by Shh (Bhatia *et al.*, 2006, Pan *et al.*, 2006). These studies showed that Gli2 exists primarily in a full length activator form, rather than the proteolytically processed repressor form. They further showed that PKA and CK1-driven phosphorylation of C-terminal serine residues in Gli2 allows for direct interaction of Gli2 with βTrCP. This association leads to ubiquitination and proteosomal degradation of Gli2. Stability and proteolytic degradation of Gli1 are known to be controlled by two independent degradation signals, and one of these signals is also present in Gli2, suggesting a role for this degron in controlling Gli2 accumulation, as well (Huntzicker *et al.*, 2006).

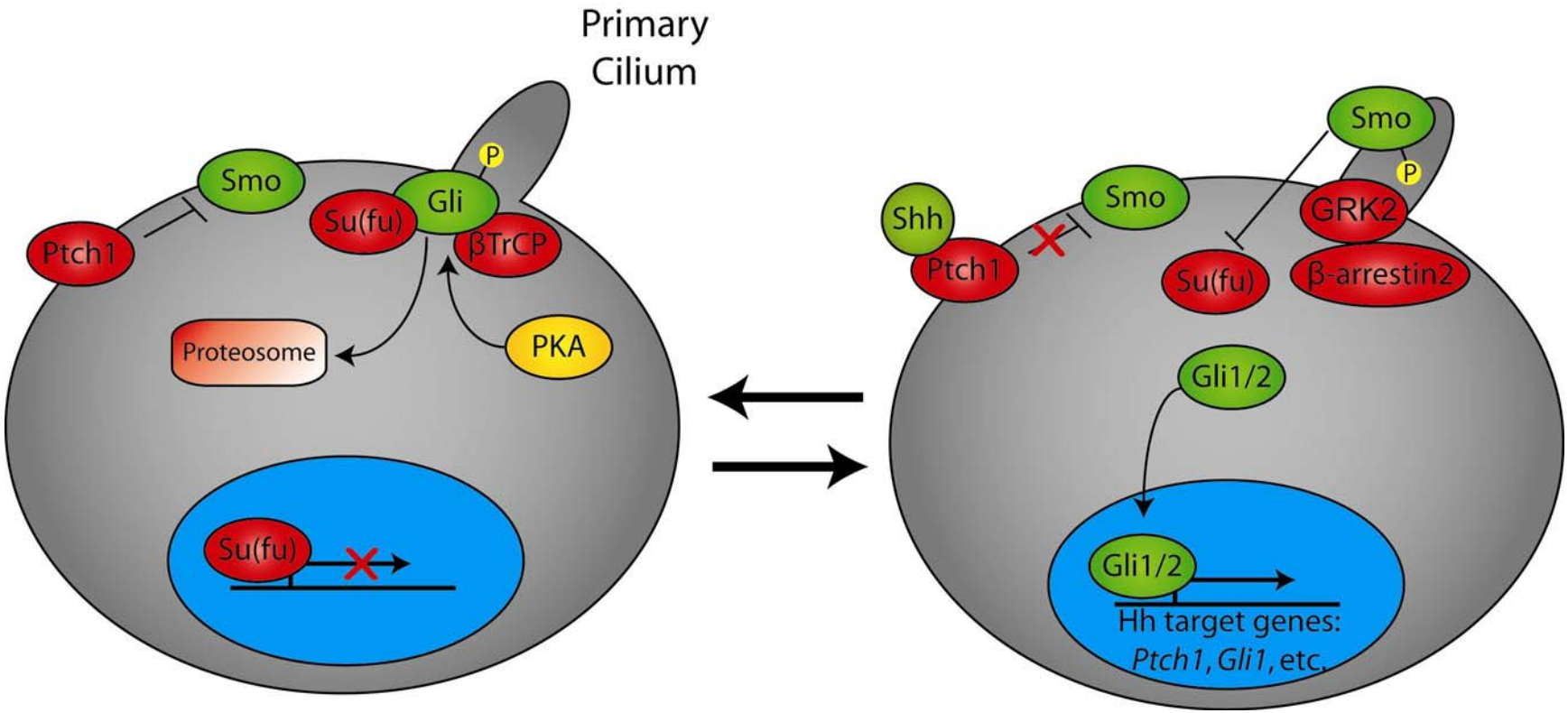

Figure 1-1. Physiologic activation of the Hedgehog pathway. In a resting cell, the Hh pathway is maintained in an "off" state by the inhibitory effects of Ptch1 on Smo. Sufu either binds to Gli proteins, sequestering them in the cytoplasm, binds to Gli-responsive promoter elements, inhibiting transcription, or both. PKA phosphorylates Gli proteins, leading to βTrCP-mediated ubiquitination and proteosomal degradation. When Shh binds to Ptch1, its inhibitory effects on Smo are blocked, leading to translocation of Smo to the primary cilium. Smo is phosphorylated by GRK2, which facilitates association of β-arrestin2 with Smo and clathrin-mediated endocytosis. Smo-mediated repression of Su(fu) results in translocation of the active forms of Gli1 or Gli2 to the nucleus, resulting in transcription of Hh target genes. In physiologic signaling, this process is entirely reversible, depending on the presence or absence of Hh ligands.

Cerebellar Development – a Hedgehog Driven Process

The cerebellum is an extremely neuron-dense structure that resides in the infratentorial space in the posterior cranium. The cerebellum, which is responsible for coordination of movement, contains more neurons than the rest of the brain combined (Wechsler-Reya *et al.*, 1999). Despite this remarkable density of neurons in the adult organism, the majority of cerebellar neurogenesis occurs postnatally. The cerebellar anlage of a newborn mouse is largely devoid of mature granule neurons. It is instead covered with a thin layer of cerebellar granular neural precursors (CGNPs), the cells which will give rise to mature cerebellar granule neurons. As the cerebellum develops in the first few weeks of life, these CGNPs proliferate extensively, expanding to form the external granular layer (EGL). This proliferation occurs in response to Shh secreted by the neurons of the underlying Purkinje layer and, transiently, by early CGNPs themselves (Dahmane *et al.*, 1999, Wechsler-Reya *et al.*, 1999). Treatment of *in vitro* CGNP or cerebellar slice cultures with Shh results in an increase in BrdU incorporation in the EGL and an inhibition of neuronal differentiation of isolated CGNPs (Wechsler-Reya *et al.*, 1999). Conversely, conditional knockout of *Shh* in EGL and Purkinje cells or *Gli2* in rhombomere 1 (which gives rise to the cerebellar anlage) impairs EGL proliferation and disrupts proper murine cerebellar patterning and foliation, and similar results have been observed with Hh-neutralizing antibody in chick embryos (Dahmane *et al.*, 1999, Lewis *et al.*, 2004, Corrales *et al.*, 2006). This proliferative response of CGNPs to Shh is dependent on the proto-oncogene N-Myc (Oliver *et al.*, 2003).

As cerebellar development progresses, the EGL begins to stratify into an outer EGL and an inner EGL. While the cells in the outer layer of the EGL continue to

proliferate, those in the inner EGL become post-mitotic, lose expression of *Gli1*, and begin to differentiate (Dahmane *et al.*, 1999, Wechsler-Reya *et al.*, 1999). As the CGNPs differentiate, they take on a marker expression pattern similar to that of mature IGL neurons; *Math1* expression decreases, and the expression of mature neuronal markers such as NeuroD1, NeuN, Zic1 and TrkC increases (Kim *et al.*, 2003). The nature of the signal that causes this phenotypic change is not entirely clear. However, it appears that the Hh antagonist REN^{KTCD11} may play a role in this process by upregulating expression of the cyclin-dependent kinase inhibitor *p27/Kip1* (Argenti *et al.*, 2005). It has also been demonstrated that upregulation of the developmental adapter protein Numb in the inner EGL may be partially responsible for abrogating CGNP response to Shh (Marcotullio *et al.*, 2006).

Whatever the nature of the inductive signal, the differentiating CGNPs in the innermost layers of the EGL, having lost responsiveness to Shh, begin to migrate deeper into the cerebellum. They pass through the developing molecular layer (ML), a region consisting primarily of the axons of granular cells and the dendrites of Purkinje cells (Hatten, 1999). The migration continues deep past the Purkinje cell layer, and the mature cerebellar granular neurons take up their permanent residence in the region known as the internal granular layer (IGL) (Fig. 1-2). Mature IGL neurons make synaptic connections to Purkinje neurons, Golgi neurons, and mossy fibers (Weyer *et al.*, 2003). In mice, this wave of proliferation, differentiation and migration is complete by two weeks after birth, by which time the EGL no longer exists, all of the cells having differentiated and migrated into the IGL. The same process occurs in humans, and is complete within the first year of life (Wang *et al.*, 2001).

Figure 1-2. Hedgehog-driven development of the cerebellum. At birth (P0), the cerebellar anlage consists of a thin layer of CGNPs (round red cells) overlying the Purkinje layer (PL) of neurons (gray rectangular cells). The PL secretes Shh, inducing the CGNPs to proliferate (indicated by anaphase nuclei in CGNPs). This causes significant expansion of the CGNP population, forming the external granular Layer (EGL). As CGNPs lose responsiveness to the Shh signal, they withdraw from the cell cycle and begin to differentiate and migrate inwards (indicated by oblong green cells). These cells migrate through the growing molecular layer (ML) and past the PL, taking up residence as the fully differentiated, mature granule neurons in the internal granular layer (round blue cells). By P21, this process is complete, and the EGL has completely disappeared. The ML is formed primarily of the axons of granule cells and the dendrites of Purkinje cells, and is sparsely populated with the nuclei of basket and stellate cells (round black cells.) The CNGPs of the EGL are believed to function as a cell of origin for medulloblastomas, potentially secondary to forced continued responsiveness to Hh signaling, as shown.

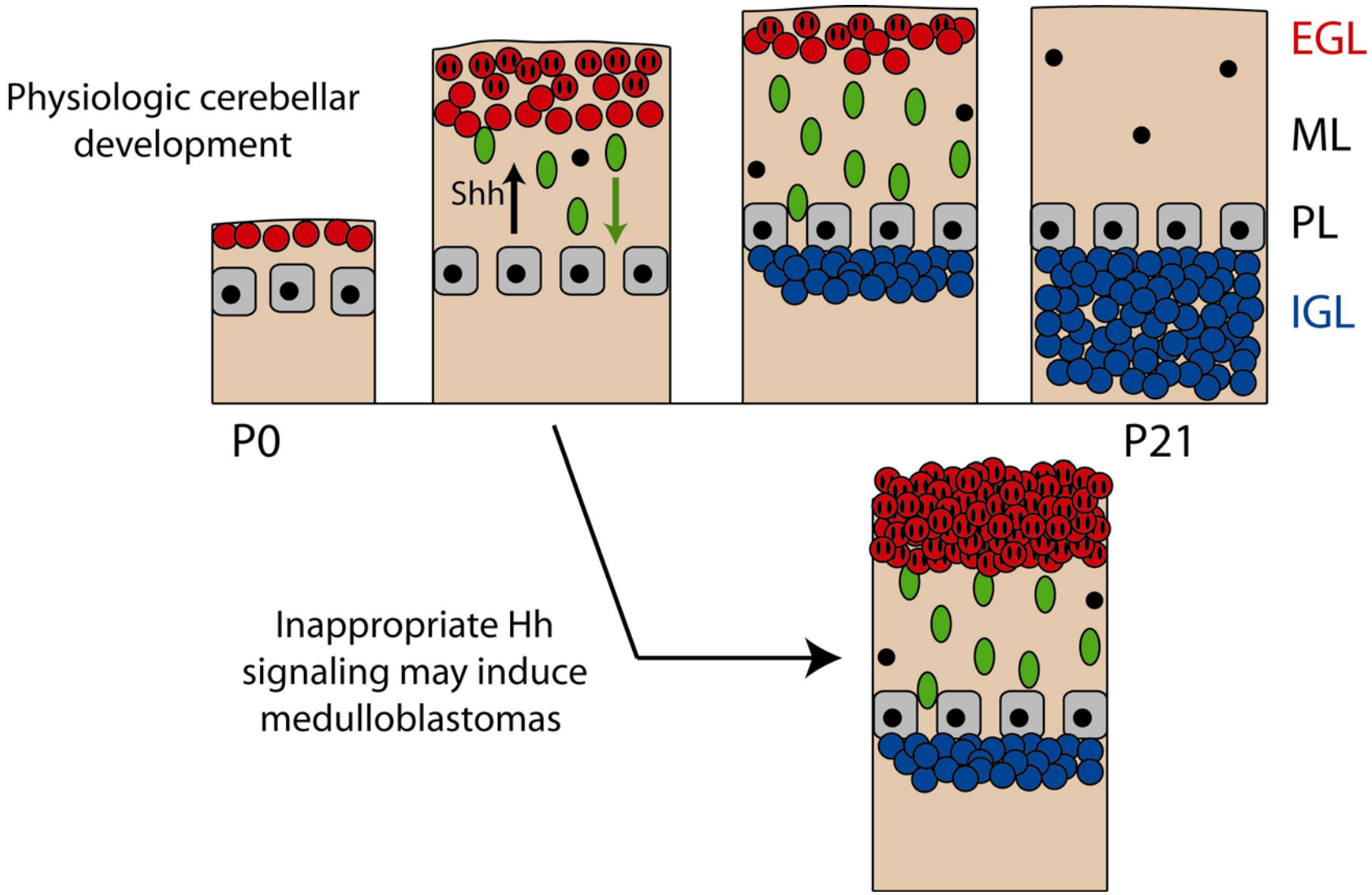
Physiologic cerebellar development
Shh
EGL
ML
PL
IGL
P0
P21
Inappropriate Hh signaling may induce medulloblastomas

The Hedgehog Pathway and Cancer – a Connection Between Development and Tumorigenesis

In contrast to the important role of physiologic Hh signaling in normal embryonic development, hyperactivation of the Hh pathway has been linked to the development of multiple cancers. Patients with the autosomal dominant disorder Gorlin Syndrome harbor an inactivating germline mutation in one allele of the HH receptor and signaling repressor PTCH (Gorlin, 2004). Gorlin Syndrome, also known as Nevoid Basal Cell Carcinoma Syndrome, is characterized by the early development of multiple basal cell carcinomas (BCCs), with some individuals developing more than one thousand of these tumors over the course of their lives (Gorlin, 2004). Gorlin Syndrome is also associated with the development of additional neoplasms, including ovarian and cardiac fibromas, fibrosarcomas, rhabdomyosarcomas, meningiomas, and medulloblastomas (Booth, 1999).

Inappropriate activation of the HH pathway is seen not only in familial tumor susceptibility, but also in sporadic cancer development. HH activation has been identified in a variety of neoplasms, including breast, prostate, pancreatic and small cell lung cancers, and others (Pasca di Magliano *et al.*, 2003, Watkins *et al.*, 2003, Sanchez *et al.*, 2005a, Lau *et al.*, 2006, Hatsell *et al.*, 2007), involving alterations at multiple levels of the pathway (Fig. 1-3). Additionally, expression of direct HH target genes, indicating activation of the pathway, is a unifying feature of sporadic human BCC (Unden *et al.*, 1997). This is attributable to *PTCH* mutations in the majority of sporadic BCCs, and mutations in *SMO* or *SUFU* in a smaller subset (Reifenberger *et al.*, 1998, Xie *et al.*, 1998, Reifenberger *et al.*, 2005, Evangelista *et al.*, 2006).

The nearly universal activation of HH in BCCs provides an important clue to the relationship between normal organ development and tumorigenesis in the skin, as both processes are driven by activation of the Hh pathway. Basal cell carcinomas are thought to arise primarily from progenitor cells within hair follicles, which are dependent on Hh signaling for appropriate development (Gerdes *et al.*, 2005, Hutchin *et al.*, 2005). While *Shh* null mice form hair germs consisting of epidermal placodes and dermal condensates, early structures indicating preliminary specification of hair follicles, these structures are unable to develop into fully-formed follicles (Chiang *et al.*, 1999).

Hh is similarly important in cycling of the adult hair follicle, an organ which is unique in that it undergoes multiple rounds of regeneration, which include phases of extensive proliferation and invasion into the underlying tissue (anagen), apoptotically-driven regression (catagen), and quiescence (telogen) throughout the life of the organism. Progression through the hair cycle is controlled by Shh, among other signals, as several studies have demonstrated that brief Shh stimulation of resting telogen skin is sufficient to induce *de novo* anagen (Sato *et al.*, 1999, Paladini *et al.*, 2005), whereas inhibition of Hh signaling blocks postnatal hair follicle growth during anagen . Together, these observations link physiologic formation and cycling of hair follicles with BCC development, and suggest that this most common skin tumor may result from the disordered development of normal hair follicles.

In addition to its role in sporadic BCC development, HH pathway activation is also associated with the development of sporadic medulloblastoma. Medulloblastoma is the most common malignant pediatric brain tumor, affecting as many as 1 in every 150,000 children (Hallahan *et al.*, 2004, Romer *et al.*, 2004). As with BCC, the

connection between HH and medulloblastoma first came from the observation that Gorlin Syndrome patients have an elevated risk for medulloblastoma development. 20 – 25% of sporadic medulloblastomas were later revealed to carry pathway-activating mutations in HH signaling components, as well (Raffel *et al.*, 1997, Wetmore, 2003, Marino, 2005). Although there has been some discrepancy in the literature about what fraction of sporadic medulloblastomas display elevated levels of HH activity, several recent reports demonstrated expression of target genes in approximately 60% of examined tumors (Hallahan *et al.*, 2004, Leung *et al.*, 2004). Furthermore, the most common genetic lesion in medulloblastoma, occurring in up to 50% of cases, is loss of chromosome 17q, which includes the region that codes for the Hh antagonist REN^{KTCD11} (Gulino *et al.*, 2007). Taken together, these data suggest that HH signaling may be important in a larger subset of human medulloblastomas than previously believed.

As mentioned above, the early postnatal proliferation of developing CGNPs is dependent on Shh. It has been hypothesized that these neural precursor cells in the EGL represent a cell of origin for medulloblastomas, secondary to forced prolongation of Hh pathway activity. Several lines of evidence support this idea. First, medulloblastoma is primarily a pediatric tumor. Although the reason for this predilection for occurring in children is not entirely clear, it is consistent with a precursor cell population that is present only during childhood, such as the CGNPs of the EGL. Second, medulloblastomas resemble CGNPs or more differentiated granule neurons in their expression of markers such as synaptophysin, NeuroD, NeuN, TRKC, NSE, Zic, PAX5, PAX6 and ATOH1/Math1, albeit often in a deregulated manner (Kozmik *et al.*, 1995, Kim *et al.*, 2003, Grimmer *et al.*, 2008). As with the hair follicle-BCC connection, it

appears that dysregulation of Hh activation, which is normally very tightly controlled, leads to medulloblastomagenesis in a manner that diverges from normal cerebellar development. However, despite these suggestive observations, additional support that the EGL serves as a pool of potential medulloblastoma precursors is needed.

Finally, the role of Hh in development and tumorigenesis of the forebrain should be considered. As with cerebellar development, Shh is a key mediator of proper formation of the forebrain. Historically speaking, the effects of blocking Hh in the developing embryo were first appreciated in lambs born to sheep grazed on *Veratrum californium*, the corn lily. This plant produces the alkaloid cyclopamine, which inhibits Smo function, rendering the Hh pathway inactive irrespective of ligand status. These animals were born cyclopic and holoprosencephalic (Bale, 2000). Holoprosencephaly, disrupted ventral patterning of the telencephalon and cyclopia were subsequently confirmed in *Shh* knockout mice, as well as in human patients with Shh mutations (Chiang *et al.*, 1996, Schell-Apacik *et al.*, 2003).

In addition to its role in embryonic development of the forebrain, Hh is also important for maintenance and activation of adult neural stem cells. These cells reside primarily in the subventricular zone (SVZ) lining the lateral ventricles and the subgranular zone (SGZ) of the hippocampal dentate gyrus (Taupin *et al.*, 2002). Confirmation that signaling through the Hh pathway is required for maintenance of this stem cell population came from experiments in which *Shh* or *Smo* was ablated in a *Nestin* promoter-specific manner. Nestin is a broadly expressed marker of neural progenitors, including the stem cells of the SVZ and SGZ. Conditional abrogation of Hh signaling in these cells resulted in reduced size of the SVZ and SGZ, and impaired proliferation and

increased apoptosis in these regions. These mice also gave rise to reduced numbers of multipotent neurospheres, a functional assay of stem cell number (Machold *et al.*, 2003). *Shh* and *Gli1* are both expressed in the adult germinal zones, and *de novo* mature neurons form from neural stem cells in mice in a Hh-dependent, cyclopamine inhibited manner (Ahn *et al.*, 2005, Palma *et al.*, 2005).

In keeping with the idea that Hh-driven tumorigenesis can be viewed as a paradevelopmental process, it follows that gliomas, which are thought to arise from Hh-responsive neural stem cells (Sanai *et al.*, 2005), may well depend on Hh for their development. In fact, *GLI1* was first identified as a gene amplified in a human glioma (Kinzler *et al.*, 1987). Following this discovery, this proposed role of Hh pathway in gliomas went largely unsupported for some time. In the past several years, however, increasing evidence has bolstered this hypothesis. The observation that human gliomas express *PTCH* and *GLI1*, confirmed both by RT-PCR and by *in situ* hybridization, was published in 2004 (Ruiz i Altaba *et al.*, 2004). Several subsequent studies indicated that gliomas of all grades and histological subtypes display Hh activation, and that increasing Gli activity correlates with worsening tumor grade (Clement *et al.*, 2007, Becher *et al.*, 2008). Furthermore, Hh blockade with cyclopamine was shown to deplete a population of neurosphere-forming, cancer stem-like cells from human glioblastomas multiforme, indicating that targeting the Hh pathway may serve as a useful therapeutic target in glioma patients. However, the story is complicated by the observation that unrestricted Hh signaling in adult neural stem cells results in apoptosis and arrested progression through the cell cycle (Galvin *et al.*, 2008). This suggests that Hh activation is necessary but not sufficient for gliomagenesis, although it is also possible that a more moderate

upregulation of the Hh pathway may lead to tumor development without inducing arrest and apoptosis of neural stem cells.

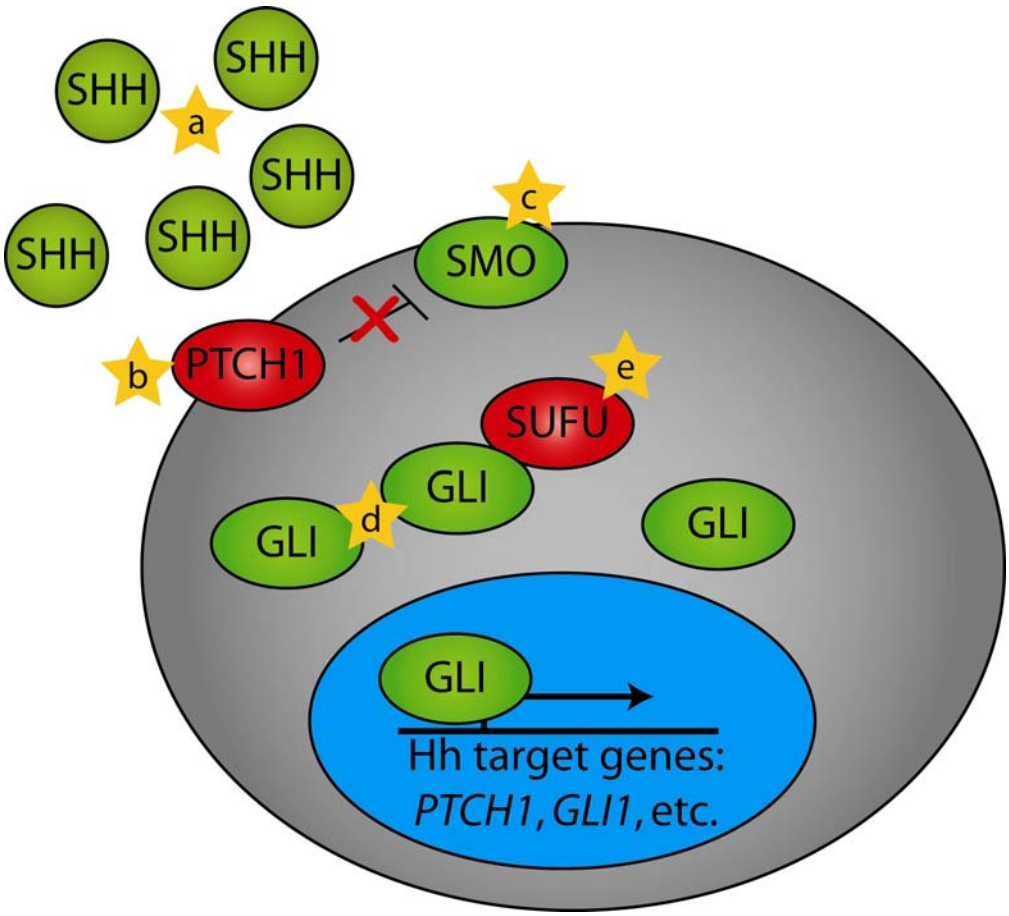

Figure 1-3. Activating alterations in the Hedgehog pathway in human cancer. a) HH overexpression is associated with esophageal, gastric, pancreatic, breast, prostate and small-cell lung cancer. b) Loss of function mutations in *PTCH1* are seen in basal cell carcinoma and medulloblastoma. c) Pathway-activating *SMO* mutations have been found in basal cell carcinomas and medulloblastomas, as well. These mutations render SMO insensitive to PTCH1 inhibition, irrespective of HH ligand status. d) GLI2 amplification is seen in squamous cell carcinoma. e) Loss of function mutations of SUFU are seen in medulloblastoma and BCC. Modified from (Pasca di Magliano *et al.*, 2003).

Hh-Driven Mouse Models of Basal Cell Carcinoma

Inspired by the well-recognized connection between HH deregulation and BCC in humans, numerous groups have made strides towards developing mouse models for BCC (reviewed in (Dlugosz *et al.*, 2002)). Approximately one third of mice carrying a heterozygous inactivating germline mutation of *Ptch* develop microscopic lesions resembling basal cell carcinomas, and UV or ionizing radiation induces BCC-like tumors in 100% of $Ptch^{+/-}$ mice by 3 months of age or older (Aszterbaum *et al.*, 1999). Another study indicated a link between anagen induction and BCC-like tumor formation in X-ray irradiated *Ptch* heterozygote mice (Mancuso *et al.*, 2006). This provides a genetically faithful model of Gorlin Syndrome; tumor latency is relatively long, however, and requires repeated, significant, long-term radiation exposure, which may lead to a variety of additional genetic alterations.

Overexpression of SHH from the *keratin 14* (*K14*) promoter results in the development of microscopic basal cell-like epithelial proliferations at birth (Oro *et al.*, 1997). *K14-SHH* mice are not viable postnatally, and so it is difficult to observe if these lesions are able to progress to full-blown BCCs. Likewise, it is not known if induction of deregulated SHH expression in an adult animal skin is sufficient to give rise to frank BCCs (Oro *et al.*, 1997). Similar basal cell-like lesions are seen in newborn transgenic mice expressing a constitutively activated mutant allele of human *SMO*, *M2SMO*, from the full length *keratin 5* promoter (Xie *et al.*, 1998). As with *K14-SHH* mice, *K5-M2SMO* mice are perinatally lethal, preventing analysis of progression or adult tumorigenesis in these mice. Animals in which *M2SMO* is expressed from a truncated form of the *K5* promoter (*ΔK5-M2SMO*) survive into adulthood, presumably because the

ΔK5 promoter is active in only a subset of *K5*-positive cells. These mice develop widespread basaloid follicular hamartomas (BFHs), slow-growing tumors which express low levels of the Hh target genes *Ptch1* and *Gli1*, both in mice and humans. Despite the development of BFHs, however, these mice never develop frank BCCs, even a full year after birth (Grachtchouk *et al.*, 2003). Similar, but more slowly developing, lesions are seen in mice heterozygous for *Sufu*, as well (Svärd *et al.*, 2006).

As discussed above, the primary downstream effectors of the Hh pathway are the Gli family of transcription factors. Several reports have indicated that unrestrained Hh activation at the level of Gli is sufficient to drive BCC formation. Transgenic mice expressing *Gli2* driven by the keratin 5 (K5) promoter (*K5-Gli2*) develop multiple tumors within three months of birth (Grachtchouk *et al.*, 2000). These tumors strongly resemble human BCCs in both gross and histologic morphology, and demonstrate robust expression of *Ptch1* and *Gli1*. *K5-Gli2* mice also develop less aggressive tumors displaying lower levels of Hh pathway activation; these lesions appear identical to the BFHs seen in *ΔK5-M2SMO* mice (Grachtchouk *et al.*, 2003). Expression of human GLI1 in *K5*-positive cells induced development of BCCs as well as a variety of other skin tumors (Nilsson *et al.*, 2000). When considered together, the data from these models suggest a significantly different tumorigenic potential of proximal, upstream (i.e. at the level of *Shh*, *Ptch* or *Smo*) vs. distal, downstream (i.e. at the level of *Gli*) activation of the Hh pathway, possibly secondary to differing levels of Hh pathway activation.

In addition to the models described above, our laboratory also developed an inducible, doxycycline-regulated model for epithelial Hh pathway activation (Hutchin *et al.*, 2005). To generate this model, transgenic mice were developed in which

transcription of *Gli2* was driven by the tetracycline response element (TRE). These mice were then crossed with *K5-tTA* mice (Diamond *et al.*, 2000), in which expression of the tetracycline transactivator is driven by the K5 promoter. In the absence of doxycycline treatment, double transgenic *K5-tTA;TRE-Gli2* mice express *Gli2* in K5 promoter-active cells. 100% of these mice develop proliferative BCCs with robust Hh activation by 6 months of age. Treatment with doxycycline inhibits expression of transgenic *Gli2* and induces regression of tumors over approximately three weeks. Residual transgene-independent cells remain following regression, and tumors regrow following reactivation of exogenous Gli2 expression (Hutchin *et al.*, 2005). Although it is difficult to definitively identify the cells which give rise to re-grown tumors, some returning tumors in this model do appear to arise from within residual tissue when examined shortly after transgene reactivation. The presence of presumptive dormant tumor cells in this model raises the possibility that shut-down of Hh signaling in other Hh-driven tumors may also leave behind a small population of potential tumor cells.

The *K5-tTA;TRE-Gli2* model provides two pieces of information. First, conditional epithelial expression of a Hh-pathway activating transgene is sufficient to generate BCCs. A conditional model has the significant advantage of allowing for postnatal transgene activation, bypassing any potential embryonic or perinatal lethality. This, then, suggests a novel way to induce high level, upstream activation of the Hh pathway, either embryonically or postnatally, to examine its tumorigenic potential. In order to achieve this, I generated the *TRE-SmoA1HA* line of transgenic mice. By employing the doxycycline-repressible *K5-tTA* or doxycycline-inducible *K5-rtTA* driver mice, I used these mice to examine the consequences of pre- and postnatal doxycycline-

regulated epithelial activation of *SmoA1HA*. SmoA1HA is an HA epitope-tagged, oncogenic, constitutively active allele of Smo. In Chapter 2, I describe the generation of this mouse model and its epithelial phenotype, which includes BFH-like hyperplasia but not frank BCC development. Second, the *K5-tTA;TRE-Gli2* model demonstrates that Hh-driven BCCs remain dependent on continued Hh activation for tumor maintenance. This raises the question of whether oncogene "addiction" is seen in other Hh-driven tumors, such as medulloblastoma. This issue is especially relevant at the present time because Hh pathway antagonists are currently in Phase II clinical trials (ClinicalTrials.gov reference # NCT00636610).

The Hedgehog Pathway in Mouse Models of Medulloblastoma

In order to study the biology of medulloblastoma, as well as to investigate potential therapeutic avenues in a pre-clinical setting, robust, faithful animal models are required. *In vivo* models are particularly critical for the study of medulloblastoma, as the Hh pathway is dramatically down-regulated in medulloblastoma cells grown in culture, and is not restored by allografting cultured cells into the flanks of recipient mice (Sasai *et al.*, 2006). The mechanism for this downregulation of Hh activity is not understood. Over the past ten years or so, significant progress has been made in our understanding of the molecular biology of medulloblastoma development, and multiple murine models of the disease have been developed. As reviewed above, a subset of human medulloblastomas harbor demonstrable mutations in genes encoding members of the HH pathway, and a larger fraction show HH pathway activity. Definitive demonstration of an etiologic role for Hh in medulloblastoma came from the generation of *Ptch1* heterozygous knockout mice. While *Ptch1*$^{-/-}$ mice die *in utero*, *Ptch1*$^{+/-}$ mice are viable,

and between 10 and 14% develop medulloblastoma, with peak onset between 16 and 27 weeks of age (Goodrich *et al.*, 1997, Hahn *et al.*, 1998, Wetmore *et al.*, 2000, Kim *et al.*, 2003). Development of these tumors is partially reliant on appropriate expression of *Gli1* (Kimura *et al.*, 2005), although a separate study indicates that virally-delivered *Shh* is able to induce medulloblastomas in *Gli1*$^{-/-}$ mice (Weiner *et al.*, 2002). Tumor latency can be decreased and incidence increased by breeding *Ptch1*$^{+/-}$ mice onto a *p53*$^{-/-}$ background (Wetmore *et al.*, 2001). However, this model may no longer faithfully recapitulate the genetic basis of human medulloblastoma, as inactivation of the *p53* pathway is rare in the human disease (Saylors *et al.*, 1991, Adesina *et al.*, 1994). In a model developed by McMahon *et al.*, Cre recombinase-mediated activation of the human mutant *SMO* allele *M2SMO* resulted in 40% medulloblastoma incidence when driven by the compound *CMV/β-actin* (CAGGS) promoter. These mice develop numerous other tumors, as well, and succumb to heavy tumor burden and infection by 18 weeks of age (Mao *et al.*, 2006).

As briefly mentioned above, mouse models of medulloblastomas have been developed in which retroviruses are used to target Hh-modifying transgenes to specific cells. In the RCAS/*tv-a* system, mice are engineered to express TV-A, the receptor for the avian retrovirus ALV subgroup A, from a tissue-specific promoter. *Ntv-a* mice express TV-A in cells in which the promoter for the stem and progenitor cell marker nestin is active. Only cells which express TV-A can be infected by RCAS vectors, which are engineered to deliver specific transgenes to the target cells. When retrovirus is delivered via intracerebellar injection within 3 days after birth, RCAS-*Shh* induces tumors in 15% of animals. Tumor incidence can be raised to 40% or higher by co-infection with RCAS-*Shh* and RCAS-*c-Myc*, -*Akt*, or -*IGF2* (Rao *et al.*, 2003, Rao *et al.*,

2004). While these retroviral models are powerful, and provide important information about the interplay between Hh and other signaling pathways in tumorigenesis, they do not serve as models for spontaneous, Hh-driven medulloblastoma formation.

Perhaps the most robust Hh-driven medulloblastoma model described to date is the *ND2:SmoA1* mouse line. In this model, a truncated version of the *NeuroD2* (*ND2*) promoter controls expression of a mutant allele of *Smo*, *SmoA1*, which is very similar to the *SmoA1* used to develop the model described in this thesis. The *ND2* promoter is active in a wide range of neuronal cells throughout the CNS, including the CGNPs of the EGL (Olson *et al.*, 2001). Approximately 50% of *ND2:SmoA1* mice develop medulloblastoma at a median age of 26 weeks (Hallahan *et al.*, 2004). A very recent report indicates that increasing transgene dosage by crossing *ND2:SmoA1* mice to homozygosity increases the incidence of tumors to 85% by one month (Hatton *et al.*, 2008). While this is a significant increase in tumor penetrance, this model still falls short of the goal of complete, early tumor penetrance, an important feature for preclinical tumor therapy models, and lacks the means to rapidly and specifically activate and inactivate the transgene.

Having developed the *TRE-SmoA1HA* mouse line, we were in a unique position to examine the consequences of conditional, high level, upstream activation of the Hh pathway in the developing cerebellum. In order to achieve this, I took advantage of several previously developed lines of transgenic mice (Table 2-1). I used *GFAP-tTA* mice (Lin *et al.*, 2004, Wang *et al.*, 2004) to generate *GFAP-tTA;TRE-SmoA1HA* mice. The *GFAP* promoter used to develop these mice is active in several populations of cells throughout the CNS, including mature glial cells, adult neural stem cells, and CGNPs

within the developing EGL. *GFAP-tTA;TRE-IFN-γ* mice develop medulloblastomas associated with activation of the Hh pathway (Lin *et al.*, 2004), suggesting that *GFAP-tTA* mice would also be useful drivers for our system. As described in detail below, I also combined the advantages of the permanent Cre/loxP system with the rapid induction and inhibition of the rtTA/TRE system, using *GFAP-Cre* mice (Zhuo *et al.*, 2001) to permanently activate expression of doxycycline-induced *rtTA* from *R26-LSL-rtTA* mice (Belteki *et al.*, 2005), in which a floxed strong stop sequence is knocked into the *ROSA26* locus upstream of the reverse tetracycline transactivator (*rtTA*). This results in expression of *rtTA* in GFAP positive cells and their progeny.

In Chapter 3, I detail the development and phenotype of bitransgenic *GFAP-tTA;TRE-SmoA1HA* mice and triple transgenic *GFAP-Cre;R26-LSL-rtTA;TRE-SmoA1HA* mice. One hundred percent of both of these varieties of transgenic mice develop histologically evident medulloblastomas within two weeks of birth, but do not develop other brain tumors, despite broad transgene expression elsewhere in the CNS, including the subventricular zone (SVZ), a niche for adult neural stem cells in the forebrain. These novel models represent powerful new tools for modeling spontaneous Hh-driven medulloblastomas, and have enabled me to address several fundamental questions in tumor biology. I describe how I exploit the doxycycline-regulated nature of these transgenic models to define a very brief postnatal window of susceptibility to medulloblastoma development, supporting the notion that these tumors arise from the transient CGNPs in the EGL. Additionally, I contrast the results from these two SmoA1-based models with the phenotypes I observed in *GFAP-tTA;TRE-Gli2* and *GFAP-tTA;TRE-GLI2** mice. Neither of these downstream activation models develop

medulloblastoma, but *GFAP-tTA;TRE-GLI2** mice develop diffuse undifferentiated forebrain tumors when transgene expression is activated postnatally, suggesting that robust downstream Hh activation is sufficient to revert mature glial cells to a progenitor-like phenotype. All murine models used in this thesis are summarized in Table 2-1.

Continued Requirement for Hedgehog Signal in Medulloblastoma Maintenance

The need for specific anti-tumor therapies in the treatment of medulloblastoma is clear. Current treatment modalities include surgical resection followed by chemotherapy and/or craniospinal axis radiation. While 5-year progression-free survival rates have risen to approximately 75% for average-risk disease (Gilbertson, 2004), these therapies often have severe long-term side effects, which can significantly impact quality of life. Radiation therapy, in particular, is poorly tolerated by Gorlin Syndrome patients, as they have an exquisite sensitivity to radiation-induced BCC development (Kimonis *et al.*, 1997). As previously discussed, there is a discrepancy between the percentage of human medulloblastomas with identifiable mutations in Hh pathway components and the notably higher proportion of these tumors in which the Hh pathway is activated. This suggests that even in tumors with disparate etiologic mechanisms, the Hh pathway may play a role in tumor pathogenesis. If true, this would argue for a role in anti-Hh therapy in perhaps as many as 60% of patients with this malignancy.

It is important to take into account the ideas of oncogene addiction and tumor dormancy when considering the targeting of specific pathways as clinical therapeutic modalities. Oncogene addiction is the idea that tumors remain dependent on a specific oncogenic stimulus for continued maintenance. In keeping with this idea, discussed in (Weinstein, 2002), tumors which remain "addicted" to an oncogene would be susceptible

to treatment by inhibition of the specific oncogenic pathway involved. The observation of specific gene fusions or amplifications, such as the recurrent *BCR/ABL* fusion in chronic myelogenous leukemia and HER2 overexpression in a subset of breast cancer, have lead to major advances in tumor-specific therapies for these diseases via treatment with Gleevec and Herceptin, respectively (reviewed in (Ross *et al.*, 2004)). Regression of BCCs in *K5-tTA;TRE-Gli2* mice (Hutchin *et al.*, 2005) suggests that Hh-driven tumors may remain addicted to Hh signaling, perhaps providing an effective therapeutic target, as reflected in the clinical trials mentioned above.

Tumor dormancy can be viewed as the flip side to oncogene addiction. As seen in *K5-tTA;TRE-Gli2* mice and several other conditional mouse models of cancer, tumors which appear to be addicted to an oncogenic stimulus may regress following abrogation of the critical oncogene, only to leave behind small populations of dormant tumor cells (Boxer *et al.*, 2004, Shachaf *et al.*, 2004, Hutchin *et al.*, 2005). These cells retain the capacity to develop into full-blown tumors when the oncogenic stimulus is reactivated. The presence of dormant tumor cells would significantly complicate the use of oncogene-specific anticancer therapy, potentially requiring long-term treatment to prevent relapses or targeting additional pathways involved in tumor dormancy. As such, examination of both oncogene addiction and tumor dormancy are critical to understanding the biology of tumors.

In keeping with the observed dependence of BCCs on Hh stimulus, additional reports indicate that Hh-driven medulloblastomas may also remain dependent on continued oncogenic stimulus for their maintenance. Treatment with the Hh pathway antagonist cyclopamine of either *in situ* $Ptch^{+/-}/p53^{-/-}$ medulloblastomas or allografts of

cell lines derived from these tumors results in inhibition of tumor proliferation (Berman *et al.*, 2002, Sanchez *et al.*, 2005b). Use of a synthetic Smo inhibitor results in a more robust inhibition of tumors, and can induce short-term tumor regression (Romer *et al.*, 2004). Consistent with the observation that Hh pathway activation is seen in human tumors without identifiable Hh pathway mutations, *GFAP-tTA;TRE-IFNγ* medulloblastomas express *Shh* and *Gli1*, and medulloblastomas derived from *Cxcr6*$^{-/-}$ mice display activation of the Hh pathway and are inhibited by pharmacologic blockade of Smo function, consistent with a downregulation of *Ptch1* expression in these tumors (Sasai *et al.*, 2007).

Despite these encouraging results, no studies have yet demonstrated that inhibition of the Hh pathway can completely and permanently eliminate medulloblastomas, and previous reports have relied on pharmacological Hh inhibitors (Berman *et al.*, 2002, Romer *et al.*, 2004, Sanchez *et al.*, 2005b), making it extremely difficult to rule out off-target effects. With the development of our double and triple transgenic *TRE-SmoA1*-based medulloblastoma models, we are in a unique position to test the hypothesis that abrogation of the Hh pathway will lead to complete tumor elimination. Our models are robust and 100% penetrant, do not require introduction of additional engineered genetic alterations such as p53 deficiency, and are doxycycline-regulated, allowing us to begin studies earlier, and perform them with the precision afforded by genetically manipulated, as opposed to pharmacologically manipulated, mice. In Chapter 4, I describe the use of both our double and triple transgenic models to demonstrate that Hh-driven medulloblastomas remain absolutely dependent on continued

Hh activity, and that focal abrogation of *SmoA1* induces focal, regional tumor regression, whereas complete *SmoA1* inhibition results in total, durable tumor elimination.

Bmi1 in Stem and Progenitor Cells and Cancer

Bmi1 is a member of the polycomb group of multiple transcriptional repressors. It functions primarily via its inhibition of the *Ink4a/Arf* locus (Jacobs *et al.*, 1999), which encodes $p16^{Ink4a}$ and $p19^{Arf}$ ($p14^{ARF}$ in humans). By repressing transcription of $p16^{Ink4a}$, *Bmi1* allows activation of CyclinD and Cdk4/6, resulting in phosphorylation and inactivation of pRB and activation of E2F, ultimately resulting in progression through the cell cycle. Additionally, by repressing transcription of $p19^{Arf}$, itself an inhibitor of MDM2, *Bmi1* also contributes to inhibition of p53 function, preventing apoptosis and cell cycle arrest (reviewed in (Park *et al.*, 2004)).

Bmi1 is an important regulator of stem and progenitor cells in multiple tissues, and is believed to be important in tumors, as well. Park *et al.* demonstrated a requirement for Bmi1 in self-renewal of hematopoietic stem cells, as $Bmi1^{-/-}$ fetal liver cells were unable to successfully reconstitute lethally irradiated recipient mice (Park *et al.*, 2003). Likewise, while $Bmi1^{-/-}$ hematopoietic stem cells form leukemia following transformation with *Hoxa9* and *Meis1*, these tumors cells are unable to induce frank leukemia in secondary recipients (Lessard *et al.*, 2003). Several laboratories have demonstrated a dependence on *Bmi1* for adult neural stem cells, mediated by $p16^{Ink4a}$ and $p19^{Arf}$ (Molofsky *et al.*, 2003, Bruggeman *et al.*, 2005, Molofsky *et al.*, 2005), and *BMI1* is expressed in human glial tumors and required for a virally-mediated grafting-based mouse model of glioma, which, as discussed above, may arise from neural stem cells (Bruggeman *et al.*, 2007, Hayry *et al.*, 2008).

Furthermore, *Bmi1*, in a manner known to be at least partially dependent on *Ink4a/Arf*, regulates proliferation and apoptosis of CGNPs (Leung *et al.*, 2004, Bruggeman *et al.*, 2005). Bmi1 is expressed in both EGL cells as well as in mature cerebellar neurons of the IGL (Leung *et al.*, 2004). This observation is particularly interesting in light of the fact that, at least in *in vitro* CGNP culture, *Bmi1* expression is upregulated upon stimulation with Shh (Leung *et al.*, 2004). When considered in conjunction with the leukemia findings discussed above and the observation that BMI1 expression correlates well with PTCH expression in human medulloblastomas (Leung *et al.*, 2004), these data suggest a role for BMI1 in Hh-driven medulloblastoma development. Indeed, an initial report indicates that knockdown of *Bmi1* inhibits growth of a medulloblastoma cell line and tumor xenografts (Wiederschain *et al.*, 2007). However, these studies do not show an absolute dependence on *Bmi1* in medulloblastoma, nor do any studies exists in the literature which demonstrate a requirement for *Bmi1* in the *de novo* development of a spontaneously-arising solid tumor.

In keeping with the idea that *Bmi1* is required for maintenance of multiple adult tissue stem cells, I employed the *Bmi1*$^{-/-}$ mouse model to briefly begin exploring whether *Bmi1* is required for proliferation and maintenance of keratinocytes. These data, which suggest a role for *Bmi1* in keratinocyte stem cell function, are presented in Chapter 5. We also employed *Bmi1*$^{-/-}$ mice to test the hypothesis that medulloblastoma development requires proper *Bmi1* function. In order to achieve this, we bred our *GFAP-tTA;TRE-SmoA1* mice onto a *Bmi1*$^{-/-}$ background, an experiment made possible by the short tumor latency and complete penetrance of this model. As reported in Chapter 5, we discovered that, while apparently not necessary for tumor initiation, *Bmi1* is required

for progression to full-blown medulloblastoma. In contrast to the complete penetrance of medulloblastomas in *GFAP-tTA;TRE-SmoA1* mice, these mice do not develop frank medulloblastomas on a *Bmi1*$^{-/-}$ background. *Bmi1*$^{-/-}$, SmoA1-expressing mice initiate tumorigenesis, but the lesions are small, unproliferative and apoptotic, and display loss of the nestin expression, indicating a loss of progenitor cell-like phenotype in the absence of *Bmi1*.

Summary

The Hh signaling pathway plays a central role in many developmental processes, both physiological and pathological. In order to address several fundamental questions in Hh-driven tumor biology, I generated a novel transgenic mouse line, the *TRE-SmoA1* line, on which the work described in this thesis is based. I describe the generation of these animals in Chapter 2. I observed that activation of this transgene in squamous epithelia prenatally resulted in perinatal lethality due to numerous developmental abnormalities, while postnatal activation induced epithelial hyperplasia consistent with basaloid follicular hamartomas, but not full-blown BCCs, confirming the resistance of murine skin to BCC development (Chapter 2). I also exploited the *TRE-SmoA1* mouse line to activate the Hh pathway in the CGNPs of the developing cerebellum, inducing completely penetrant medulloblastoma development. In so doing, I defined a narrow developmental window for tumor susceptibility, which strongly implicates CGNPs as the cell of origin for these tumors. By contrasting these results with data generated using *TRE-Gli2* and *TRE-GLI2** mice, I observed a differential tumorigenic response in the brain to proximal versus distal activation of the Hh pathway, suggesting strong inhibition of the Hh pathway in cells which are not normally regulated by Shh (Chapter 2). Taking advantage

of the conditional nature of our medulloblastoma model, we demonstrated that Hh-driven medulloblastomas remained entirely dependent on Hh signaling for their maintenance, and that relatively brief inhibition of this signal resulted in complete disappearance of tumors, an observation with potentially significant impact for treatment of the human disease (Chapter 3). Finally, I used our robust new model for medulloblastoma to address the question of the necessity for *Bmi1* in medulloblastoma development, demonstrating that while *Bmi1* is apparently not required for tumor initiation, it is required for progression to full-blown medulloblastoma (Chapter 4).

Chapter 2

SmoA1 is Sufficient to Induce Medulloblastomas but not Forebrain Tumors or Basal Cell Carcinomas

Introduction

Basal cell carcinoma (BCC) and medulloblastoma are the most common skin cancer in light-skinned people, and the most common malignant brain tumor in children, respectively (Hallahan *et al.*, 2004, Hutchin *et al.*, 2005). There are between 750,000 and one million new cases of BCC diagnosed each year in America (Hutchin *et al.*, 2005, Athar *et al.*, 2006), whereas medulloblastomas account for roughly 20% of pediatric brain malignancies, affecting approximately 1 in 150,000 children (Hallahan *et al.*, 2004, Romer *et al.*, 2004). Development of both of these relatively undifferentiated tumors has been linked to inappropriate activation of the Hedgehog (HH) signaling pathway.

The first clue to the link between BCC and HH signaling came from the observation of *PTCH* mutations in patients with Gorlin Syndrome. These patients are at greatly elevated risk for BCC development, often developing many of these tumors over their lives (Gorlin, 2004). *PTCH* normally functions as both a receptor for HH ligands and a repressor of HH signaling activity (see Fig. 1-1), and loss of *PTCH* leads to uncontrolled activation of the pathway. Mutations in the HH pathway are not limited to BCCs arising in the context of Gorlin Syndrome, and have been detected in nearly all examined sporadic BCCs, either at the level of *PTCH*, *SMO*, or *SUFU* (Reifenberger *et*

al., 1998, Xie *et al.*, 1998, Bale *et al.*, 2001, Reifenberger *et al.*, 2005, Evangelista *et al.*, 2006).

As discussed in Chapter 1, numerous murine models for BCC-like tumors have been developed based on activation of the Hh pathway. *Ptch*$^{+/-}$ mice develop full-blown BCCs, but only after significant doses of UV or ionizing irradiation (Aszterbaum *et al.*, 1999, Corcoran *et al.*, 2001). Distal pathway activation at the level of *Gli* transcription factors, however, leads to robust BCC development in the absence of other genetic alterations (Grachtchouk *et al.*, 2000, Nilsson *et al.*, 2000, Hutchin *et al.*, 2005). Despite the robust tumor development seen in *Gli*-driven models, full-blown BCCs have not been observed in mice in which the Hh pathway is activated proximally at the level of Shh or Smo. Overexpression of SHH from the *K14* promoter results in development of basaloid proliferations in newborn mice, but no BCCs (Oro *et al.*, 1997). *M2SMO*, a constitutively active mutant allele of *SMO* cloned from a BCC, is able to transform rat embryonic fibroblasts in conjunction with E1A. However, mice expressing *M2SMO* from either the full-length *K5* promoter or the truncated *ΔK5* promoter, which drives patchy activation in squamous epithelium, develop microscopic basaloid proliferations or basaloid follicular hamartomas, but not frank tumors, an outcome ascribed to insufficient activation of the Hh pathway (Xie *et al.*, 1998, Grachtchouk *et al.*, 2003). Although these results suggest that proximal activation of the Hh pathway in murine skin is not sufficient to induce BCC development, it is entirely possible that activated murine Smo may more efficiently activate Hh signaling, leading to tumor formation.

In contrast to the identification of HH pathway mutations in nearly every BCC, medulloblastoma, a primitive neuroectodermal tumor (PNET), represents a

heterogeneous disease, without a defined genetic lesion common to all tumors (Marino, 2005). Nevertheless, a clear link has been established between dysregulation of the Hedgehog (Hh) pathway and medulloblastomagenesis, based on the observation that approximately 1 in 20 Gorlin syndrome patients develop medulloblastoma, a 7500-fold increase over the risk of medulloblastoma in the general population (Gorlin, 1995, Packer *et al.*, 1999). Activating mutations in components of the HH pathway have been detected in spontaneous medulloblastomas, and approximately 25% of all medulloblastomas examined harbor such a mutation (Wetmore, 2003, Marino, 2005). Additional studies indicate that the pathway is activated in an even greater fraction of human medulloblastomas, as measured by expression of HH target genes (Hallahan *et al.*, 2004, Leung *et al.*, 2004). Several mouse models have subsequently confirmed that inappropriate activation of the Hh pathway can give rise to medulloblastoma development (Goodrich *et al.*, 1997, Rao *et al.*, 2003, Hallahan *et al.*, 2004, Mao *et al.*, 2006).

Development of medulloblastomas is tightly linked to the physiologic development of the cerebellum. As described in Chapter 1 and reviewed in (Wetmore, 2003), the majority of cerebellar development occurs postnatally. In normal neonatal cerebellum, a thin layer of cerebellar granule neuron precursors (CGNPs) lines the external surface of the cerebellar anlage. These cells are stimulated by sonic hedgehog (Shh) secreted by the neurons of the underlying Purkinje layer (PL). Activation of the Hh pathway induces proliferation and significant expansion of the CGNP population, forming the external granular layer (EGL.) Cells within the EGL eventually become refractory to the Shh signal and abstract themselves from the cell cycle. As they do so,

they differentiate and migrate inwards, passing through the developing molecular layer (ML) and past the PL, settling in the internal granular layer (IGL) as the mature cerebellar neurons. This process is complete by P21 in the mouse, and within the first year of life in humans (Wang *et al.*, 2001, Marino, 2005). Due in part to the location and timing of medulloblastoma development, the Shh-responsive CGNPs of the EGL are thought to comprise a pool of potential medulloblastoma precursor cells (Marino, 2005, Ueba *et al.*, 2008), although this model awaits definitive proof.

In addition to the well-supported contribution of HH pathway deregulation to medulloblastoma development, several lines of evidence suggest a role for HH signaling in the development of glial tumors, as well. *GLI1*, one of the primary transcriptional effectors of the HH pathway, was originally identified as a gene overexpressed in glioma (Kinzler *et al.*, 1987). More recently, additional studies have indicated that the entire spectrum of glial tumors display Hh pathway activation, and have linked increasing pathway activity to worsening tumor grade (Ruiz i Altaba *et al.*, 2004, Clement *et al.*, 2007, Becher *et al.*, 2008). Furthermore, glial tumors are believed to arise from SHH-responsive neural stem cells in the forebrain (Sanai *et al.*, 2005), providing further support for the idea that deregulation of the HH pathway contributed to CNS tumors other than PNETs. However, as yet no experimental models have demonstrated that activation of Hh signaling is sufficient to induce or promote, with other genetic alterations, gliomagenesis.

In this chapter, I will describe the use of a novel mouse model to examine the consequences of conditional, high level, proximal activation of the Hh pathway in skin, cerebellum, and forebrain. To generate this model, I placed HA epitope-tagged *SmoA1*, a

constitutively active mutant *Smo* allele (Taipale *et al.*, 2000), under control of the tetracycline response element (TRE), and generated transgenic mice carrying the *TRE-SmoA1* construct. I initially bred the resulting mouse lines with doxycycline-regulated, squamous epithelium-specific *K5-tTA* activator mice (Diamond *et al.*, 2000), allowing me to test the hypothesis that activated murine SmoA1 can induce BCC formation. I observed that postnatally activated adult SmoA1-expressing mice developed basaloid follicular hamartoma-like lesions, but not full-blown BCCs, in keeping with the phenotype observed in M2SMO-expressing mice (Xie *et al.*, 1998, Grachtchouk *et al.*, 2003).

Taking advantage of the power and flexibility of the *TRE-SmoA1* mice, I induced high-level proximal Hh activation in the CGNPs of the developing EGL by activating transcription from the *glial fibrillary acidic protein* (*GFAP*) promoter. We achieved this either in bitransgenic mice also expressing the *GFAP-tTA* transgene (Lin *et al.*, 2004), or in triple transgenic mice, by way of the Cre-loxP system, using combinatorial expression of *GFAP-Cre* (Zhuo *et al.*, 2001) and a Cre-mediated, *ROSA26*-driven rtTA (Belteki *et al.*, 2005). One hundred percent of mice expressing SmoA1 in the cerebellum using either of these models developed medulloblastomas within two weeks of birth. Characterization of these mice revealed many similarities to human medulloblastomas and other published mouse models. By controlling the timing of transgene activation, we were able to define a window of susceptibility to tumor development that extends to at least the seventh postnatal day, but not past 21 days old, supporting the hypothesis that these tumors arise from the transient EGL.

Since SmoA1-expressing mice do not develop forebrain tumors, we also employed several additional models for inducing distal activation of the Hh pathway in order to assess the sufficiency of the Hh pathway to drive glioma formation. By crossing *GFAP-tTA* mice with *TRE-Gli2* mice (Hutchin *et al.*, 2005) or *TRE-GLI2** mice (which express a Myc-tagged, repressor domain-deleted *GLI2* allele), we were able to compare the outcome of postnatal Hh activation at the level of Smo to the outcome of activation at the level of Gli. While neither SmoA1-expressing nor *GFAP-tTA;TRE-Gli2* mice developed forebrain tumors, *GFAP-tTA;TRE-GLI2** mice developed large numbers of small, undifferentiated tumors consisting of clusters of progenitor-like cells scattered throughout both the cerebellum and the cerebrum. Notably, none of these models developed glioma, suggesting that by itself, activation of the Hh pathway in *GFAP*-expressing cells is not sufficient to induce gliomagenesis.

Materials and Methods

Generation of TRE-SmoA1 mice.

A plasmid containing the *SmoA1* allele was generously provided by Dr. Phil Beachy (Taipale *et al.*, 2000). Dr. Alex Ermilov appended an HA epitope tag to the 3' end of *SmoA1* in the pEGFP plasmid. In order to place *SmoA1HA* under control of the tetracycline response element (TRE), the *SmoA1HA* insert was liberated by digestion with *Not*I and *Hind*III, then blunted with Klenow polymerase. The ~2.7 kb insert was isolated by agarose gel separation and DNA purification using the Qiaquick kit (Qiagen). pTet-Splice acceptor plasmid (Invitrogen) was linearized by digestion with *Eco*RV and agarose gel purified as above. Linearized pTet-Splice vector and insert were blunt-end ligated using the Roche rapid DNA ligation kit (Roche). Transformation-competent

JM109 *E. coli* (Promega) were transformed with the resulting ligation product and grown on agar plates with ampicillin selection. Picked colonies were grown as mini-preps, and plasmid DNA was isolated using the Qiagen Plasmid Mini kit (Qiagen). Presence of a single insert copy was ascertained by digestion with *Xba*I, and proper insert orientation was ascertained by digestion with *Xho*I. The resulting plasmid contained the TRE, comprising seven copies of the tetracycline operator and the minimal CMV promoter upstream of the *SmoA1HA* sequence and the SV40 intron and polyadenylation sequence downstream (Figure 2-1A).

The *TRE-SmoA1HA*/SV40 intron + pA fragment was liberated by digestion with BsshII and purified as above. The purified fragment was microinjected into (C57BL/6 X SJL)F1 X (C57BL/6 X SVJ)F1 eggs by the University of Michigan Transgenic Animal Core. Potential founder animals were screened by PCR for presence of the transgene as described below, and five transgenic *TRE-SmoA1* lines were established by backcrossing to C57BL/6 mice. The identity of our transgenic construct was confirmed by sequencing at the University of Michigan Sequencing Core. Comparison of obtained primary sequence data with RefSeq mRNA sequence (NM_176996.3) confirmed the presence of the expected W539L mutation, and also revealed the presence of an unexpected second point mutation, T425R. As indicated by robust expression of *Ptch1* and *Gli1* in tumors (Figure 2-4), this second mutation does not appear to affect the ability of SmoA1 to activate the Hh pathway.

Housing, breeding and genotyping of mice

All mice were maintained in the University of Michigan Cancer Center animal facility under specific pathogen-free conditions in accordance with university and federal

guidelines. All animals were given food and water *ad libitum*. In order to activate SmoA1 expression in squamous epithelium, I crossed *TRE-SmoA1* mice with *K5-tTA* ("Tet-off") or *K5-rtTA* ("Tet-on") mice, generously provided by Dr. Adam Glick (Diamond *et al.*, 2000).

GFAP-tTA mice (Lin *et al.*, 2004) were a gift from Dr. Brian Popko at the University of Chicago. *TRE-Gli2* mice were generated as described previously (Hutchin *et al.*, 2005). *TRE-GLI2** mice were developed by Dr. Marina Grachtchouk in the Dlugosz laboratory (Grachtchouk *et al.*, in preparation). *GFAP-Cre* (Zhuo *et al.*, 2001) and *R26-LSL-rtTA* (Belteki *et al.*, 2005) mice were purchased from Jackson Labs (Bar Harbor, ME). *TRE-lacZ* mice were a gift from Dr. Julie Segre at the National Human Genome Research Institute of the NIH. *GFAP-tTA* mice were crossed with *TRE-SmoA1*, *TRE-Gli2*, *TRE-GLI2** or *TRE-lacZ* mice to generate double transgenic *GFAP-tTA*;*TRE-SmoA1* (designated *tTA-SmoA1*), *GFAP-tTA*;*TRE-Gli2* (designated *tTA-Gli2*), *GFAP-tTA;TRE-GLI2** mice (designated *tTA-GLI2**) or *GFAP-tTA;TRE-lacZ* mice (designated *tTA-lacZ*). To obtain rapidly inducible "Tet-on" mice expressing SmoA1 in the developing EGL, triple transgenic mice were obtained using a multi-step breeding scheme. Initially, *GFAP-Cre* mice were bred with *R26-LSL-rtTA* mice to obtain double transgenic *GFAP-Cre*;*R26-LSL-rtTA* progeny. These offspring were then bred with *TRE-SmoA1* mice to obtain triple transgenic *GFAP-Cre;R26-LSL-rtTA;TRE-SmoA1* animals (designated *rtTA-SmoA1*). Single and double transgenic progeny from these crosses were also intercrossed as appropriate to generate additional *rtTA-SmoA1* animals. See Table 2-1 for summary of transgenic mice.

To repress transgene expression in *K5-tTA;TRE-SmoA1*, *tTA-SmoA1* and *tTA-GLI2** mice, pregnant and nursing dams or weaned animals were fed chow containing 1 g/kg or 200 mg/kg doxycycline *ad libitum* after weaning (BioServ). To activate transgene expression in *K5-rtTA;TRE-SmoA1* and *rtTA-SmoA1* mice, animals were fed chow containing 1 g/kg doxycycline. *K5-rtTA;TRE-SmoA1* animals were provided water containing 200 μg/ml doxycycline for the first three days of treatment, after which time they were returned to regular water.

To genotype animals, tail snips were taken between 14 and 21 days old and digested overnight using Proteinase K to obtain DNA for genotyping PCR. *K5-tTA*, *K5-rtTA*, *GFAP-tTA* and *R26-LSL-rtTA* genotypes were ascertained by performing PCR with primers specific for the tetracycline transactivator: 5'-ctcgcccagaagctaggtgt-3' and 5'- ccatcgcgatgacttagt-3' (Diamond *et al.*, 2000). *TRE-SmoA1* and *TRE-GLI2** genotypes were ascertained by performing PCR with primers specific for the SV40 polyA sequence: 5'-ggaactgatgaatgggagca-3' and 5'-gggaggtgtgggaggttt-3'. Genotyping for *TRE-Gli2* was performed as previously described (Hutchin *et al.*, 2005)). Animals were genotyped for *GFAP-Cre* status by PCR using primers specific for Cre recombinase (5'-catgcttcatcgtcggtcc-3' and 5'-gatcatcagctacaccagag-3'), and for *TRE-lacZ* by using PCR primers specific for *lacZ* (Li *et al.*, 2003) (5'-gctgggatccgccattgtcagacatg-3' and 5'-gctggaattccgccgatactgac-3') . For some experiments, mice were injected intraperitoneally with 100 μg 5-bromo-2-deoxyuridine (BrdU) per gram body weight one hour prior to sacrifice. For long-term BrdU treatment, mice were given a loading dose of 50 μg/gram body weight injected intraperitoneally, and then maintained on drinking water containing1.5 mg/ml BrdU for one week.

Tissue harvesting, processing and sectioning

Animals were sacrificed by CO_2 narcosis. For general histology and immunohistochemistry, whole brains were removed and fixed overnight in 10% neutral buffered formalin, then transferred to 70% EtOH. For fixation of skin, a 2 cm^2 section of full-thickness epithelium was blunt dissected away from the underlying tissue and stretched, dermis-side down, on nitrocellulose filter paper. Tissue was then cut into strips and fixed in the same manner as brain tissue. All other post-fixation processing, including paraffin embedding, mounting, and initial sectioning and hematoxylin and eosin staining was performed by Histoserv, Inc., of Bethesda, MD. All subsequent sections for immunostaining were cut at 5 μm thick, either by Paula Arrowsmith of the Unit for Laboratory Animal Medicine at the University of Michigan or by LEM. Serial coronal sections were cut by LEM and James Diener. Additional tissue from the ventrolateral region of *tTA-SmoA1* cerebella, the region of greatest tumor burden, was collected for RNA analysis by stabilization in RNAlater and RNA extraction using the RNEasy kit (Qiagen). For X-gal staining, animals were sacrificed as above, and brains were briefly fixed in 4% PFA at 4° C. Tissues were then rinsed and treated with X-gal staining solution overnight at 37° C. Following staining, tissues were post-fixed in 10% NBF and processed as above, with nuclear fast red staining in place of hematoxylin and eosin.

Immunohistochemistry and *in situ* hybridization

For all immunohistochemistry and immunofluorescence, slides were stripped of paraffin and rehydrated by passing through xylenes followed by a graded series of ethanol washes. Slides were then subjected to antigen retrieval by boiling in pH 6.0

sodium citrate buffer for 10 minutes, followed by cooling on the benchtop for 15 minutes. For all non-mouse primary antibodies, blocking was performed for one hour with 10% normal goat serum and 2 mg/ml BSA in PBS. All primary antibodies were applied overnight at 4° C. For immunohistochemistry, species-appropriate biotinylated secondary antibody (Vector Labs) was used at 1:200 dilution for 30 minutes, followed by treatment with ABC reagent (Vector Labs). Color was developed using DAB as the chromogenic substrate (Sigma-Aldrich). For immunofluorescence, species-appropriate fluorescein- or Texas red-conjugated secondary antibody (Jackson ImmunoResearch) was used at 1:75 dilution. For all mouse primary antibodies, the Mouse on Mouse kit (Vector Labs) was used according to manufacturer's instructions, with the exception of extending primary antibody incubation to overnight at 4° C. Primary antibodies, host species and concentrations used include rat α-HA High Affinity, 1:100 (Roche Applied Science, 1 867 423); rat α-BrdU, 1:100 (Abcam, ab6326); rabbit α-GFAP, 1:200 (Lab Vision/NeoMarkers, RB-087-A0); rabbit α-Ki67, 1:2000 (Vector Labs, VP-K451); rabbit α-cleaved Caspase-3, 1:500 (Cell Signaling Technologies, #9661); rabbit α-phospho-histone H3, 1:1000 (Upstate/Millipore, 06-570); rabbit α-GABRA6, 1:2000 (Chemicon, AB5610); rabbit α-$p27^{Kip1}$, 1:100 (LabVision/NeoMarkers, BR-9019-P0); mouse α-NeuN, 1:200 (Chemicon, MAB377); mouse α-synaptophysin, 1:1000 (Chemicon, MAB5258); mouse α-nestin, 1:4 (Developmental Studies Hybridoma Bank, Rat-401); mouse anti-Myc tag, 1:50 (Developmental Studies Hybridoma Bank, 9E 10). For immunohistochemistry, species-appropriate biotinylated secondary antibodies were used, followed by use of the ABC avidin-biotin complex kit (Vector Labs) per manufacturer's instructions. DAB or DAB + Co enhancer (Sigma) was used as the chromogenic

substrate, and slides were lightly counterstained with dilute hematoxylin. For immunofluorescence, FITC- or TXRed-conjugated species-specific secondary antibody was used, followed by mounting in DAPI-containing aqueous mounting medium (Vector Labs.)

Non-radioactive *in situ* hybridization for detection of *Ptch1*, *Gli1*, and *SmoA1* was performed essentially as described in detail elsewhere (Grachtchouk *et al.*, 2003). *SmoA1* was detected using riboprobe specific to the *SV40 small t poly(A)*, as described.

Real time quantitative rt-PCR

RNA was prepared from the cerebella of control and tumor-bearing *tTA-SmoA1* and *rtTA-SmoA1* mice using the RNEasy kit (Qiagen). Following treatment with DNAseI (Invitrogen), 1 µg of total RNA was reverse transcribed to first strand cDNA with SuperScript II reverse transcriptase (Invitrogen). The RT reaction was performed using random hexamer primers in accordance with the manufacturer's instructions. Quantitative real time rt-PCR was performed on a LightCycler 2 (Roche Applied Science) using $1/20^{th}$ of the resulting cDNA per reaction and the following primer sets:

Actin: 5'-tgttaccaactgggacgaca-3' and 5'-tctcagctgtggtggtgaag-3'.

Math1: 5'-tgcgctcactcacaaataag-3' and 5'-taacaacacaatagtccgtgttc-3'.

N-myc: 5'-gctgcggtcactagtgtgtc-3' and 5'-ggagaagcctcgctcttgat-3'.

Ptch1 (Takabatake *et al.*, 1997): 5'-aacaaaaattcaaaccaaacctc-3' and 5'-tgtcttcattccagttgag-3'.

Ptch2: 5'-ggtaatcctcgtggcctctat-3' and 5'-ggagacagctccatcagtca-3'.

Gli1 (Allen *et al.*, 2003); 5'-gtcggaagtcctattcacgc-3' and 5'-cagtctgctctcttccctgc-3'.

CyclinD1 (Berman *et al.*, 2002): 5'-ctctggctctgtgcctttct-3' and

5'-ccggagactcagagcaaact-3'.

CyclinD2 (Berman *et al.*, 2002): 5'-ttcagcaggatgatgaagtga-3' and

5'-gagaaggggctagcagatga-3'.

P-values were calculated using the t-test assuming unequal variances.

Full name	Abbreviation	Nature of transgene	Location of transgene expression	Activated or repressed by doxycycline	Epitope tag	Tumor phenotype
K5-tTA;TRE-SmoA1	none	Activated murine SmoA1	Basal layer and hair follicles of squamous epithelium	Repressed	HA	Basaloid Follicular Hamartoma
K5-rtTA;TRE-SmoA1	none	Activated murine SmoA1	Basal layer and hair follicles of squamous epithelium	Activated	HA	Basaloid Follicular Hamartoma
GFAP-tTA;TRE-SmoA1	*tTA-SmoA1*	Activated murine SmoA1	Scattered EGL cells; stem cells of SVZ; mature glia	Repressed	HA	Medulloblastoma
GFAP-tTA;TRE-Gli2	*tTA-Gli2*	Full length murine Gli2	Scattered EGL cells; stem cells of SVZ; mature glia	Repressed	n/a	None
*GFAP-tTA;TRE-GLI2**	*tTA-GLI2**	Repressor-deleted active human GLI2	Scattered EGL cells; stem cells of SVZ; mature glia	Repressed	Myc	"Progenitoroma"
GFAP-tTA;TRE-lacZ	*tTA-lacZ*	β-galactosidase	Scattered EGL cells; stem cells of SVZ; mature glia	Repressed	n/a	n/a
GFAP-Cre;R26-LSL-rtTA; TRE-SmoA1	*rtTA-SmoA1*	Activated murine SmoA1	*GFAP*-positive cells and their progeny, includes all EGL cells; undetermined cells in skin.	Activated	HA	Medulloblastoma

n/a = not applicable

Table 2-1. Summary of transgenic mice.

Results

Postnatal Epithelial SmoA1 activation induces basaloid follicular hamartoma-like lesions

Unrestricted embryonic epithelial SmoA1 expression caused neonatal lethality associated with multiple developmental abnormalities. To bypass this and examine adult epithelial response to SmoA1 expression, expression of SmoA1 was activated postnatally by removing *K5-tTA;TRE-SmoA1* mice from doxycycline or placing *K5-rtTA;TRE-SmoA1* mice on doxycycline after birth. Doxycycline-switch transgene activation experiments were performed at postnatal day 7, during the initial round of postnatal hair follicle growth, at 4 weeks of age, just prior to the first true postnatal anagen cycle, and at 8 weeks old, during the first prolonged telogen. Similar results were seen regardless of whether *K5-tTA* or *K5-rtTA* was used to drive *SmoA1* expression.

In all experiments, the first appreciable phenotypic change was the development of a greasy appearance, in which the pelage fur clumped together and became matted down. This greasy appearance was initially evident at the most posterior region of the dorsal skin, and moved progressively forward. This initial change was appreciable between 8 days and 3 weeks after transgene activation. Greasy fur was poorly attached to the animals, and came away easily with gentle pulling, an observation made following sacrifice of affected animals. Within several weeks of the appearance of the greasy phenotype, animals began losing their hair in a posterior to anterior pattern that mirrored the initial appearance of the phenotype. The underlying skin was thickened, scaly and hyperpigmented. In animals which had progressed to the point of significant hair loss,

thickening and hyperpigmentation of the ear which bore the identification tag was appreciable (Figure 2-1 A). This phenotype was confined to the tagged ear, suggesting an involvement of wound healing response. In additional to the skin changes, animals began to appear cachectic and slow-moving, generally between the time of the appearance of the greasy phenotype and the beginning of hair loss. Affected animals sat hunched, moved very little, and appeared to be in significant distress. As such, double transgenic animals were terminated within no more than 9 weeks of transgene activation. The same phenotype was evident in both *K5-tTA;TRE-SmoA1* and *K5-rtTA;TRE-SmoA1* double transgenic animals.

Histological examination of skin from postnatally activated transgenic mice revealed the presence of generalized hyperplasia of the epidermis, consistent with a proliferative response of basal keratinocytes to Hh activation. The affected ears contained large collections of densely packed cells (Figure 2-1 B). Thickening of the basal layer of dorsal skin was evident, and follicles had become badly distorted. Rather than the well-ordered follicular structures of control animals, the affected skin bore a collection of immature follicle-like structures, some of which had evident remaining hair shafts (Figure 2-1 C). The same phenotype was observed in ventral skin (not shown.) The hyperpigmentation seen grossly in the dorsal skin and ears of bitransgenic animals can be appreciated histologically as collections of brown melanin evident in hematoxylin and eosin-stained sections. Immunophenotyping of dorsal skin confirmed widespread expression of SmoA1 (Figure 2-1 D) and a high level of proliferation in both the distorted follicles and the interfollicular epidermis (Figure 2-1 E). Distorted follicles in adult mice ubiquitously expressed K5, indicating a lack of appropriate differentiation (Figure 2-1 F).

Figure 2-1. Hair loss and epithelial hyperplasia following post natal SmoA1 activation. (A) Gross photographs of control animal (left) and *K5-tTA;TRE-SmoA1* double transgenic animal after 3 weeks of transgene activation (middle), with greasy appearance and matted fur evident. After 6 weeks of transgene activation in a *K5-rtTA;TRE-SmoA1* double transgenic mouse, loss of posterior dorsal hair and skin hyperpigmentation are evident (right), as is thickening and hyperpigmentation of the ear bearing the identification tag (right, inset). Hyperpigmentation, thickening and scale development were also evident on the ventral skin (not shown). (B – C) Hematoxylin and eosin staining of ear (B) and dorsal skin (C) from control and double transgenic mice after 6 weeks of transgene activation. Basaloid follicular hamartoma (BFH)-like lesions and melanin deposition are appreciable in both sites. (D – F) Immunohistochemical analysis of control and double transgenic skin. SmoA1 expression is evident throughout both BFHs and interfollicular epidermis, but not in control skin (D). BFHs and interfollicular epidermis are highly proliferative, as measured by Ki67 expression (E). As with newborn lesions, BFHs stain uniformly for keratin 5 (F).

A
Control
K5-tTA;TRE-SmoA1
3 weeks activation
K5-rtTA;TRE-SmoA1
6 weeks activation
B
Ear H&E
C
Dorsal H&E
D
HA
E
Ki67
F
K5
Control
K5-rtTA;
TRE-SmoA1

Proximal activation of the Hh pathway using SmoA1 in developing cerebellum induces medulloblastoma

In order to assess the impact of inappropriate activation of the Hh pathway on the cerebellum of developing mice, we used the *TRE-SmoA1* mouse lines described in Chapter 2. We activated cerebellar expression of SmoA1 by crossing *TRE-SmoA1* mice with *GFAP-tTA* mice, which express the tetracycline transactivator under the control of the human glial fibrillary acidic protein promoter (Lin *et al.*, 2004) (Fig. 2-2 A). The resulting double transgenic mice express SmoA1 in a doxycycline-repressable manner in cells in which the *GFAP* promoter is active. For brevity's sake, double transgenic *GFAP-tTA*;*TRE-SmoA1* mice are referred to simply as *tTA-SmoA1* (Table 2-1). At birth, *tTA-SmoA1* mice were grossly indistinguishable from their control littermates. Furthermore, there was no appreciable histological difference between the external granular layer (EGL) of P0 control mice and P0 *tTA-SmoA1* mice (Fig. 2-2 B, C). Small distortions and expansions of the EGL were evident in some animals by P7, however, and 100% (80/80) of animals examined at P14 or later harbored significant tumor burden (discussed below, see Fig. 2-7). By P21, the tumor burden was quite large, and often extended along the entire anterior-posterior length of the cerebellum, whereas genotype control animals or animals maintained on doxycycline from conception to harvest did not develop tumors (Fig. 2-2 D, E, data not shown). Tumors arose on the external surface of the molecular layer, a region which, by P21, is normally devoid of tissue other than the leptomeninges and vasculature. If left untreated, *tTA-SmoA1* mice developed very large tumor burden, resulting in development of hydrocephalus, which was appreciable grossly

in late stage animals as doming of the skull (Fig. 2-3). Mice also developed marked ataxia, and became generally non-responsive. Mice rarely survived past 7 weeks without displaying obvious signs of tumor burden, and by 10 – 12 weeks old, mice were extremely ill. The longest an untreated *tTA-SmoA1* mouse survived was 16 weeks.

tTA-SmoA1 medulloblastomas are highly proliferative and display dysregulated differentiation

Immunohistochemical analysis of tumors using an anti-HA antibody revealed extensive expression of the transgene throughout the tumor, but not in tissue from control mice (Fig. 2-2 F, G). The medulloblastomas were highly proliferative, as nearly every cell within the tumors stained for the proliferation marker Ki67, while control IGL was largely quiescent (Fig. 2-2 H, I). The tumors displayed a moderate baseline level of apoptosis, consistent with results seen in other medulloblastoma models as well as human medulloblastomas (Fig. 2-2 J, K) (Schiffer *et al.*, 1995, Kim *et al.*, 2003). Despite the high proliferative status of the tumors, many cells also expressed NeuN, a marker for mature, post-mitotic cerebellar granule neurons of the IGL and inner EGL (Fig. 2-2 L, M) (Kim *et al.*, 2003), and scattered expression of the neuronal marker synaptophysin was appreciable, as well (Fig. 2-2 N, O). The tumors did not express gamma-aminobutyric acid receptor, subunit alpha 6 (GABRA6), an inhibitory neurotransmitter receptor broadly expressed by mature IGL neurons (Fig. 2-2 P, Q).

Figure 2-2. 100% of double transgenic *tTA-SmoA1* mice develop medulloblastomas. (A) Breeding scheme demonstrating crossing of *GFAP-tTA* and *TRE-SmoA1* mice to generate *GFAP-tTA*;*TRE-SmoA1* (*tTA-SmoA1*) bitransgenic mice. (B, C) Hematoxylin and eosin stained sagittal sections of newborn control and *tTA-SmoA1* cerebella demonstrating no appreciable histological differences in the EGL. (D, E) Hematoxylin and eosin stained coronal sections of cerebella from 21 day old *tTA-SmoA1* mice with (D) or without (E) continuous doxycycline treatment. Large tumor burden can be appreciated in E. Insets show low magnification. (F – Q) Immunohistochemical analysis of tumors (F, H, J, L, N, P) or genotype control IGL (G, I, K, M, O, Q) for SmoA1, detected by means of the HA epitope tag (F, G), Ki67 (H, I), cleaved caspase 3 (J, K), NeuN (L, M), synaptophysin (N, O) and GABRA6 (P, Q).

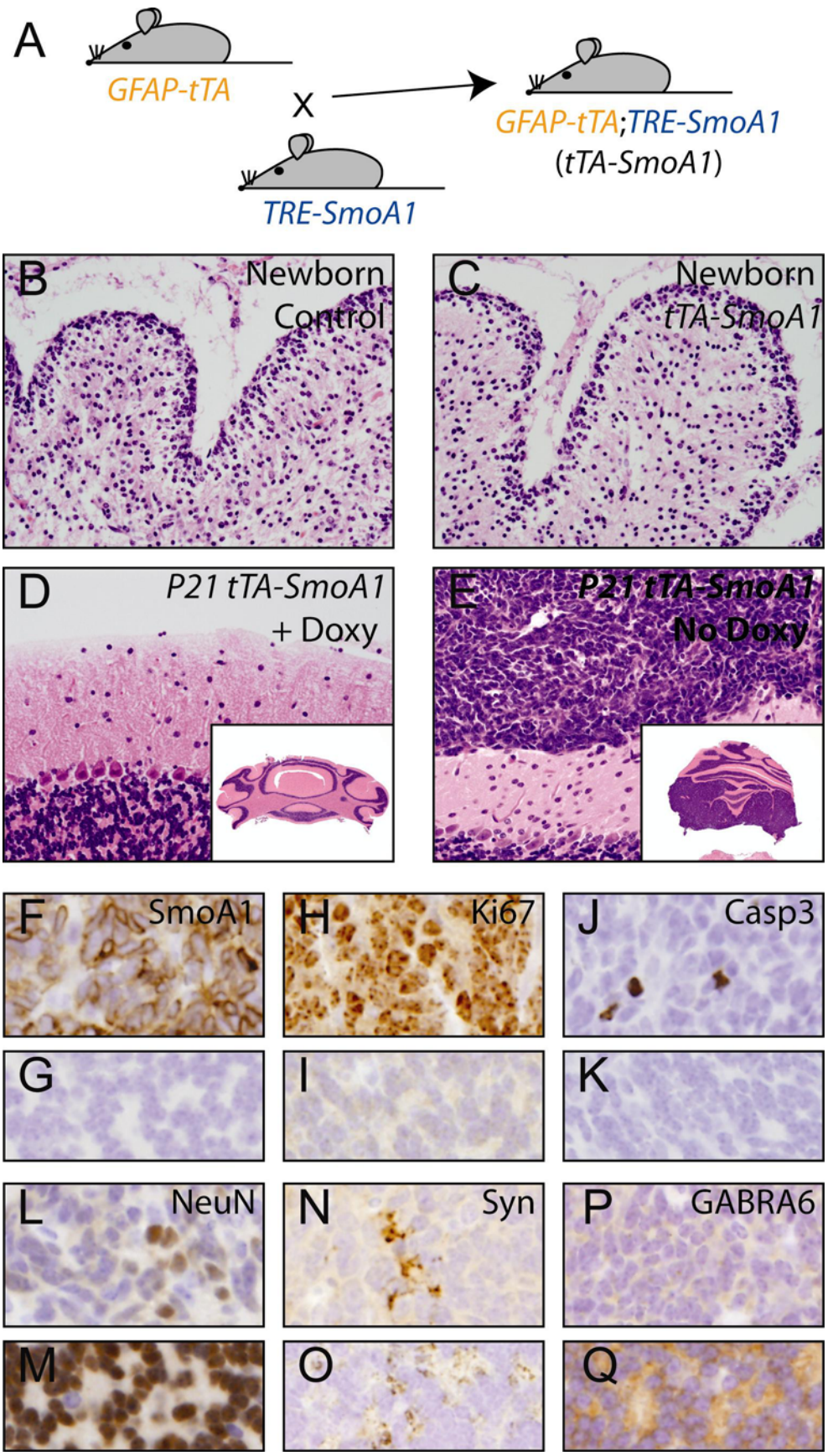
A
GFAP-tTA
X
TRE-SmoA1
GFAP-tTA;TRE-SmoA1
(tTA-SmoA1)
B
Newborn
Control
C
Newborn
tTA-SmoA1
D
P21 tTA-SmoA1
+ Doxy
E
P21 tTA-SmoA1
No Doxy
F
SmoA1
H
Ki67
J
Casp3
G
I
K
L
NeuN
N
Syn
P
GABRA6
M
O
Q

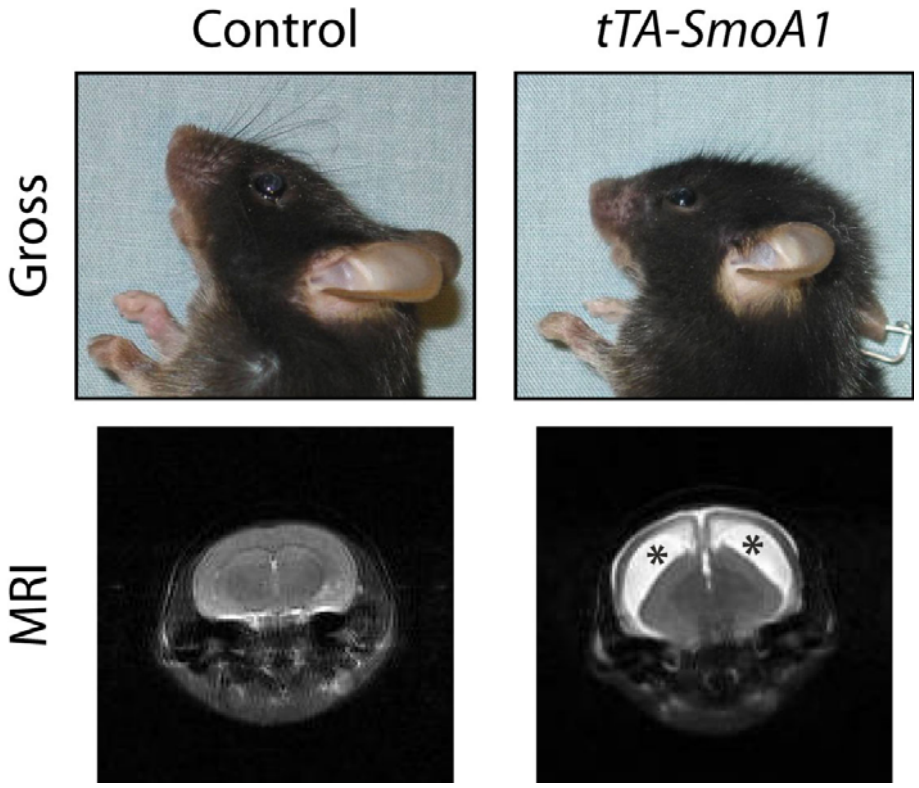

Figure 2-3. Medulloblastomas cause cranial doming and hydrocephalus. Effects of tumor burden can be appreciated grossly in an 8-week old *tTA-SmoA1* mouse as significant doming of the skull, secondary to hydrocephalus. Hydrocephalus can be appreciated as distortion of the lateral ventricles, visible on T2-weighted MRI (asterisks).

tTA-SmoA1 medulloblastomas express Hh pathway targets and key cell cycle regulators

Comparison of hematoxylin and eosin-staining (Fig. 2-4 A) and *in situ* hybridization of neighboring sections demonstrated expression of *SmoA1* (Fig. 2-4 B) and activation of the Hh pathway in tumors, as measured by expression of *Gli1* and *Ptch1* (Fig. 2-4 C, D). We also examined pathway and target gene expression in 5 wild type adult control cerebella and 5 tumor-bearing cerebella by quantitative, real time RT-PCR. Both *Gli1* and *Ptch2*, markers for Hh pathway activation, were significantly upregulated in tumor-bearing cerebella (Fig. 2-5 A, C). Surprisingly in light of the *in situ* hybridization data, *Ptch1* levels were not significantly different between control cerebellum and *SmoA1*-induced medulloblastomas when measured by qPCR (Fig. 2-5 B).

All other measures of Hh pathway activation in tumors however, both by *in situ* hybridization and qPCR, indicated a strong upregulation of pathway activity, perhaps suggesting a problem with the *Ptch1* primers or reaction conditions. *N-myc*, a key downstream target of the Hh pathway in normal cerebellar development and medulloblastoma development (Hatton *et al.*, 2006), was upregulated 17-fold in medulloblastomas (Fig. 2-5 D). *CyclinD1* was upregulated 11-fold and *CyclinD2* was upregulated 24-fold (Fig. 2-5 E, F). Both *CyclinD1* and *CyclinD2* are hedgehog target genes, and *CyclinD1* has recently been identified as a critical factor in both normal cerebellar development and the formation of medulloblastoma (Pogoriler *et al.*, 2006). Additionally, *Math1*, a marker for immature, proliferating granule cell precursors (Helms *et al.*, 1998), was overexpressed approximately 550-fold in tumors (Fig. 2-5 G). Expression of *Math1* is consistent with previous reports of Math1 in pre-neoplastic

lesions and medulloblastomas in the *Ptch*$^{+/-}$ mouse model (Oliver *et al.*, 2005) as well as in human disease (Ueba *et al.*, 2008).

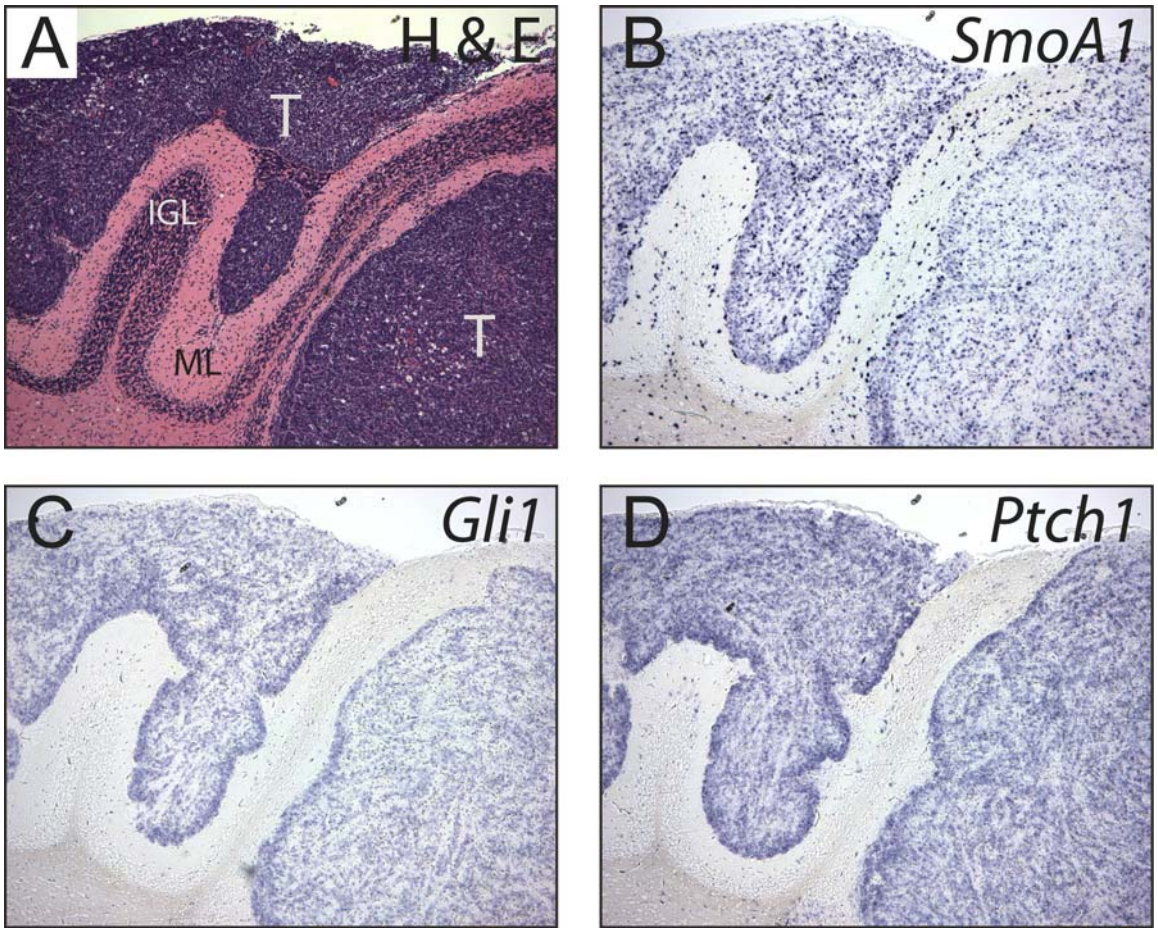

Figure 2-4. Expression of *SmoA1* and Hh pathway activation in tumors. (A) Hematoxylin and eosin staining of a parasagittal cerebellar section from a 7 week old *tTA-SmoA1* mouse. Tumor burden (T) is clearly appreciable external to the molecular layer (ML). The internal granular layer (IGL) is also visible. (B – D) *In situ* hybridization demonstrating expression of *SmoA1* (B) and activation of the Hh pathway in medulloblastoma, indicated by expression of the Hh target genes *Gli1* (C) and *Ptch1* (D).

Figure 2-5. qPCR demonstrates activation of Hh target genes in tumors. (A – G) Quantitative real-time RT-PCR using mRNA isolated from 21 day old genotype control or tumor-bearing *tTA-SmoA1* cerebellum. Significant overexpression in tumors was detected for *Gli1*, P=0.0073 (A); *Ptch2*, P=0.028 (C); *N-Myc*, P=0.012 (D); *Cyclin D1*, P=0.0026 (E); *Cyclin D2*, P=0.00064 (F); and *Math1*, P=0.0097 (G). *Ptch1* expression in tumors was not detectably different from control cerebellum (B). Error bars represent standard error of the mean and * indicates a significant difference from control cerebellum. N=5 individual samples for each group.

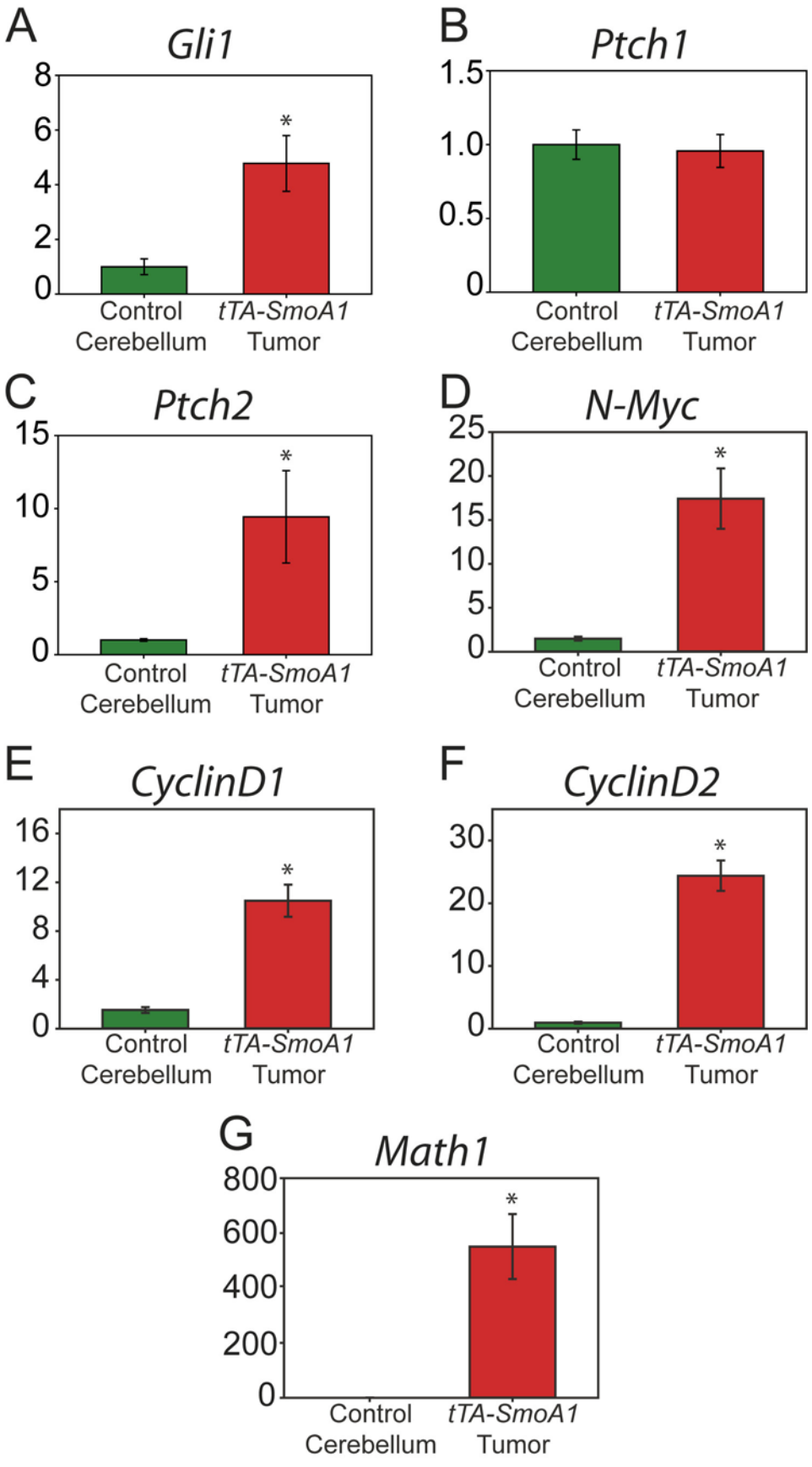
A
Gli1
8
6
4
2
0
*
Control Cerebellum
tTA-SmoA1 Tumor
B
Ptch1
1.5
1.0
0.5
0
Control Cerebellum
tTA-SmoA1 Tumor
C
Ptch2
15
10
5
0
*
Control Cerebellum
tTA-SmoA1 Tumor
D
N-Myc
25
20
15
10
5
0
*
Control Cerebellum
tTA-SmoA1 Tumor
E
CyclinD1
16
12
8
4
0
*
Control Cerebellum
tTA-SmoA1 Tumor
F
CyclinD2
30
20
10
0
*
Control Cerebellum
tTA-SmoA1 Tumor
G
Math1
800
600
400
200
0
*
Control Cerebellum
tTA-SmoA1 Tumor

Cells within tumors retain the ability to differentiate into postmitotic neurons

In addition to the gross tumor burden in *tTA-SmoA1* animals, we also observed ectopic clusters of nuclei within the molecular layer, beneath the tumor mass (Fig. 2-6 A – D). Similar populations of cells are seen adjacent to human tumors and in other mouse models of medulloblastoma. The nuclei in these ectopic foci appeared very similar histologically to post-mitotic IGL neurons, albeit inappropriately located in the molecular layer. These foci were never appreciated in control cerebella. Due to their proximity to the tumors and their IGL neuron-like appearance, we hypothesized that these rests comprised cells that originated within the tumors, recapitulating at least part of the behavior of physiologic EGL-derived neurons. The cells within the rests were non-proliferative, as they were negative for Ki67 (Fig. 2-6 B) and did not incorporate BrdU when injected intraperitoneally one hour prior to sacrifice (Fig. 2-6 G). In addition to their nuclear morphology, these cells resembled normal cerebellar IGL with respect to lineage marker expression. Cells within the clusters expressed p27 (Fig. 2-6 C) and GABRA6 (Fig. 2-6 D), both markers of mature, post-mitotic cerebellar granule neurons (Kato, 1990, Miyazawa *et al.*, 2000).

In addition to p27 and GABRA6, cells within the clusters also strongly expressed the post-mitotic neuronal marker NeuN (Fig. 2-6 E, F). As expected, NeuN-positive cells in the ML were non-proliferative, as no NeuN and BrdU co-labeled cells were detected when BrdU was injected intraperitoneally 1 hour prior to sacrifice (Fig. 2-6 H, upper timeline in Fig. 2-6 M). We also placed tumor-bearing animals on BrdU-containing water for one week prior to tissue harvest in order to track the behavior of proliferating cells (lower timeline in Fig. 2-6 M). Co-staining cerebella from long-term BrdU-treated

mice revealed the presence of numerous cells within the post-mitotic rests which both expressed NeuN and had incorporated BrdU at some point during the week of treatment. (arrows in Fig. 2-6 I – L). As indicated by the short-term BrdU labeling and Ki67 immunostaining experiments, essentially the only proliferative cells in the outer cerebella of the tumor bearing animals were within the body of the tumors; cells in the ectopic rests within the ML were non-proliferative. Therefore, these post-mitotic, NeuN- and BrdU-positive neuronal cells within the ML must have arisen from within the tumors. This suggests that some cells within tumors retain the ability to withdraw from the cell cycle, turn on expression of normal IGL neuronal markers, and migrate into the molecular layer. However, we cannot formally exclude the possibility that the cells within the rests are dividing very slowly and therefore do not incorporate BrdU during the short-term injection studies, although lack of Ki67 (Fig. 2-6 B) and NeuN positivity (not shown) in these cells argue that this is not the case.

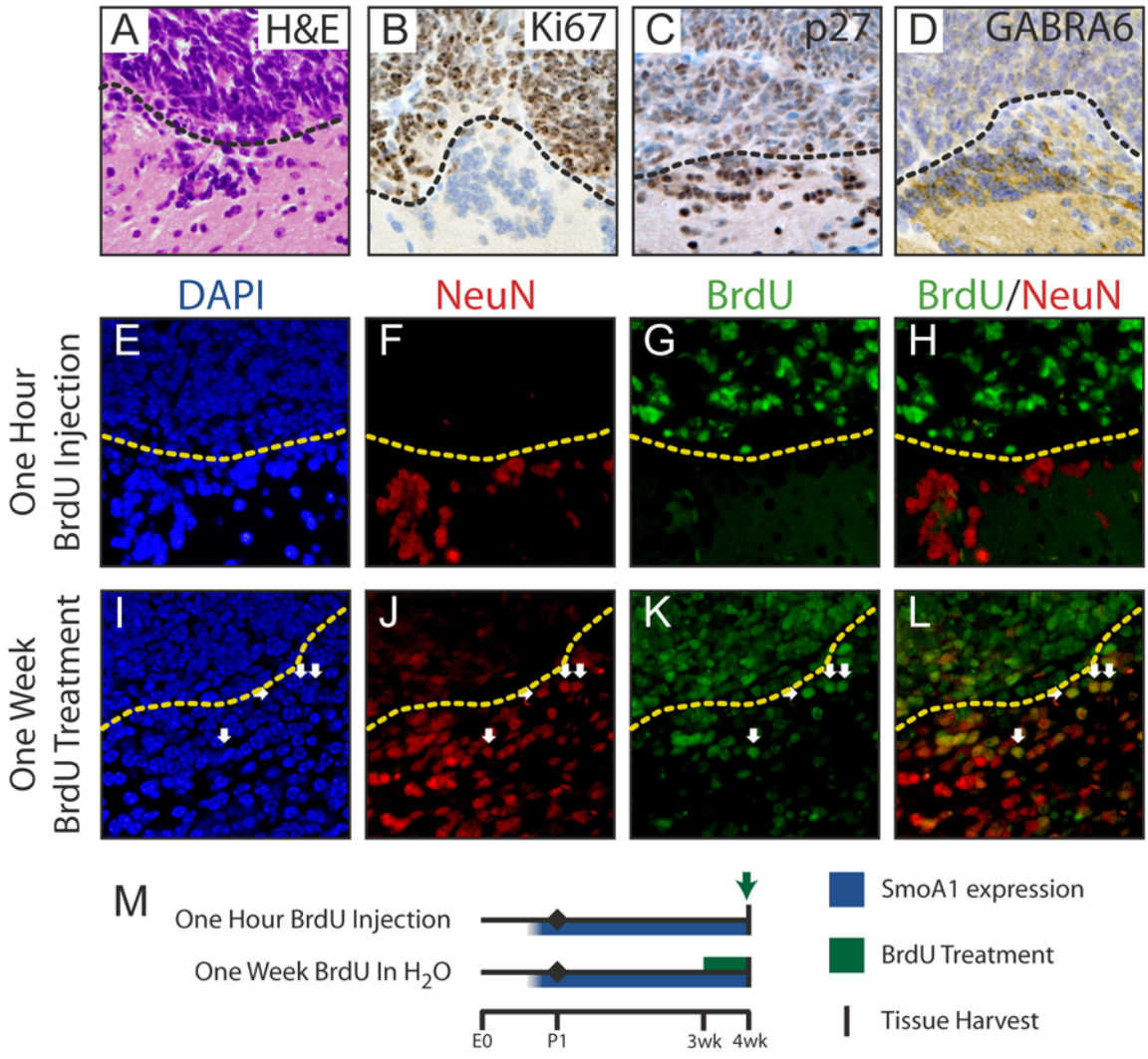

Figure 2-6. Cells within medulloblastomas can differentiate into post-mitotic neurons. (A) Hematoxylin and eosin stain of ectopic cell cluster within outer ML, underneath tumor burden. (B) Immunohistochemical staining of ectopic cell clusters for Ki67, demonstrating a lack of proliferation in these cells. (C, D) Expression of the mature neuronal markers p27 (C) and GABRA6 (D) were detected in ectopic clusters. Dotted black lines in A – D indicate outer edge of ML. (E – L) Co-immunofluorescence for NeuN and BrdU in tumor-bearing mice injected with BrdU one hour before harvest (E – H) or maintained on continuous BrdU treatment for one week prior to harvest (I – L). Panels show nuclear DAPI (E, I), NeuN (F, J) or BrdU (G, K) alone or co-staining for BrdU and NeuN (H, L). Arrows in I – L indicate some of the visible co-labeled cells. Dotted yellow lines in E – L indicate outer edge of ML. (M) Timeline of BrdU treatments prior to harvest.

SmoA1-induced medulloblastomas arise from the EGL

It has been hypothesized that medulloblastomas, particularly those driven by inappropriate Hh signaling, often arise from the cerebellar granule neuron precursors of the immature external granular layer (Eberhart, 2007), and the location of tumors in 21-day old and older *tTA-SmoA1* mice is consistent with development from the EGL. We used several approaches to provide additional evidence that this population serves as the cell of origin for SmoA1-induced medulloblastomas. We crossed *GFAP-tTA* mice with TRE-lacZ mice, in which expression of β-galactosidase is induced by tTA. We sacrificed the resulting *tTA-lacZ* pups from this cross at two days old, and stained brain tissue with X-gal to determine the location of tTA expression in the young cerebellum. In addition to the expected staining in cells scattered throughout the underlying tissue, single X-gal stained cells or small clusters of cells were also present in the very young EGL (Fig. 2-7 A, B). By postnatal day 7 (P7), the EGL of *tTA-SmoA1* mice contained small clusters of SmoA1-expressing cells, which were often associated with minor distortion of the otherwise smooth outer edge of the ML (Fig. 2-7 C, D). By 14 days old, tumors with robust SmoA1 expression were evident in all *tTA-SmoA1* mice. These tumors were contiguous with the EGL, which persisted at this age both in control and in *tTA-SmoA1* mice (Fig. 2-7 E, F). Regions of *tTA-SmoA1* EGL expressing no detectable SmoA1 were histologically indistinguishable from age-matched control EGL (Fig. 2-7 F, inset).

To further support the hypothesis that the EGL serves as the progenitor cell population for Hh-driven medulloblastomas, we took advantage of the conditional nature of our *TRE-SmoA1* mice. We maintained *tTA-SmoA1*-producing breeding pairs and nursing dams on doxycycline chow, inhibiting transgene expression. Pups were weaned

onto doxycycline-free chow, resulting in SmoA1 expression after the complete disappearance of the EGL. No tumor development was detected in 13 *tTA-SmoA1* mice removed from doxycycline between three and six weeks after birth and sacrificed between 12 and 16 months old (Fig. 2-7 G and data not shown). Likewise, no tumors were detected in four *tTA-SmoA1* mice removed from doxycycline treatment between E16 – 18 and P1 and sacrificed at 7.5 or 9 months (Fig. 2-7 G and data not shown). Expression of SmoA1 was confirmed in confirmed postnatally-activated mice by immunostaining.

In order to more precisely regulate the time point at which SmoA1 expression commences, we also employed our *TRE-SmoA1* mice in a tetracycline-induced, "Tet-on" rtTA model. To obtain *GFAP*-driven rtTA expression, we employed *GFAP-Cre* mice, in which expression of Cre recombinase is driven by the human GFAP promoter (Zhuo *et al.*, 2001). We crossed *GFAP-Cre* mice with *R26-LSL-rtTA* mice (Belteki *et al.*, 2005). In *R26-LSL-rtTA* mice, a *loxP*-flanked strong stop sequence and the reverse tetracycline transactivator are knocked into the ubiquitously active *ROSA26* locus. In the absence of Cre recombinase activity, no *rtTA* is transcribed. Following Cre recombinase-mediated excision of the stop sequence, *rtTA* is expressed in the recombined cell and all of its progeny from the ubiquitously active *ROSA26* locus. We crossed double transgenic *GFAP-Cre*;*R26-LSL-rtTA* progeny with *TRE-SmoA1HA* mice to obtain triple transgenic *GFAP-Cre*;*R26-LSL-rtTA*;*TRE-SmoA1HA* mice (Fig. 2-8 A). For brevity's sake, these triple transgenic mice will hereinafter be referred to as *rtTA-SmoA1*.

To induce SmoA1 expression, we maintained *rtTA-SmoA1* breeding cages on doxycycline-containing chow continuously, and maintained weaned mice on

doxycycline-containing chow until harvest. Mice were harvested for histological analysis at P7 (N=3), P14 (N=2), P21 (N=4) or between 4 and 8 weeks old (N=6) (timeline for all doxycycline treatment regimens and sacrifices can be seen in Fig. 2-8 B). While animals positive for zero, one or two of the transgenes did not develop tumors (Fig. 2-8 C), triple transgenic *rtTA-SmoA1* mice developed significant medulloblastoma burden (Fig. 2-8 D). Tumor penetrance was 100% in animals examined at P14 or later (12/12). By 8 weeks of age, animals were slow-moving and lethargic prior to euthanasia. Continuous activation of SmoA1 expression also led to a developmental defect in the cerebellum, resulting in abnormal foliation and a disordered IGL and Purkinje layer in young adult animals (Fig. 2-8 D), but no other obvious developmental defects.

To define the developmental window for medulloblastoma susceptibility, we fed breeding pairs normal, doxycycline-free chow during gestation, beginning doxycycline treatment either 4 or 7 days after the birth of litters, when the EGL is still actively proliferating. Histological examination revealed that activation of SmoA1 expression at either P4 (Fig. 2-8 E) or P7 (not shown) induced medulloblastoma formation by P21, with relative normalization of cerebellar foliation and IGL and Purkinje layer organization. To examine the consequences of activating SmoA1 expression after the disappearance of the EGL, we weaned *rtTA-SmoA1* mice from normal chow to doxycycline-containing chow at P21. These mice were sacrificed 3 weeks (N=3), 16 weeks (N=3) or 31 weeks (N=1) after weaning to doxycycline chow. At the time of this writing, 3 additional mice are approximately one year old, and will be sacrificed after 52 weeks of transgene activation. In stark contrast to animals in which transgene expression was activated at P7 or earlier, no tumor development was evident in any animal activated

at weaning, and cerebella were grossly indistinguishable from controls (Fig. 2-8 F). These data indicate that activation of the Hh pathway in cerebellum by SmoA1 is capable of driving tumorigenesis only in the first few weeks of life, during the developmental period in which the CGNPs of the EGL are still present and proliferating.

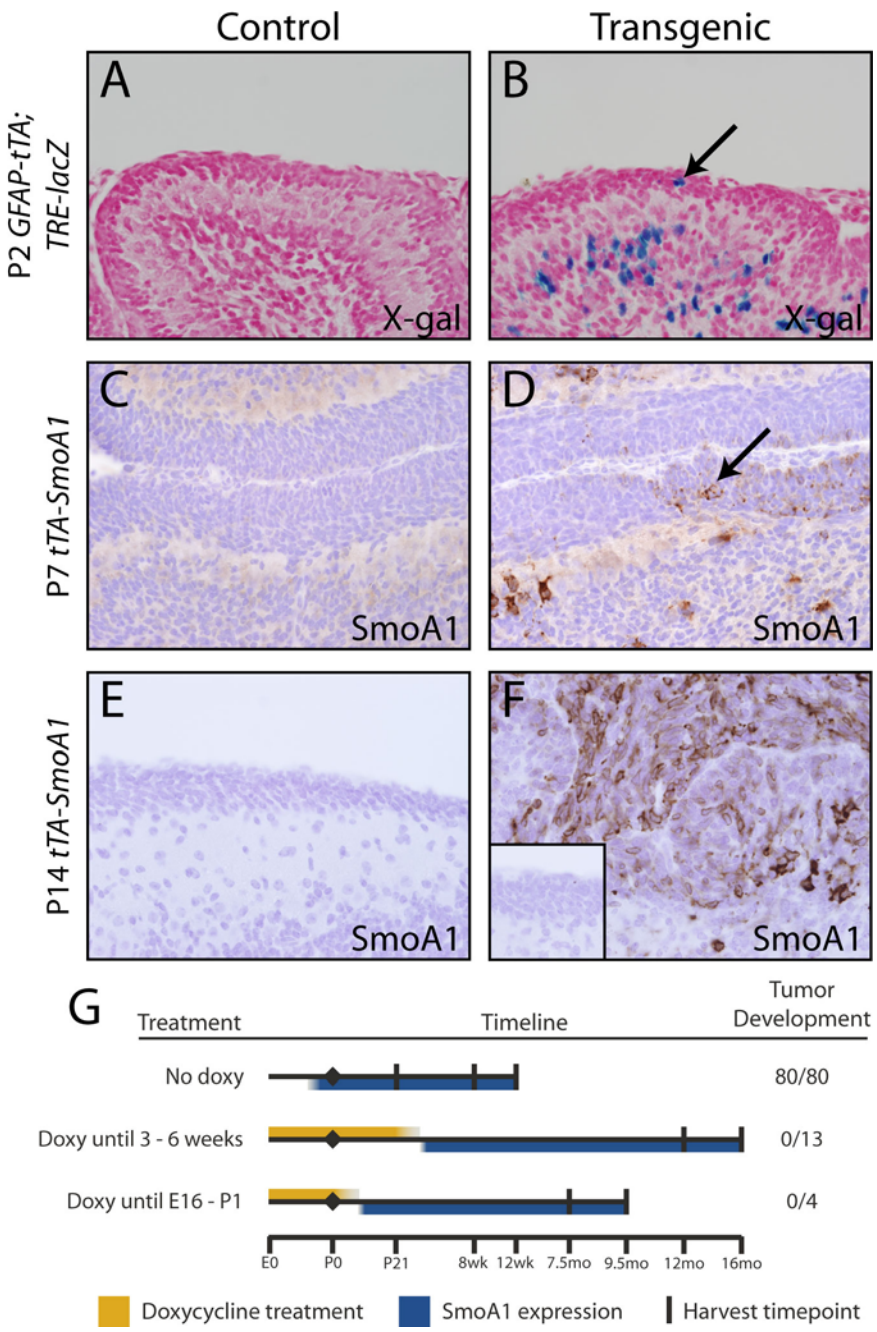

Figure 2-7. Early GFAP-tTA mediated transgene activation and SmoA1-driven distortion of the EGL. X-gal staining of cerebella from 2 day old control (A) and double transgenic *GFAP-tTA;TRE-lacZ* (B) mice revealed activation of few cells scattered throughout the EGL (arrow). (C – F) Immunohistochemical detection of HA-tagged SmoA1. No staining was evident in P7 (C) or P14 control mice (E). Small, scattered clusters of SmoA1-positive EGL cells were evident at P7 (D, arrow), and by P14, developed into early tumors contiguous with the remaining EGL (F). Inset in F shows a region from the EGL of the same cerebellum, demonstrating that regions which did not express transgene were indistinguishable from control EGL. (G) Timeline for doxycycline treatment and tumor development in *tTA-SmoA1* mice.

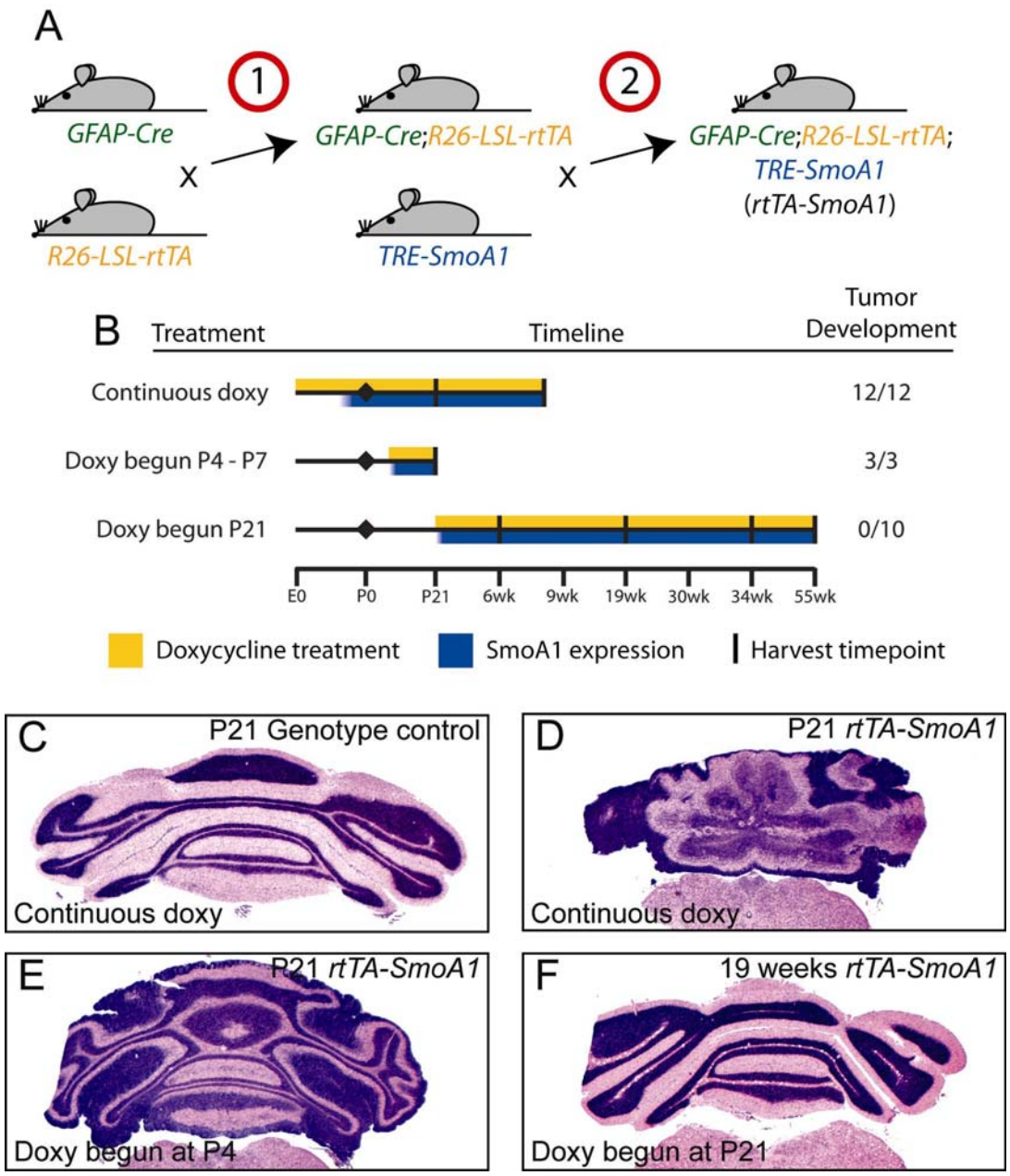

Figure 2-8. Breeding scheme and tumor development in *rtTA-SmoA1* mice. (A) Initial two step breeding scheme to generate triple transgenic *rtTA-SmoA1* mice. (B) Timeline indicating doxycycline treatment regimens and tumor development. (C – F) Low magnification of coronal cerebellar sections from genotype control and *rtTA-SmoA1* mice. No tumors were evident in genotype control mice (C). Both significant tumor development and disruption of the normal cerebellar architecture were evident in P21 *rtTA-SmoA1* mice on continuous doxycycline treatment (D). Both early tumor development and relative normalization of the cerebellar architecture were evident at P21 when doxycycline treatment was begun at P4 (E). No tumors developed when *rtTA-SmoA1* animals were placed on doxycycline at P21 (F).

Expression of repressor-deleted GLI2* in CNS, but not SmoA1 or full-length Gli2, induces formation of widespread undifferentiated tumors

To assess the potential for *GFAP-tTA* driven SmoA1 to induce tumorigenesis outside of the developing cerebellum, we examined the forebrains of medulloblastoma-bearing *tTA-SmoA1* mice. These mice exhibited no appreciable histologic abnormalities in the forebrain other than the development of hydrocephalus, and were indistinguishable from genotype control forebrain (Fig. 2-9 A, B). Immunostaining for the HA tag demonstrated expression of SmoA1 in cells within the SVZ, a niche for Sonic hedgehog-responsive adult neural stem cells (Ahn *et al.*, 2005, Palma *et al.*, 2005). However, SmoA1 was detected not only in the SVZ, but also in cells, presumably glia, scattered throughout the brain (Fig. 2-9 C). Strikingly, despite the broad expression of SmoA1, activation of the Hh pathway, as indicated by expression of *Gli1* and *Ptch1*, was essentially confined to the cells of the SVZ (Fig. 2-9 D, E). These results suggest that 'inappropriate' activation of Hh signaling by SmoA1 is blocked in glial cells, rendering them unresponsive to this potent oncogene when expressed in the cerebellar EGL.

In order to examine whether downstream activation of the Hh pathway at the level of the Gli transcription factors could bypass the apparent lack of response to SmoA1 in glial cells, we employed the *TRE-Gli2 (Hutchin et al., 2005)* and *TRE-GLI2** mouse models previously developed in our lab. We activated expression of exogenous full-length *Gli2* or Myc-tagged, repressor domain-deleted *GLI2** in the central nervous system by crossing *GFAP-tTA* mice with *TRE-Gli2* or *TRE-GLI2** mice. The resulting double transgenic mice were designated *tTA-Gli2* and *tTA-GLI2**, respectively (Table 2-1).

Double transgenic *tTA-Gli2* mice did not exhibit any obvious morphological or behavioral phenotype. We sacrificed *tTA-Gli2* mice and examined them histologically at 5.5 weeks (N=1), 22 weeks (N=1), 52 weeks (N=6) and 60 weeks of age (N=2). Contrary to our results with *tTA-SmoA1* mice, *tTA-Gli2* mice failed to develop any tumors, and were histologically indistinguishable from their control littermates (not shown). These findings suggest that, despite high-level expression of *Gli2* in several mouse models of medulloblastoma (Hallahan *et al.*, 2004, Dakubo *et al.*, 2006, Sasai *et al.*, 2007), overexpression of this transcription factor is not sufficient to drive medulloblastoma development. This is in contrast to the formation of multiple BCCs in skin engineered to overexpress Gli2 (Grachtchouk *et al.*, 2000, Hutchin *et al.*, 2005).

Conversely, 9/9 newborn *tTA-GLI2** mice, derived from two independent *TRE-GLI2** lines, developed large undifferentiated masses of proliferating cells in their forebrains, and were unable to survive past birth. The lesions in these mice appeared to be gross expansions of undifferentiated cells surrounding the lateral ventricles (Fig. 2-10 A). The masses, which expressed high levels of GLI2* (Fig. 2-10 B) and were highly proliferative (Fig. 2-8 C), were also positive for the stem and progenitor cell marker nestin, suggesting a preservation of progenitor-like phenotype (Fig. 2-10 D). They were also negative for the neuronal markers NeuN and TuJ1 (Fig. 2-10 E, F), reflecting their undifferentiated status. The striking phenotype seen in these mice is in keeping with the potent transcriptional activity of GLI2*, an 'activated' form of GLI2 which is missing the amino-terminal repressor domain (Roessler *et al.*, 2005).

To examine the consequences of *GLI2** activation in the adult forebrain, we maintained breeding cages on doxycycline chow to repress transgene expression until

after birth. We activated transgene expression by returning animals to regular, doxycycline-free chow at P2 (N=2), P21 (N=4), 1 month old (N=1) or 6 weeks old (N=7). 9 animals were sacrificed for histological examination when they began to exhibit abnormal behavior such as slow movement, general unresponsiveness or seizures. Abnormal behavior was appreciated between 6 and 14 weeks after transgene activation, and had a sudden onset, as animals subsequently deteriorated rapidly over the span of several days. 5 animals died spontaneously between 8 and 16 weeks old, and were not recovered for histological analysis.

Histological examination of postnatally activated *tTA-GLI2** mice revealed the presence of many small tumors scattered throughout both the cerebrum (Fig. 2-11 A top, B) and the cerebellum (Fig. 2-11 A bottom). The number of these small, fairly well-circumscribed tumors generally increased with greater time of transgene activation. In animals harboring very large tumor burden, adjacent small tumors coalesced into larger, confluent lesions, and minor dilation of the lateral ventricles was evident. Tumor cells expressed GLI2*, and the lesions were highly proliferative with little evidence of apoptosis (Fig. 2-11 C, D, E). Tumors appeared to represent collections of undifferentiated cells, as they were largely negative for the differentiation markers NeuN, synaptophysin, TuJ1 and GFAP (Fig. 2-11 F, G, H, I), and were positive for the neural stem and progenitor cell markers nestin, Sox2 and Sox3 (Fig. 2-11 J, K, L). Development of these numerous undifferentiated tumors from mature glia, but not of SVZ-derived gliomas, in response to GLI2* expression suggests that high level, distal activation of the Hh pathway is sufficient to induce de-differentiation of mature glia and their proliferative expansion, but not for gliomagenesis.

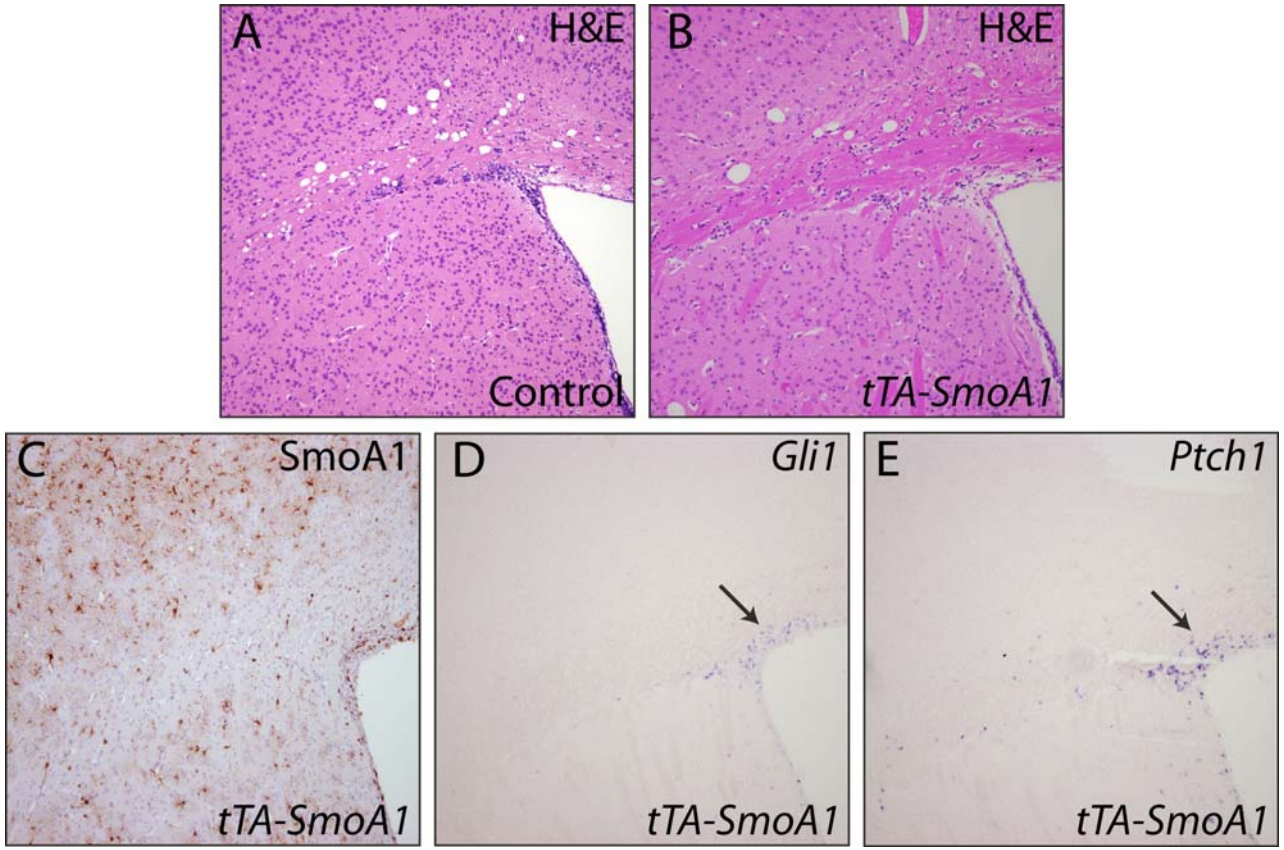

Figure 2-9. SmoA1 does not induce tumorigenesis or widespread activation of the Hh pathway in forebrain. (A, B) Hematoxylin and eosin staining of control (A) and a 6.5 week old *tTA-SmoA1* mouse with a large medulloblastoma, but no appreciable tumor development in the forebrain. (C) Immunohistochemical staining for the HA tag demonstrated broadly scattered SmoA1 expression throughout the forebrain. *In situ* hybridization for *Gli1* (D) and *Ptch1* (E) in nearby sections revealed that Hh pathway activation was essentially restricted to the SVZ (arrows), a region where the endogenous Hh pathway is normally activated.

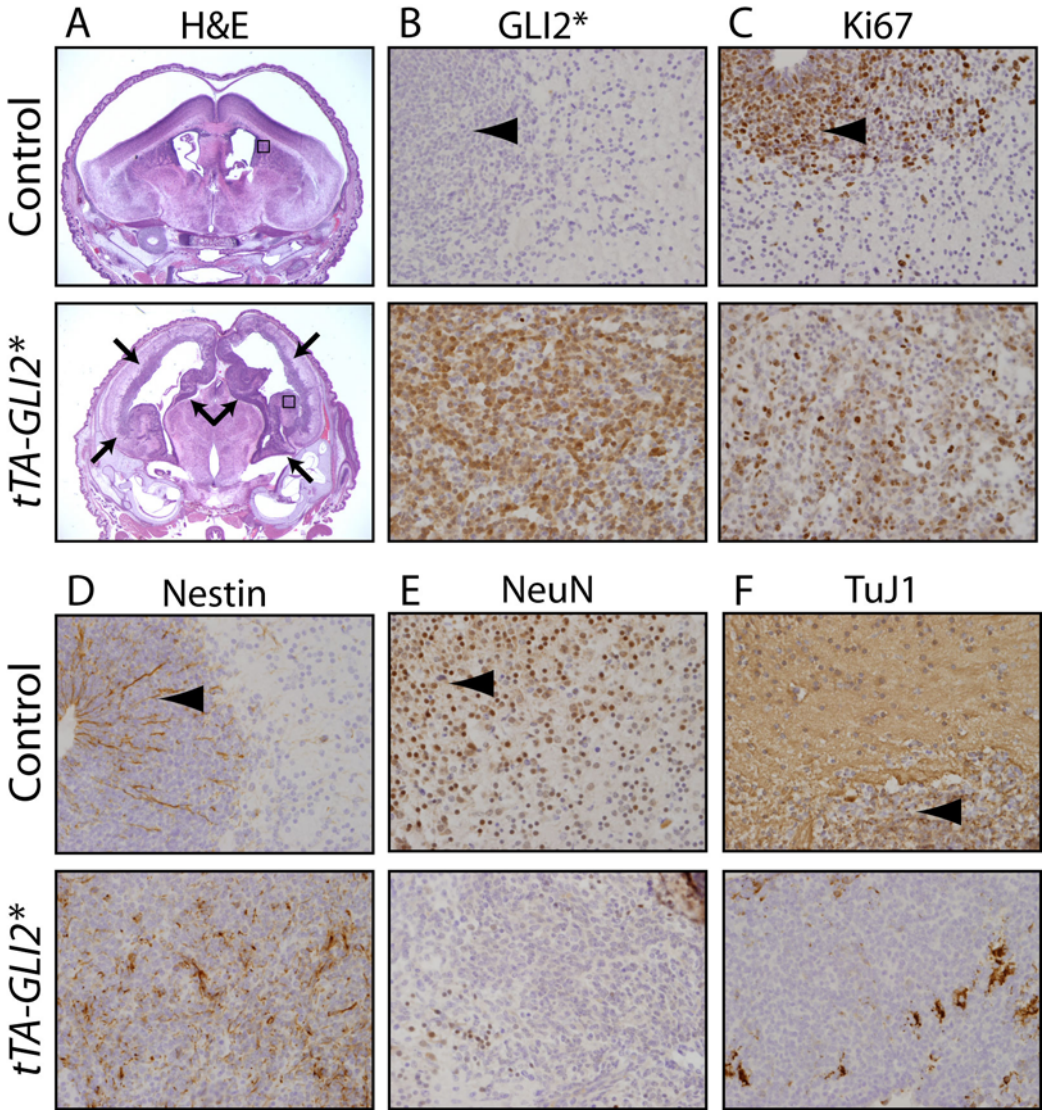

Figure 2-10. Newborn *tTA-GLI2 mice harbor large, undifferentiated forebrain tumors.** (A) Low-power hematoxylin and eosin staining of newborn control and *tTA-GLI2** mice. Arrows indicate large bilateral forebrain masses in a representative *tTA-GLI2** mouse and boxes indicate approximate regions of higher-power images. (B – F) Immunohistochemical analysis of newborn lesions revealed poorly-differentiated, progenitor-like phenotype. Arrowheads indicate control SVZ. (B) GLI2*, detected by staining for the transgenic Myc tag, was broadly expressed in lesions, which were highly proliferative (C), as was control SVZ. Many cells in both tumors and control SVZ were positive for the stem and progenitor marker nestin (D). Some cells within tumors expressed low levels of the neural markers NeuN (E) and TuJ1 (F), but the majority of the cells did not express terminal differentiation markers.

Figure 2-11. Postnatally activated *tTA-GLI2 mice develop many undifferentiated brain tumors.** (A) Hematoxylin and eosin stained section of a 12 week old *tTA-GLI2** mouse, showing the development of many tumors throughout both the forebrain (top) and cerebellum (bottom). Original magnification in A was 2.5X. (B) Higher power image of a representative lesion. Original magnification in B – L was 40X. (C – L) Immunohistochemical staining revealed proliferative, undifferentiated, progenitor-like nature of *tTA-GLI2** tumors. Myc tag staining demonstrated *GLI2** expression in the majority of cells within tumors (C). Tumors expressed the proliferation marker Ki67 (D), but not TUNEL positive (E), indicating an absence of apoptosis. As with newborn tumors, some cells within the lesions expressed low levels of NeuN (F). Tumors were negative for the differentiation markers synaptophysin (G), TuJ-1 (H) and GFAP (I). Scattered cells within the tumors expressed nestin (J), and nearly every cell expressed Sox2 (K) and Sox3 (L).

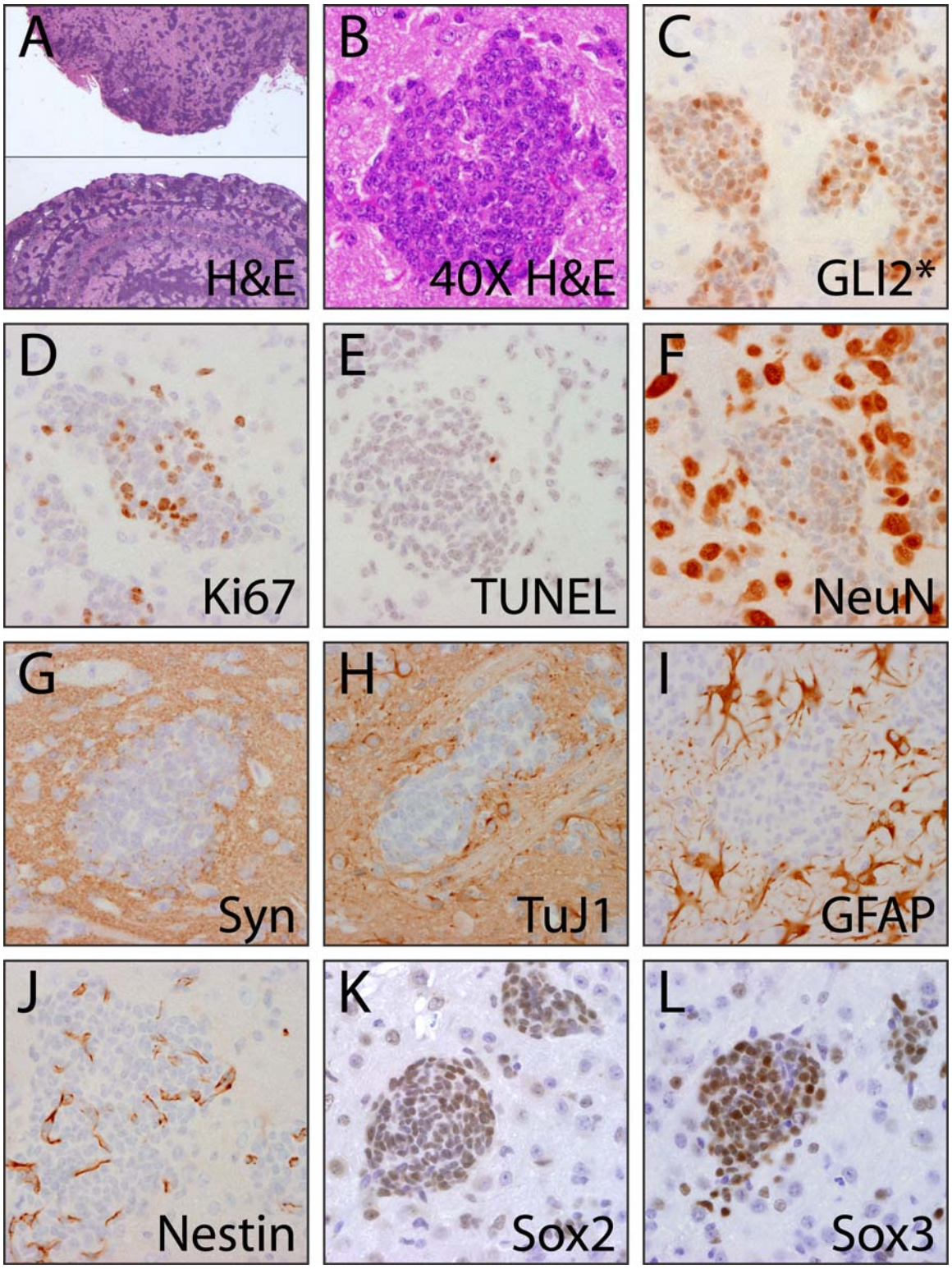
A
H&E
B
40X H&E
C
GLI2*
D
Ki67
E
TUNEL
F
NeuN
G
Syn
H
TuJ1
I
GFAP
J
Nestin
K
Sox2
L
Sox3

Discussion

In this chapter, I have described a novel inducible model for dysregulated Hh signaling in multiple tissues, driven by the constitutively active *Smo* allele *SmoA1*. Epithelial activation of SmoA1 expression in *K5-tTA;TRE-SmoA1* mice induced development of benign follicular hamartoma-like lesions very similar to the tumors induced by M2SMO, the human ortholog of SmoA1 (Grachtchouk *et al.*, 2003). This outcome is consistent with previous observations that murine skin is resistant to BCC development secondary to upstream Hh pathway activation (Dlugosz *et al.*, 2002). Conversely, SmoA1 expression in the cerebella of double transgenic *tTA-SmoA1* mice and triple transgenic *rtTA-SmoA1* mice caused development of robust medulloblastomas with 100% penetrance early in life. This represents a powerful new tool in the study of Hh-driven medulloblastoma initiation, progression, and maintenance (see Chapter 3). Because p53 mutations and MDM2 amplification are rare in human medulloblastoma (Saylors *et al.*, 1991, Adesina *et al.*, 1994), by specifically activating the Hh pathway while leaving the function of the tumor suppressor p53 intact, this system represents a genetically faithful model of human medulloblastoma, with the caveat that it is based on overexpression of a transgene. Furthermore, while demonstrable mutations in components of the HH pathway are evident in roughly 25% of human medulloblastomas (Wetmore, 2003, Marino, 2005), there is mounting evidence that the Hh pathway is activated across a larger subset of human medulloblastomas. I have used the conditional SmoA1 mouse model to address several key questions in medulloblastoma biology related to developmental window for tumor susceptibility, cell of origin, and sufficiency of proximal vs. distal Hh pathway activation to induce tumor formation.

Multiple independent studies have reported activation of Hh target genes in up to 60% of human medulloblastomas (Hallahan *et al.*, 2004, Leung *et al.*, 2004). A possible explanation for this phenomenon may come from the observation that up to 50% of medulloblastomas harbor a loss of the short arm of chromosome 17 (reviewed in (Gulino *et al.*, 2007)). *REN*^{KCTD11}, a functional repressor of the HH pathway, maps to chromosome 17p (Di Marcotullio *et al.*, 2004), suggesting that loss of this region may lead to unrestrained HH signaling in a large fraction of medulloblastomas. Additionally, several mouse models generated by activating disparate pathways result in medulloblastomas with Hh pathway activation; both IFN-γ driven medulloblastomas (Lin *et al.*, 2004) and tumors arising following *Cxcr6* inactivating mutation (Sasai *et al.*, 2007) display an increase in Hh signaling.

Morphological and biochemical features of medulloblastomas which developed in *tTA-SmoA1* mice resembled both human medulloblastomas and tumors arising in previously established mouse models. Tumors were highly proliferative, and displayed a moderate baseline level of apoptosis. Expression of typical medulloblastoma markers such as NeuN, synaptophysin, *Math1*, *N-Myc*, and *Cyclin D1* and *D2* was evident in tumors from our models. Likewise, Hh pathway activity in medulloblastomas was confirmed by *in situ* hybridization and quantitative real-time RT-PCR. Additional characterization of *rtTA-SmoA1* medulloblastomas will be described in Chapter 4.

During the course of our studies, we observed ectopic foci of cells within the outer regions of the ML of *tTA-SmoA1* mice, just deep to tumor burden. The ML is normally sparsely populated with the nuclei of basket and stellate cells (Voogd *et al.*, 1998), and should never harbor clusters of nuclei. These rests of cells were non-

proliferative, and they were both morphologically and biochemically similar to normal cerebellar neurons. Due to their location and biochemical properties, we hypothesized that these cells arise from within the tumor mass. By long-term labeling with BrdU, we were able to confirm that post-mitotic cells within these rests arise from proliferating cells in the tumor mass. This indicates that a subset of cells within tumors retain the ability to become non-responsive to the Hh signal, become post-mitotic, express neural differentiation markers, and migrate into the ML, behavior which partially recapitulates that of normal CNGPs, arguing that these cells serve as the cell of origin for the medulloblastomas described herein. However, we cannot formally exclude the possibility that the cells in question are normal CGNPs which have been trapped within tumors and continue to proliferate. NeuN-positive clusters of cells in the ML have been reported in other murine medulloblastoma models (Uziel *et al.*, 2005, Hatton *et al.*, 2008), and ectopic rests of cells have been seen within the ML deep to human medulloblastomas (Franks, 1988, Kleihues *et al.*, 1997), although it is unclear how closely these cells resemble those observed in our model.

To more definitively address the question of medulloblastoma cell of origin, we took advantage of the doxycycline-regulated nature of our model to perform timed tumor induction studies. When transgene expression was unimpeded, all *tTA-SmoA1* and *rtTA-SmoA1* mice developed medulloblastomas. Examination of P2 *tTA-lacZ* and P7 and P14 *tTA-SmoA1* mice revealed activation of lacZ in individual cells in the EGL of P2 mice, followed by small clusters of SmoA1-expressing cells at P7, and presence of tumors contiguous with EGL at P14. Regions of P14 EGL not expressing SmoA1 were histologically indistinguishable from control EGL. Activation of SmoA1 expression as

late as P7, when the external granular layer is still actively proliferating, resulted in formation of tumors in *rtTA-SmoA1* animals. However, activation of transgene at weaning, by which point the EGL had completely disappeared, failed to lead to tumor development in either *tTA-SmoA1* or *rtTA-SmoA1* animals. These data, together with the presence of the ML-bound neuronal rests and lineage marker studies described above, strongly argue that the transient, Shh-dependent CNGPs of the EGL serve as a cell of origin for medulloblastomas. However, it should be noted that this study does not rule out additional pools of medulloblastoma precursors in human disease, particularly for non-HH driven tumors.

Prenatal activation of transgene in *rtTA-SmoA1* animals resulted not only in development of medulloblastoma, but also in distortion of normal cerebellar architecture (See Fig. 2-8 D). A possible explanation for the altered cerebellar morphology seen in these mice comes from a recent study indicating that high level Hh signaling in neural stem cells leads to G2/M cell cycle arrest and apoptosis, as opposed to an increase in proliferation of committed CGNPs (Galvin *et al.*, 2008). Because the entirety of the cerebellar anlage has undergone Cre-mediated recombination at birth (Zhuo *et al.*, 2001), is it likely that the GFAP promoter is active in the early progenitor cells of the rhombic lip, which give rise to the CGNPs of the EGL. In the *rtTA-SmoA1* model, this may lead to high level Hh pathway activation and an increased risk for apoptosis or G2/M arrest in all precursor cells for the EGL, resulting in the smaller EGL and distorted cerebella seen in these mice. However, initiation of doxycycline treatment at P4 or P7 led both to tumor development and to a normalization of cerebellar architecture (See Fig. 2-8 E). Postnatal activation of transgene expression presumably allows for normal initiation of cerebellar

development analogous to that seen in *tTA-SmoA1* mice in which relatively few cells in the early EGL activate transgene expression (see Figure 2-7).

We next examined the consequences of activating the Hh pathway in the forebrain, both proximally with SmoA1, and distally at the level of the Gli2 transcription factor. To do this, we made use of the *TRE-Gli2* and *TRE-GLI2** mouse lines previously developed in our lab. When Gli2 expression is driven by the keratin 5 promoter in the basal layer of the epithelium, the resulting *K5-tTA*;*TRE-Gli2* mice develop basal cell carcinomas with 100% penetrance by 6 months after birth (Hutchin *et al.*, 2005), and *MMTV-tTA;TRE-GLI2** mice develop tumors in multiple sites (manuscript in preparation). When we crossed *GFAP-tTA* mice with *TRE-Gli2* mice, we were somewhat surprised to discover that the resulting bitransgenic offspring failed to develop any tumors. This suggests that the wild-type *Gli2* transgene, which contains both the transcriptional activator and repressor domains (Roessler *et al.*, 2005), may not activate the Hh pathway strongly enough during the critical window of medulloblastoma susceptibility, as discussed above. The observation that full length Gli2 displays weaker oncogenic activity than Gli1 supports this idea (Sheng *et al.*, 2002). The necessity and sufficiency of Gli protein expression for medulloblastoma development is still an open question. Conflicting reports indicate that *Gli1* either is (Kimura *et al.*, 2005) or is not important for development of medulloblastomas driven by Hh activation (Weiner *et al.*, 2002).

However, when we crossed *GFAP-tTA* mice with *TRE-GLI2** mice, the resulting double transgenic *tTA-GLI2** pups did not survive past birth and harbored large, undifferentiated forebrain tumors. By activating *GLI2** after weaning, we were able to

bypass the perinatal lethality and observe the effects of unimpeded distal activation of the Hh pathway in mature, fully developed brains. These animals developed large numbers of small, well-circumscribed, proliferative, undifferentiated tumors. The tumors arose in widely scattered regions throughout both the forebrain and the hindbrain. This suggests that, rather than originating from the GFAP-positive adult stem cells within the subventricular or subgranular zones, these lesions instead appeared to arise from mature, GFAP-positive glia scattered throughout the CNS. Although it is possible that GLI2* expression in glia induced a tumorigenic response in neighboring cells, this scenario seems unlikely, both because GLI2* induces a cell-autonomous activation of the Hh pathway, and because GLI2* expression appeared to be largely confined to tumor lesions in mature mice. A clue as to why tumors do not appear to arise from adult neural stem cells may come from the recent finding that forced expression of Gli1 causes apoptosis and cell cycle arrest of neural stem cells (Galvin *et al.*, 2008), although we did not observe grossly apparent alterations in apoptosis in the SVZ of *tTA-GLI2** mice in a pilot experiment (data not shown). These findings suggest that high-level Hh pathway activity is sufficient to return mature glial cells to an undifferentiated, proliferative state, but only when the pathway is activated directly at the level of the Gli transcription factors. Furthermore, despite the link between increasing levels of HH signaling and decreasing glioma prognosis (Becher *et al.*, 2008), these results suggest that neither proximal nor distal Hh pathway activation is sufficient to induce gliomas in mice. However, we cannot exclude the possibility that the level of Hh pathway activation may have been too high in transgenic mice, resulting in cell death or cell cycle arrest, as previously observed (Galvin *et al.*, 2008), rather than glioma formation. Moreover, although deregulated Hh

signaling may not be sufficient to drive glioma development, it may synergize with other pathways known to be active in forebrain tumorigenesis. Platelet-derived growth factor receptor, for example, is a target of Hh signaling both in skin, where it contributes to BCC proliferation (Xie *et al.*, 2001), and in brain (Nery *et al.*, 2001), where excessive activation of the PDGF/PDGFR pathway can induce glioma-like growths from the SVZ (Jackson *et al.*, 2006).

Chapter 3

Hedgehog Signaling is Required for Tumor Maintenance in Medulloblastoma

Introduction

As discussed in Chapter 2, activation of exogenous Hh signaling in the developing cerebellum of *tTA-SmoA1* and *rtTA-SmoA1* mice induces the development of medulloblastomas with complete penetrance and short latency. As I will describe in this chapter, I used these models to investigate whether Hh-driven medulloblastomas remain dependent on continued Hh signaling for maintenance. This is a particularly important question in terms of treatment of the human disease. Current treatment for medulloblastoma is limited to the standard anticancer therapies of surgical resection, multiagent chemotherapy, and craniospinal axis radiation therapy. These modalities are reasonably successful, and 5-year progression-free survival rates have risen to between 43% and 94%, depending on tumor subtype and specific therapeutic regimen (Gilbertson, 2004). However, these treatments are not without significant adverse sequelae such as ataxia, mutism, and cognitive, neuroendocrine and neuropsychological defects (Chintagumpala *et al.*, 2001, Mulhern *et al.*, 2004, Robertson *et al.*, 2006). It is clear that tumor-specific, mechanism-based medulloblastoma therapies are needed, both to increase treatment efficacy and to avoid potentially devastating sequelae. This is particularly critical in patients with Gorlin syndrome, who cannot tolerate significant radiation dose without developing extraordinary basal cell carcinoma burden (Kimonis *et al.*, 1997), and

thus would benefit greatly from rational tumor-specific therapies that reduce the required radiation dose for effective treatment.

Previously published studies in mice suggest that some medulloblastomas remain dependent on Hh signaling. Initial reports indicated that growth of cultured *Ptch*$^{+/-}$*/p53*$^{-/-}$ medulloblastoma cell lines and subcutaneous allografts can be inhibited by cyclopamine, a Hh inhibitor which acts at the level of *Smo* (Berman *et al.*, 2002). However, cyclopamine treatment did not lead to complete elimination of tumors, and additional studies revealed that cultured medulloblastoma cells downregulate the Hh pathway, calling into question the usefulness of such studies in understanding tumor biology (Romer *et al.*, 2004, Sasai *et al.*, 2006). Subsequent studies demonstrated that pharmacological blockade of the Hh pathway in *Ptch*$^{+/-}$*/p53*$^{-/-}$ medulloblastomas lead to inhibition of tumor growth (Romer *et al.*, 2004, Sanchez *et al.*, 2005b). Similar results were seen in medulloblastoma allografts from *Cxcr6*$^{-/-}$ mice, tumors which also demonstrate elevated Hh pathway activity (Sasai *et al.*, 2007). However, none of the previous studies demonstrate complete, durable elimination of medulloblastomas following pharmacological blockade of Hh signaling.

These observations suggest a potential role for HH inhibition in the treatment of human medulloblastoma. Given the significant proportion of human medulloblastomas that display activation of HH signaling (Wetmore, 2003, Hallahan, 2004 #13, Leung *et al.*, 2004, Marino, 2005), inhibition of this powerful mitogenic pathway may represent an important therapeutic adjunct for many patients. Translational investigation of HH inhibition for antitumor therapy is already underway, as a small molecule inhibitor

developed by Curis and Genentech is currently in Phase II clinical trials for HH-driven metastatic colon cancer (ClinicalTrials.gov reference # NCT00636610).

An important question remains when considering anti-HH therapy for use in medulloblastoma patients. If HH pathway inhibitors induce regression of tumor burden, would such therapy confer a permanent benefit to patients, or would tumors return following discontinuation of therapy? Work previously published by our lab provides important insight into the analogous question in a murine model of basal cell carcinoma. In *K5-tTA;TRE-Gli2* mice, skin-targeted activation of distal Hh signaling leads to the development of basal cell carcinomas that develop within six months after birth (Hutchin *et al.*, 2005). Inhibition of *Gli2* expression by doxycycline treatment causes rapid regression of tumors, correlated with a decrease in proliferation and an increase in apoptosis. However, following tumor regression, small populations of non-proliferative cells remain. When doxycycline treatment is discontinued, a subset of the regressed, quiescent tumors re-grow, indicating that a pool of dormant tumor-initiating cells remains following inhibition of exogenous Hh pathway activation (Hutchin *et al.*, 2005), and suggesting the potential existence of similar cells following regression of other Hh-mediated tumors.

I investigated whether SmoA1-induced medulloblastomas exhibit a continued dependence on exogenous Hh signal and, if so, whether dormant tumor cells remain after transgene inhibition. To achieve this, I took advantage of the conditional nature of the *TRE-SmoA1* mouse. I treated medulloblastoma-bearing *tTA-SmoA1* mice with doxycycline, and observed focal abrogation of *SmoA1* expression, perhaps due to difficulties achieving sufficiently high drug levels in the CNS. Regardless, in areas

where SmoA1 transgene expression was extinguished, I observed corresponding focal inhibition of Hh signaling and regression of tumor burden, indicating that these tumors remain dependent on continued activation of the Hh pathway. To globally inhibit transgene expression, I removed tumor-bearing *rtTA-SmoA1* ("Tet-on") mice from doxycycline treatment. Complete loss of transgene expression in these mice resulted in total disappearance of tumors within three weeks. Tumor regression was coupled to loss of Hh pathway activation, impaired proliferation, and increased apoptosis. While residual tissue remained on the surface of the cerebella of regressed mice, these regions did not harbor dormant tumor-inducing cells, as tumors never recurred, either with or without resumption of doxycycline treatment to reactivate transgene expression. These data suggest that relatively brief treatment of patients with HH-driven medulloblastomas may be sufficient for potentially curative therapy.

Materials and Methods

Mice were obtained, housed and genotyped as described on pp. 38 - 41. SmoA1 expression was induced by maintaining breeding pairs, nursing dams and weaned animals on doxycycline-containing chow, as previously described on p. 41. SmoA1 expression was inhibited by replacing available chow with doxycycline-free chow. Tissue fixation and processing and immunohistochemistry were performed as previously described. Phospho-histone H3 and TUNEL positive cells per high power field were quantified by counting ten high power fields' worth of cells per animal for each of three animals. Comparisons were performed between the average count per field for each animal. Quantitative real time RT-PCR was performed as described on pp. 44 - 45. Magnetic

resonance imaging was performed by the University of Michigan Center for Molecular Imaging.

Results

Focal Hh pathway inhibition results in focal medulloblastoma regression

In order to examine whether continued Hh pathway activation was necessary for the maintenance of medulloblastoma, I placed tumor-bearing *tTA-SmoA1* animals on doxycycline to repress expression of SmoA1. I began doxycycline treatment between three and six weeks of age (Fig. 3-1 A). Doxycycline-treated animals were monitored by magnetic resonance imaging (MRI) for one month following inception of treatment. The greatly enlarged tumor-bearing cerebellum is readily appreciable in T2-weighted images at the beginning of the course of doxycycline treatment (Fig. 3-1 B, C). Following one month of therapy, the overall size of the cerebellar region had not decreased, but the cerebellum had changed dramatically in appearance on T2-weighted MRI. Instead of the relatively uniform appearance of an untreated animal, very bright regions appeared along the outer edges of the cerebellum and in the region of the cerebellar aqueduct, indicative of the presence of greater a amount of cerebrospinal fluid in these regions (Figure 3-1 D). This pattern suggests a focal loss of tumor mass, leaving behind space which is filled by CSF.

Histological examination of treated *tTA-SmoA1* animals confirmed the presence of focal tumor regression. In 10/10 animals treated with doxycycline, the cerebella contained both normal-appearing tumor and focal regions of loose collections of cells with light pink cytoplasm and a low nuclear-cytoplasmic ratio (Fig. 3-1 E). *In situ* hybridization revealed persistent expression of *SmoA1* (Fig 3-1 F) and activation of the

Hh pathway in regions of unregressed tumor tissue (Fig. 3-1 G), whereas loss of *SmoA1* expression (Fig. 3-1 F) and inhibition of the Hh pathway were evident in regressed areas (Fig. 3-1 G). Regressed areas contained few proliferating cells, in comparison to the highly proliferative unregressed tumor (Fig. 3-1 H). Regressed regions were also strongly positive for expression of GFAP, indicative of the presence of astroglial cells in these areas (Fig. 3-1 I), indicating either infiltration of glia from outside the tumor in a glial scarring phenomenon or differentiation of tumor cells down a glial lineage. Additionally, although regressed areas were largely negative for NeuN-positive cells, clusters of cells adjacent to the internal borders of regressed regions strongly expressed this mature neuronal marker. Strikingly, expression of the stem and progenitor cell marker Nestin, which was appreciable in cells scattered throughout unregressed regions of tumor, was completely absent from regressed regions (Fig. 3-1 J), suggesting that a loss of progenitor cell-like character contributes to tumor regression.

Figure 3-1. Doxycycline treatment of *tTA-SmoA1* mice induces focal tumor regression. (A) Timeline showing doxycycline treatment and resultant tumor regression. (B – D) Coronal T2-weighted magnetic resonance imaging showing cerebella of control (B) or tumor-bearing *tTA-SmoA1* mice before treatment (C) and after one month of doxycycline treatment (D). Dotted yellow lines in B – D demarcate the cerebellum. (E) hematoxylin and eosin staining of cerebellum of mouse treated with doxycycline for 3 weeks. Arrows in E – J indicate unregressed tumor, also shown at higher magnification in left inset; arrowheads indicate regressed regions of tumor, also shown at higher magnification in right inset. (F, G) *In situ* hybridization for *SmoA1* (F) and *Ptch1* (G) showing loss of transgene expression and Hh pathway activity in regressed regions of tumors. (H – J) Immunohistochemical staining for Ki67 (H), GFAP (I) and nestin (J), demonstrating relative lack of proliferation, robust GFAP staining, and loss of nestin expression in regressed medulloblastoma regions relative to unregressed tumor.

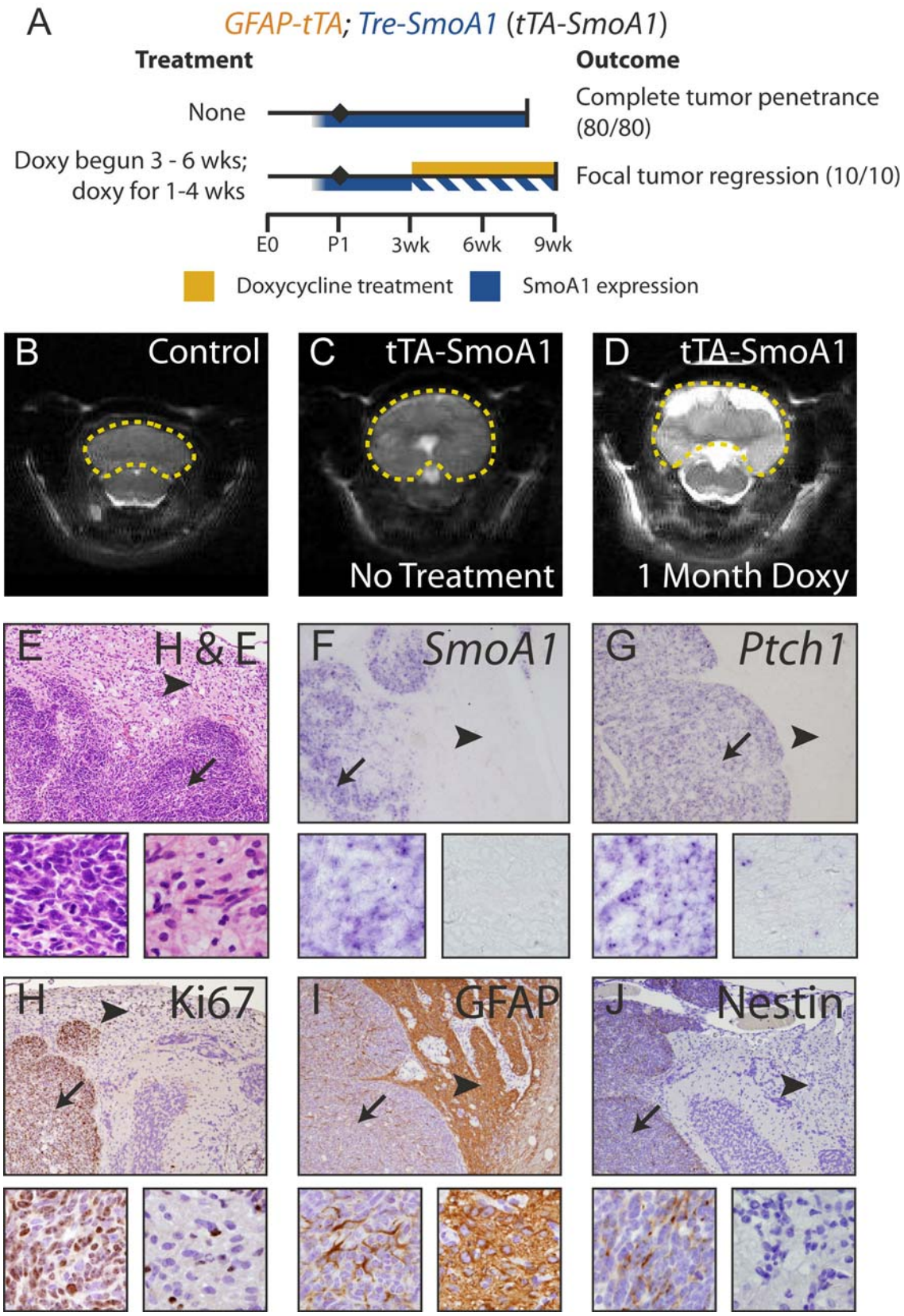
A
GFAP-tTA; Tre-SmoA1 (tTA-SmoA1)
Treatment
Outcome
None
Complete tumor penetrance (80/80)
Doxy begun 3 - 6 wks; doxy for 1-4 wks
Focal tumor regression (10/10)
E0
P1
3wk
6wk
9wk
Doxycycline treatment
SmoA1 expression
B Control
C tTA-SmoA1
No Treatment
D tTA-SmoA1
1 Month Doxy
E H & E
F SmoA1
G Ptch1
H Ki67
I GFAP
J Nestin

Total transgene inhibition results in complete and durable tumor regression

To investigate whether transgene repression leads to total abolition of tumor, I employed the triple transgenic *rtTA-SmoA1* mouse model described on p. 41. One advantage to this model is that expression of transgene requires continuous supplementation with doxycycline-containing chow. Therefore, discontinuation of doxycycline treatment should lead to complete abrogation of SmoA1 expression, in contrast to the focal inhibition seen in double transgenic *tTA-SmoA1* mice (which may be due to inadequate local levels of doxycycline).

I maintained breeding pairs on doxycycline throughout gestation to generate tumors in *rtTA-SmoA1* mice. At P21, I either sacrificed animals for histological examination or weaned them to regular chow for tumor regression studies (Fig. 3-2 A, 3-2 B left). All mice examined at P21 harbored significant tumor burden, and all mice examined after discontinuation of doxycycline chow harbored either regressing tumor or regressed regions indicative of previously existent tumor, as discussed below. One week after weaning mice to doxycycline-free chow, significant changes had already begun to occur in the tumors, although there was significant viability in tumor regression within individual brains at this stage (N=4). While regions of tumor were still appreciable, the tumors appeared less dense, with a lower nuclear to cytoplasmic ratio (Fig. 3-2 B middle). In other regions, tumors had already fully regressed, leaving behind residual cells as described below.

Three weeks after removal from doxycycline, medulloblastomas had completely regressed, and no tumor mass remained in any of the animals examined at this time point (N=6). Instead, residual clusters of leftover cells were appreciable on the outer surface of

the ML, a region normally devoid of cells other than the leptomeninges. These clusters of cells persisted in animals maintained on regular chow for 6 weeks (N=6), 16 weeks (N=1), 27 weeks (N=1) or 34 weeks (N=2) (Fig. 3-2 B right). In order to verify complete elimination of tumor burden in sacrificed animals, we examined the entire rostral-caudal length of the cerebella of selected regressed animals by cutting serial coronal sections. Animals were examined by serial coronal sectioning after 3 weeks (N=3), 6 weeks (N=5), 16 weeks (N=1) and 27 weeks of transgene inhibition (N=1). No regrowth of tumor was evident in any mice, indicating a complete and durable loss of tumor burden. At the time of this writing, 2 additional *rtTA-SmoA1* mice, treated with doxycycline until weaning, have been maintained on doxycycline-free chow for approximately 52 weeks, and show no signs of re-developed tumors.

To confirm loss of transgene expression in mice removed from doxycycline, we examined expression of SmoA1 by immunohistochemical staining for the HA epitope tag. Significant transgene expression was readily appreciated in nearly every cell within unregressed tumors. However, mice rapidly lost expression of transgene following removal from doxycycline. Very faint staining for SmoA1 could be appreciated in residual tumors one week after discontinuation of doxycycline treatment, and no SmoA1 was detectable in residual cells three weeks or longer after regression (Fig. 3-2 C).

Following loss of transgene expression, tumors rapidly changed their proliferative and apoptotic status. While the majority of tumor cells were positive for the proliferation marker Ki67, a partial loss of Ki67 positivity was evident following one week of regression, and the residual cells left following complete tumor regression were entirely non-proliferative (Fig. 3-2 D). A significant decrease in proliferation, as measured by

density of phospho-histone H3 positive cells within the lesions, was evident within one week of discontinuation of doxycycline treatment (Fig. 3-2 F left). Although baseline apoptosis was appreciable in tumors from animals maintained on doxycycline, the apoptotic index significantly increased during regression (Fig. 3-2 E, F right). Residual cells remaining following regression were no longer apoptotic.

Regression was also coupled with loss of Hh pathway activity, target gene expression, and medulloblastoma marker expression. qPCR indicated a loss of *Gli1* and *Ptch1* expression in regressing tumors, indicating inhibition of Hh signaling, that reached significance within one week of regression (Fig. 3-3 A, B). *Ptch2* expression also quickly dropped following discontinuation, and expression in tumors was significantly different from that in control cerebellum (Fig. 3-3 C). While expression of *CyclinD1*, a critical gene for Hh-mediated tumorigenesis (Pogoriler *et al.*, 2006), was increased approximately 4-fold over regressing tumors and control cerebellum, P-values did not reach significance, due to relatively high variance among tumor samples (Fig. 3-3 D). Expression of *N-Myc*, another key Hh target in medulloblastoma development (Hatton *et al.*, 2006), quickly dropped off with tumor regression, reaching significance by three weeks after doxycycline removal (Fig. 3-3 E). Lastly, *Math1*, a marker for EGL cells and medulloblastomas, was overexpressed nearly 300-fold in medulloblastomas compared to wild-type cerebellum, and was significantly reduced within three weeks of regression (Fig. 3-3 F).

Figure 3-2. Complete medulloblastoma disappearance following SmoA1 inhibition is associated with decreased proliferation and increased apoptosis. (A) Timeline of tumor regression studies. (B – E) Hematoxylin and eosin staining and immunohistochemical analysis of *rtTA-SmoA1* mice showing unregressed tumors (continuous doxycycline treatment), regressing tumors (one week following discontinuation of doxycycline) or residual clusters following complete regression of tumors (4 months following discontinuation of doxycycline). Little transgene expression is seen after one week off doxycycline, and none is seen in long-term regression (C). Ki67 expression drops off shortly after discontinuation of doxycycline, and residual cells are entirely quiescent (D). Cleaved caspase 3-positive cells are evident in tumors, but are more numerous in regressing tissue. Fully regressed regions are no longer apoptotic (E). (F) Quantification of decreased proliferating phospho-histone H3-positive cells (P=0.041) and increased apoptotic TUNEL-positive cells (P=0.0029) in unregressed tumors vs. tumors from mice removed from doxycycline treatment for one week. Error bars represent standard error of the mean, and * indicates a significant difference from unregressed tumors. N=3 animals for each group.

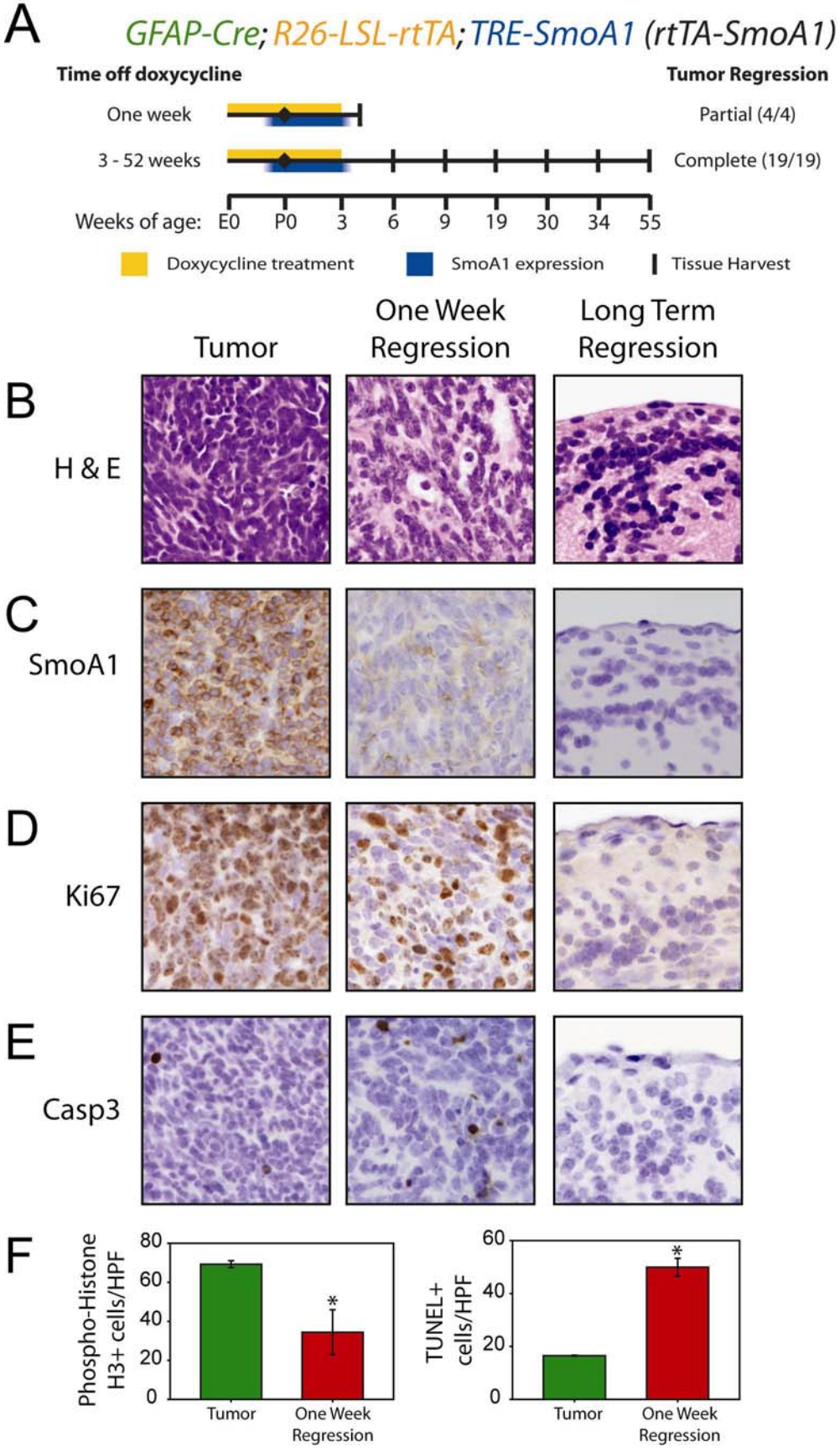
A
GFAP-Cre; R26-LSL-rtTA; TRE-SmoA1 (rtTA-SmoA1)
Time off doxycycline
Tumor Regression
One week
Partial (4/4)
3 - 52 weeks
Complete (19/19)
Weeks of age: E0 P0 3 6 9 19 30 34 55
Doxycycline treatment
SmoA1 expression
Tissue Harvest
Tumor
One Week Regression
Long Term Regression
B
H & E
C
SmoA1
D
Ki67
E
Casp3
F
Phospho-Histone H3+ cells/HPF
80
60
40
20
0
Tumor
One Week Regression
TUNEL+ cells/HPF
60
40
20
0
Tumor
One Week Regression

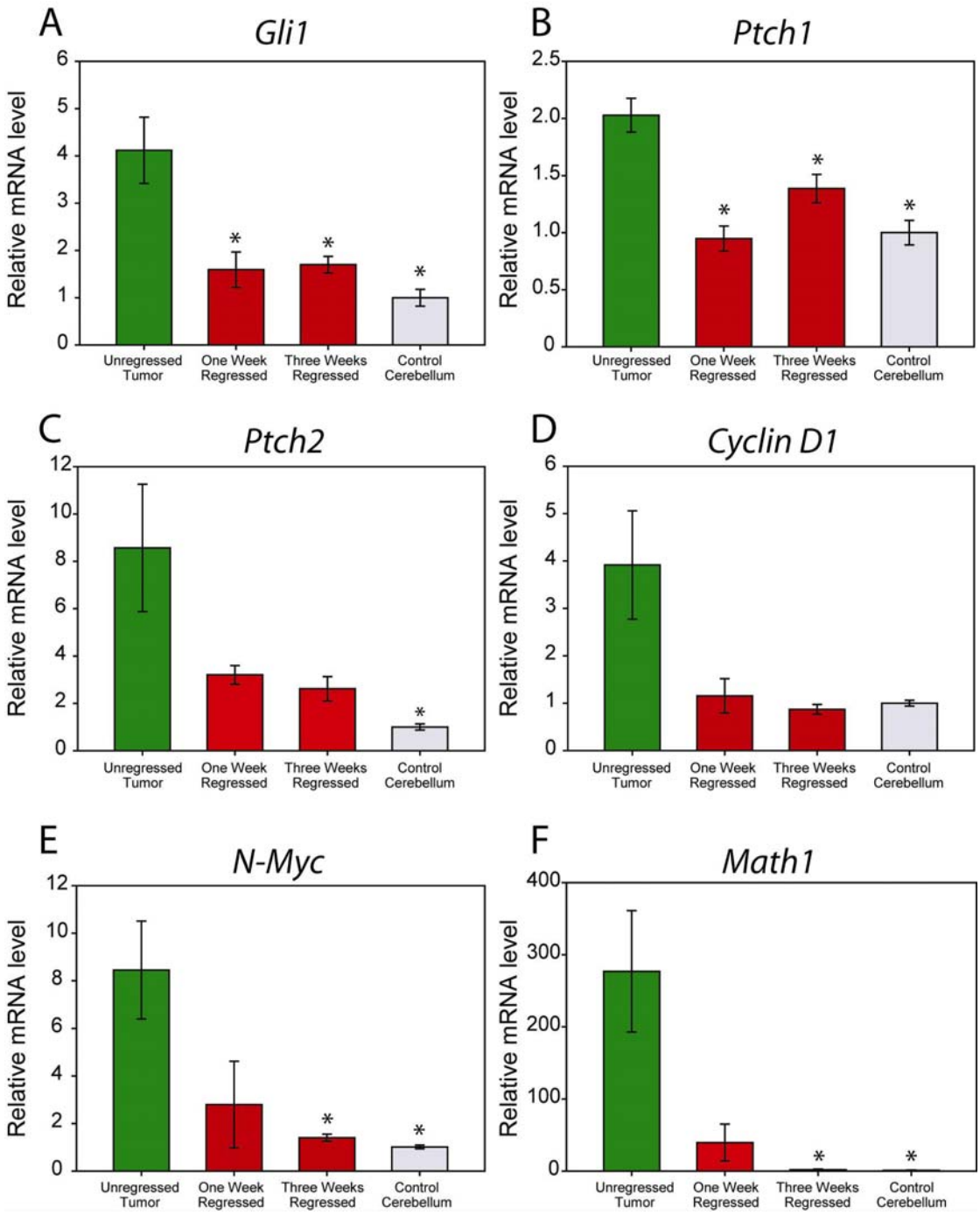

Figure 3-3. Tumor regression is coupled to loss of Hh pathway activation and target gene expression. (A – F) qPCR on RNA isolated from tumors, control cerebella, and cerebella from tumor-bearing mice removed from doxycycline for one or three weeks. N=3 for each group. Expression of *Gli1* (A), *Ptch1* (B), and *Ptch2* (C) was decreased in control cerebella or regressing lesions compared to tumors. Expression of *CyclinD1* was also decreased, but the difference did not reach significance (D). Expression of *N-Myc* (E) and *Math1* (F) was significantly inhibited by three weeks of regression. * indicates significant difference from unregressed tumor ($P<0.05$).

Tumor regression is associated with loss of nestin-positive progenitor-like cells and terminal differentiation of residual population

In order to further characterize the nature of tumor regression and the non-proliferative residual cells that remain, I examined both progenitor cell and differentiation markers. In unregressed tumor, a subset of the cells expressed the stem and progenitor cell marker nestin, suggesting a subpopulation of progenitor-like cells within the tumors. Nestin positivity quickly disappeared from the tumors after discontinuing doxycycline treatment, and no nestin was detectable in the residual cells following tumor disappearance (Fig. 3-4 A). Both expression of nestin in active tumor and focal loss of nestin positivity in regressed regions were also seen in tumors from *tTA-SmoA1* mice, as described above (Fig. 3-1 J).

Scattered cells within active *rtTA-SmoA1* medulloblastomas stained relatively weakly for the neuronal marker NeuN. This pattern remained largely unchanged early on in the regression process, although some regions of more densely NeuN-positive cells could be appreciated within the disappearing tumor mass. Immunostaining revealed that the clusters of strongly NeuN-positive residual nuclei persisted in the outer region of the molecular layer following regression (Fig. 3-4 B), indicating that these quiescent cells had differentiated along a neural lineage.

As seen in the foci of regression in *tTA-SmoA1* medulloblastomas, residual regions following tumor disappearance in *rtTA-SmoA1* mice stained very strongly for GFAP (Fig. 3-4 C). Although sparse GFAP expression was detected scattered through active tumor, likely indicating the astrocytic stroma of the tumor, a peripheral increase in GFAP intensity was appreciated one week after doxycycline removal. This GFAP

positivity increased, leaving behind a persistent population of astroglial cells in regions of tumor regression. Whether these cells represent a glial scar generated by glia from outside the tumor or indicate differentiation of tumor cells along a glial lineage is unclear. In keeping with the latter hypothesis, CGNPs of the EGL can be induced to differentiate into mature astroglial cells (Okano-Uchida *et al.*, 2004), suggesting that tumor cells derived from the EGL may have the same ability.

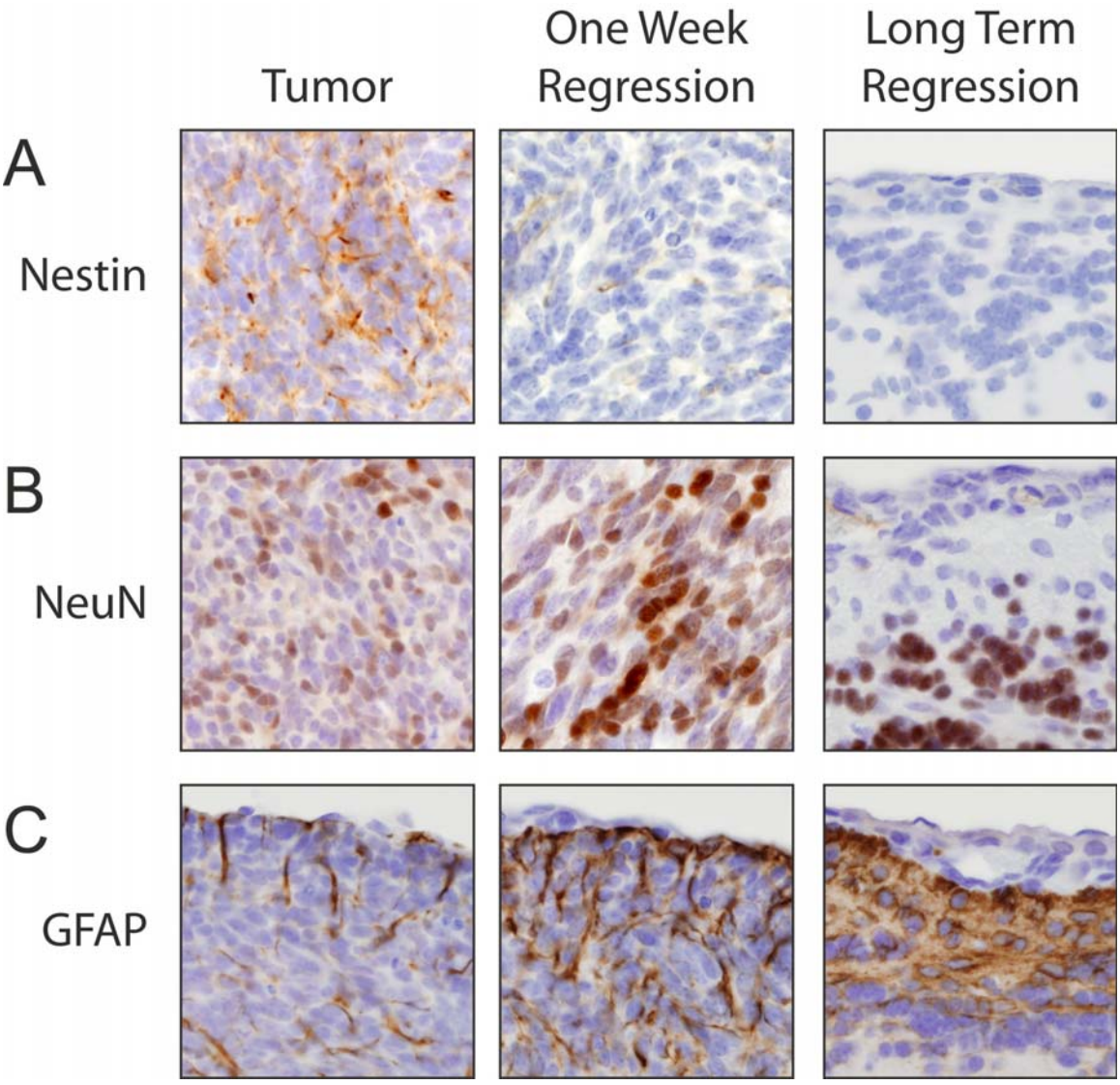

Figure 3-4. Loss of nestin positive cells and increased differentiation marker expression in regressing tumors. (A – C) Immunohistochemical stains of unregressed, one week regressed and 4 month regressed tumors. (A) Nestin expression was appreciable in tumors, but was rapidly lost following discontinuation of doxycycline. (B) Increased density of NeuN positive neurons could be seen early during regression. Clusters of cells staining strongly for NeuN remained permanently in the molecular layer in areas of tumor regression. (C) Increased peripheral GFAP positivity began within one week of regression and persisted indefinitely.

Regressed tumors do not recur after resuming doxycycline treatment

To determine if dormant residual tumor cells persisted following tumor regression, I returned regressed mice to doxycycline treatment. First, I weaned tumor-bearing animals to doxycycline-free chow at P21 to induce tumor regression, as described above. Following either three or four weeks of regression, animals were returned to doxycycline-containing chow until sacrifice. Mice were sacrificed and examined after 3 weeks (N=1), 6 weeks (N=3), 8 weeks (N=2) or 28 weeks (N=1) of transgene reactivation. No regrowth of medulloblastomas was evident either grossly or histologically (Fig. 3-5 A). Long-term transgene reactivation induced variable levels of alopecia and skin lesions resembling basaloid follicular hamartomas, as with postnatal transgene activation since the GFAP promoter is active in skin (not shown). The development of this epithelial phenotype indicates that SmoA1 expression was reactivated to a sufficient level to give rise to benign tumors in another organ. At the time this thesis was written, three additional mice were being maintained for long-term transgene reactivation studies; transgene had been reactivated for 9 months in one mouse 10.5 months in two others. None of these mice displayed behavioral evidence of tumor recurrence, although they had developed variable levels of alopecia or skin lesions.

Reactivation of SmoA1 expression in scattered cells within the EGL and ectopic regions was confirmed by immunohistochemistry (Fig. 3-5 B). However, relatively few SmoA1-positive cells were evident in the cerebella of examined mice. Cells within the residual regions of reactivated mice were neither proliferative nor apoptotic (Fig. 3-5 D, E). Nestin expression did not return following resumption of doxycycline treatment (Fig.

3-5 F), and expression of NeuN and GFAP in residual regions was unchanged as well (Fig. 3-5 G, H). Timeline of regression/reactivation studies is shown (Fig. 3-5 I).

When compared with unregressed tumors, relatively few cells within the cerebellum expressed SmoA1 following resumption of doxycycline treatment. One possible explanation for this phenomenon is that transgene reactivation may induce high enough levels of Hh pathway activity to drive apoptosis in SmoA1 re-expressing cells. To test this hypothesis, I performed a short-term reactivation experiment. Mice were maintained on doxycycline until weaning to regular chow for three weeks as above. Mice were sacrificed for histological analysis one, three, five and seven days after resumption of doxycycline treatment. Transgene expression and apoptosis were assayed in serial sections. While scattered SmoA1-positive cells were seen in cerebella 3, 5, and 7 days after resumption of doxycycline treatment (Fig. 3-6 A and not shown), no apoptotic cells were detected (Fig. 3-6 B). This suggests that apoptotic deletion of SmoA1-expressing cells following reactivation does not account for the relative scarcity of SmoA1-positive cells in reactivated cerebellum.

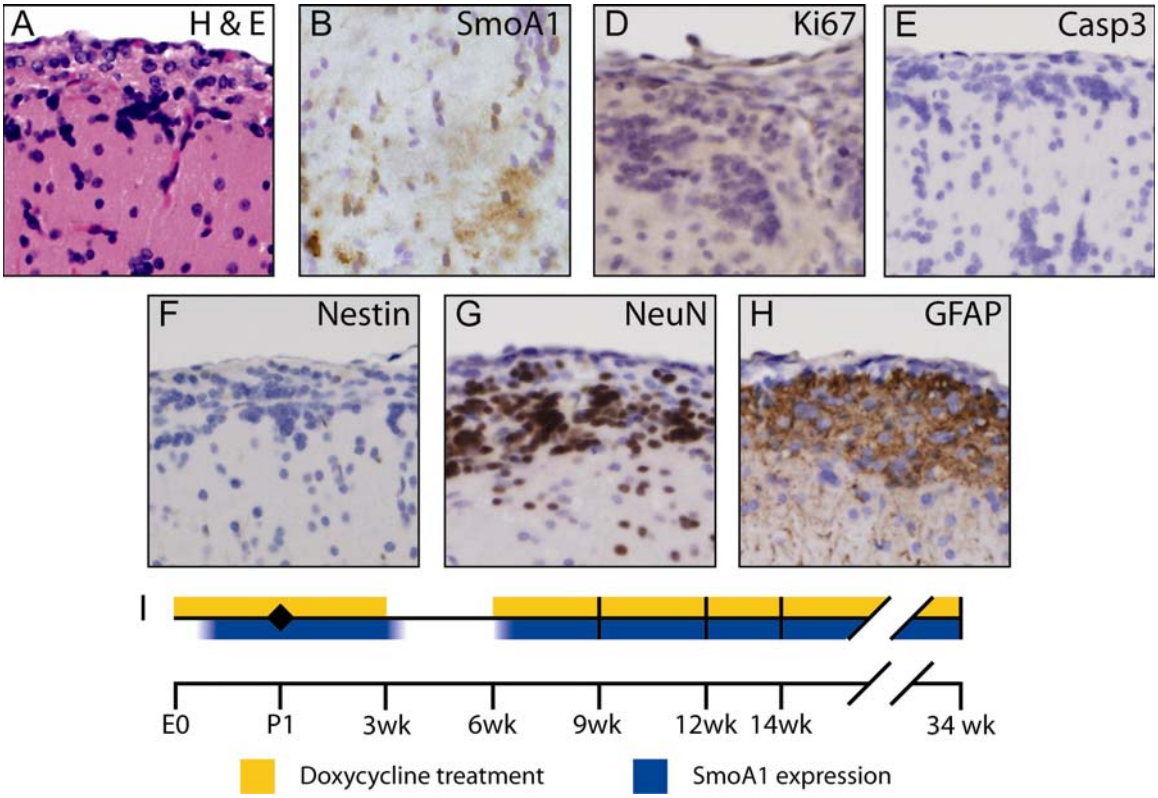

Figure 3-5. Reactivation of transgene expression does not lead to regrowth of medulloblastomas. Hematoxylin and eosin staining (A) and immunohistochemistry (B – H) examining residual regions 6 weeks after resumption of doxycycline treatment. (B) Transgene expression was detected in cells scattered throughout the IGL and residual tissue. Residual cells did not express Ki67 (D), cleaved caspase 3 (E) or nestin (F). Strong staining for NeuN (G) and GFAP (H) were detected in residual regions. (I) Timeline for regression/reactivation studies.

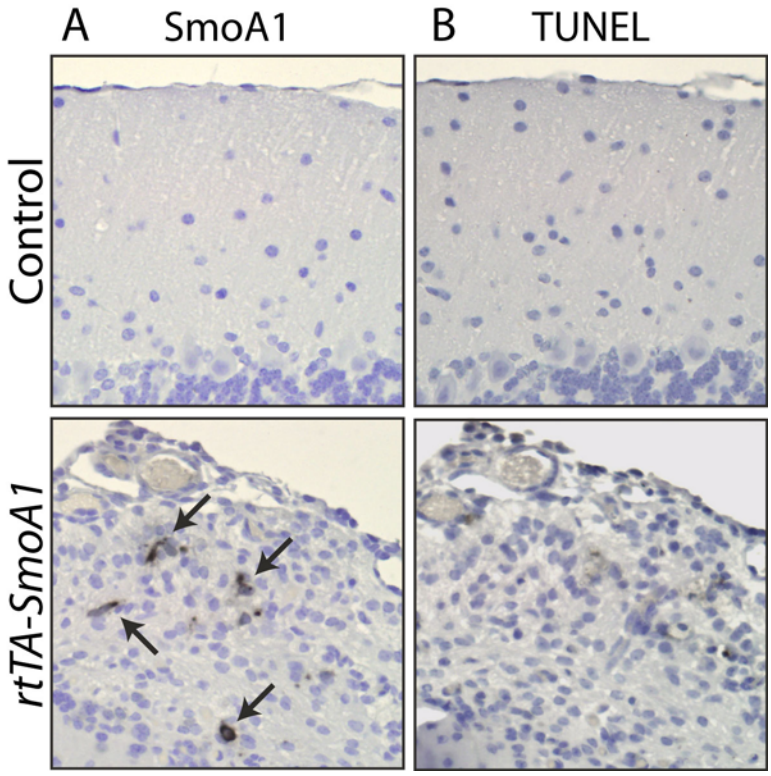

Figure 3-6. Brief reactivation of SmoA1 does not induce apoptosis. Expression of SmoA1 can be seen in a few scattered cells with residual regressed tissue following 7 days of transgene reactivation (arrows in A). No TUNEL positive, apoptotic cells are detected in either control or transgenic cerebella (B). Because DAB + Co enhancer was used as the chromogenic substrate on these sections, positive staining is indicated by development of black color.

Discussion

Previously published studies have suggested that pharmacologic inhibition of the Hh pathway inhibits the growth of medulloblastomas from both the *Ptch*$^{+/-}$*/p53*$^{-/-}$ model and a recently described *Cxcr6* mutant model (Romer *et al.*, 2004, Sanchez *et al.*, 2005b, Sasai *et al.*, 2007). Phase II clinical trials of a small molecule HH pathway inhibitor for treatment of solid epithelial cancers are currently in progress (ClinicalTrials.gov reference # NCT00636610), underscoring the importance of understanding the biological responses of Hh-mediated tumors to pathway inhibition. A previous study from our lab demonstrated that Gli2-induced BCCs remain dependent on continued transgene expression for survival and proliferation (Hutchin *et al.*, 2005), demonstrating "addiction" to the Hh pathway. However, regressed tumors in these mice harbored dormant, quiescent cells capable of regrowth following transgene reactivation, raising the possibility that such cells may also exist in medulloblastomas.

With the work described in this chapter, I demonstrated that, as with Gli2-induced BCCs, the medulloblastomas arising in our *tTA-SmoA1* and *rtTA-SmoA1* mouse models are addicted to exogenous Hh signaling, remaining completely dependent on continued SmoA1 expression for survival. I began by examining the consequences of SmoA1 inhibition in *tTA-SmoA1* mice. In order to achieve this, I exploited the conditional nature of the model, treating tumor-bearing *tTA-SmoA1* mice with doxycycline to suppress transgene expression. Histological examination revealed focal regression of tumors in these animals; both regions of diffuse, pale pink collections of cells indicative of tumor regression and regions of persistent tumor were appreciated in 10/10 animals. All tumor and regressed tissue was located outside the external surface of the molecular layer,

which represents the outer edge of physiologic cerebella. Regions interpreted as regressed tissue bore notable histological resemblance to regressed *Ptch*$^{+/-}$*/p53*$^{-/-}$ tumors following short-term, high-dose treatment with HhAntag, a small molecule Hh inhibitor (Romer *et al.*, 2004). *In situ* hybridization revealed loss of *SmoA1*, *Gli1*, and *Ptch1* from regressed regions, but with persistent transgene expression and Hh pathway activation in non-regressing regions of tumor. This observation suggested that tumors persisted because of incomplete transgene inhibition, presumably due to insufficient doxycycline delivery to the tumor.

These initial results confirmed the dependence of Hh-driven medulloblastomas on continued activation of the pathway, but did not allow us to address the question of persistent, dormant tumor-forming cells. Investigating the potential presence of such cells following regression required complete elimination of active tumor. Accordingly, I modified my experimental approach, employing a combinatorial model utilizing both the Cre/loxP and rtTA-TRE systems to generate *rtTA-SmoA1* mice. In these "Tet-on" mice, expression of SmoA1 is induced by doxycycline treatment, and ablation of transgene expression is achieved by withholding doxycycline. Continuous doxycycline supplementation throughout gestation and until harvest resulted in the development of medulloblastomas by P14, as described in Chapter 2.

When we removed medulloblastoma-bearing *rtTA-SmoA1* mice from doxycycline treatment, tumors began regressing quickly, and tumor burden had completely disappeared within three weeks of doxycycline discontinuation, leaving behind residual tissue histologically similar to regressed regions in *tTA-SmoA1* mice. Loss of tumor burden was coupled to decreased Hh pathway activity, inhibited proliferation, and

increased levels of apoptosis. Regressed tissue from both *tTA-SmoA1* and *rtTA-SmoA1* mice displayed significant upregulation of GFAP density, and ectopic clusters of NeuN-positive neurons were evident in the molecular layer near regressed lesions. The presence of robust GFAP staining raises two possibilities: first, loss of tumor tissue may induce reactive astrocytosis, a common response to CNS injury (Sofroniew, 2005); second, some EGL-derived cells within the tumors may differentiate down an astroglial lineage once Hh signaling is repressed. This latter possibility is suggested by the observation that CGNPs of the EGL can differentiate into astroglial cells (Okano-Uchida *et al.*, 2004), and may also account for the presence of NeuN-positive clusters. This hypothesis could be investigated by combining the *tTA-SmoA1* tumor model with the *Math1-CreER*^{T2} mouse (Machold *et al.*, 2005) on a *ROSA26* background. Pulsing animals with tamoxifen prior to inducing regression would label only the *Math1*-positive tumor cells and allow lineage tracing of these cells following regression. This hypothesis is also consistent with the observation that inhibition of transgene expression induces differentiation of tumor cells in a mouse model of hepatocellular cancer (Shachaf *et al.*, 2004). Perhaps most significant, however, was the observation that nestin-positive cells disappeared prior to complete medulloblastoma regression. The fact that expression of this stem and progenitor cell marker disappears before the bulk of the tumor burden was eliminated suggests that nestin-expressing cells may be critical for tumor maintenance, and is consistent with loss of *nestin* seen in cyclopamine-treated medulloblastoma cell lines (Berman *et al.*, 2002) and loss of nestin-positive progenitor-like cells in *Bmi1*-deficient SmoA1-expressing cerebella (discussed in Chapter 4).

Ultimately, the data from this study indicate that Hh-driven medulloblastomas remain dependent on continued activation of the Hh pathway. Inhibition of *SmoA1* expression resulted in complete and durable resolution of tumor *in vivo*. Following disappearance of tumors, small residual populations of quiescent cells remained. These populations persisted throughout the life of the animal, and never gave rise to additional medulloblastomas, even after 7 months of transgene inhibition, and two additional mice display no behavioral or gross phenotypic evidence of tumor regrowth approximately one year after initial repression of transgene. These observations are in contrast to numerous other conditional tumor models, in which emergence of transgene-independent tumors frequently occurs following transgene inactivation (Ewald *et al.*, 1996, Chin *et al.*, 1999, Felsher *et al.*, 1999, D'Cruz *et al.*, 2001, Moody *et al.*, 2002, Gunther *et al.*, 2003, Boxer *et al.*, 2004).

To test the hypothesis that dormant tumor cells persist in regressed tissue, I re-initiated doxycycline treatment after three or four weeks of tumor regression. In striking contrast to the tumor regrowth observed following transgene reactivation in conditional models of other tumors (Boxer *et al.*, 2004, Shachaf *et al.*, 2004, Hutchin *et al.*, 2005), no medulloblastomas reappeared in *rtTA-SmoA1* mice which were returned to doxycycline chow following tumor regression. The Hh pathway was clearly reactivated in these mice, as indicated by the appearance of basaloid follicular hamartoma-like lesions in the skin of long-term reactivated mice. I observed that, following reactivation, SmoA1 was detectable in relatively few cells in the cerebellum. Several possibilities may explain this phenomenon. First, the vast majority of potential SmoA1-reactivating cells may die via apoptosis during the initial regression stage, and the residual tissue may represent mostly

non-recombined tissue. Second, forced high-level reactivation of the Hh pathway in regressed tissue may lead to early apoptosis, resulting in few remaining SmoA1 expressing cells in later stage reactivation. I eliminated the latter possibility by performing brief periods of transgene re-induction, and observing that while reactivation of transgene was evident three, five and seven days after returning mice to doxycycline chow, no TUNEL-positive cells were evident in regressed tissue at these early time points. Because expression of transgene requires sufficient delivery of doxycycline to cells, I cannot formally exclude the possibility that tumors fail to recur because of insufficient secondary induction of transgene. Doxycycline delivery to regressed tumor regions may be impaired because of the observed increased astrocytic density along the outer edges of the cerebellum, as astrocytes are known to play a role in maintenance of the blood-brain barrier (Sofroniew, 2005). This possibility could be tested by using intracranial osmotic pumps to deliver increased levels of doxycycline directly into the cerebellum, bypassing the blood-brain barrier function.

Taken together, the results presented in this chapter demonstrate an absolute dependence of SmoA1-induced medulloblastomas on continued oncogenic activation of the Hh pathway. Inhibition of Hh signaling in tumors resulted in impaired proliferation, increased apoptosis, and possibly terminal differentiation of tumor cells, culminating in complete, durable regression of tumors, without the development of transgene-independent recurrence seen in many other transgenic mouse models of cancer. Furthermore, the regressed tumors do not appear to harbor dormant tumor cells, as resumption of doxycycline treatment failed to induce regrowth of regressed tumors, although, as mentioned above, we cannot exclude the possibility of insufficient transgene

reactivation. These data strongly argue for the potential utility of anti-HH therapy in at least a subset of patients with medulloblastoma, a goal which may soon be achievable, as evidenced by ongoing Phase I and II clinical trials of a small molecule pathway inhibitor in several HH-mediated cancers. Studies of anti-HH therapies in children must be approached with caution, however, in light of a recent study demonstrating that even brief treatment of young mice with a small molecule Hh pathway inhibitor induced permanent defects in bone development (Kimura *et al.*, 2008).

Chapter 4

Bmi1 is Required for Normal Keratinocyte Proliferation and Medulloblastoma Expansion

Introduction

Bmi1 is a member of the Polycomb group of transcriptional repressor proteins and regulates stem cell self-renewal, partially by repressing the senescence and apoptosis-related genes $p16^{Ink4a}$ and $p19^{Arf}$ (Valk-Lingbeek *et al.*, 2004). In the epithelium, BMI1 is expressed in both *in vivo* and in cultured keratinocytes, and contributes to cell survival and proliferation by inhibiting apoptosis and modifying cell cycle machinery (Lee *et al.*, 2008), in keeping with its role as a repressor of the *Ink4a/Arf* locus. Expression of BMI1 in human skin is inversely correlated with chronological age, and as BMI1 decreases, $p16^{INK4A}$ increases (Ressler *et al.*, 2006). Additionally, cultured epithelial stem cells from the bulge region of rat follicles express *Bmi1* (Claudinot *et al.*, 2005), further supporting the idea that Bmi1 is important in epithelial stem cell function. However, no studies have demonstrated a requirement for Bmi1 in epithelial stem cells.

In keeping with the idea that normal organ development and maintenance is related to tumor formation in a paradevelopmental manner, *Bmi1* has also been implicated in Hh pathway-mediated self-renewal of both normal mammary stem cells and cancer stem cells (Liu *et al.*, 2006b). Likewise, *Bmi1* is a key determinant of the proliferative potential of both normal hematopoietic stem cells and leukemic stem cells (Lessard *et al.*, 2003). In developing cerebellum, Bmi1 appears to act downstream of the

Hh pathway to control proliferation of cerebellar granule neuron precursors (CGNPs) (Leung *et al.*, 2004). Accordingly, *Bmi1*-null mice develop smaller cerebella secondary to impaired production of granular neurons; however, overall cerebellar organization and cell specification and differentiation appear relatively normal (Leung *et al.*, 2004, Bruggeman *et al.*, 2005, Molofsky *et al.*, 2005). In humans, BMI1 is aberrantly overexpressed in a number of solid tumor types, including medulloblastoma (Leung *et al.*, 2004), where BMI1 expression correlates with activation of the Hh pathway.

These data suggest that Bmi1 may be important in the development of medulloblastomas, which appear to arise from CGNPs in response to deregulated Hh signaling (Kozmik *et al.*, 1995, Kim *et al.*, 2003, Grimmer *et al.*, 2008), (Chapter 2 of this thesis). While several recent studies suggest a role for *Bmi1* in maintenance of cultured or grafted tumor cells (Bruggeman *et al.*, 2007, Cui *et al.*, 2007, Wiederschain *et al.*, 2007), a requirement for Bmi1 in the spontaneous development of *de novo* solid tumors has not been demonstrated. In this chapter, I describe work in which I investigated the role of *Bmi1* both in the function of epithelial cells from skin and in the pathogenesis of Hh-driven medulloblastoma. To accomplish these aims, I used the *Bmi1* knockout mouse line generated by van der Lugt *et al*. (van der Lugt *et al.*, 1994), and the robust, fully penetrant *GFAP-tTA;TRE-SmoA1* medulloblastoma model described in Chapter 2. For the sake of simplicity, double transgenic *GFAP-tTA;TRE-SmoA1* are referred to as *SmoA1* in this chapter.

Materials and Methods

Maintenance, breeding, and genotyping of knockout and transgenic mice

Bmi1$^{-/-}$ mice were obtained for skin experiments by intercrossing *Bmi1*$^{+/-}$ mice (van der Lugt *et al.*, 1994). I generated *SmoA1* mice on *Bmi1*$^{+/-}$ and *Bmi1*$^{-/-}$ backgrounds by crossing *GFAP-tTA* and *TRE-SmoA1* mice separately with *Bmi1*$^{+/-}$ mice and then intercrossing the resulting *GFAP-tTA*;*Bmi1*$^{+/-}$ and *TRE-SmoA1*;*Bmi1*$^{+/-}$ progeny. Pups were genotyped between P14 and P21, by which point *Bmi1*$^{-/-}$ animals were readily distinguished by their smaller body size and elongated ear hair. *Bmi1*, *GFAP-tTA* and *TRE-SmoA1* genotypes were confirmed by PCR. *Bmi1* genotype was confirmed by multiplex PCR for both the hygromycin cassette in the *Bmi1* knockout allele (5'-cgccgtgcacagggtgtcacgttgcaagac-3' and 5'-caagccaaccacggcctccagaag-3') (Molofsky *et al.*, 2005) and the wild-type *Bmi1* allele (5'-ccaccacaacacctcatcac-3' and 5'-cgggtgagctgcataaaaat-3'). *SmoA1* genotype was ascertained by individual PCR for the tetracycline transactivator to identify *GFAP-tTA* and the SV40 poly-A tail to identify *TRE-SmoA1*, as described in Chapter 2. In total, 90 litters were screened, comprising 417 pups from 70 of the litters, and an additional 20 litters of unrecorded size which contained no *Bmi1*$^{-/-}$ pups by phenotype and were therefore sacrificed without further analysis. All mice used in the experiments described in this chapter were on a pure C57BL/6 background, and *TRE-SmoA1* mice were from line #140.

To induce anagen, mice were anesthetized by intraperitoneal injection of a ketamine/xylazine mixture. Pelage fur was clipped, and over-the-counter Nair depilatory cream was applied for five minutes. Due to impaired hematopoietic function and increased risk of infection in *Bmi1*$^{-/-}$ mice, all animals were maintained on water supplemented with 0.1214 mg/mL Polymixin B sulfate (Sigma) and 1.1 mg/mL Neomycin trisulfate (Sigma). Maintenance of mouse colonies and experimental

procedures were approved by the University of Michigan University Committee on the Use and Care of Animals.

Cell culture, colony formation assay, total cell output assay and *in vitro* BrdU incorporation

To establish keratinocyte cultures (Dlugosz *et al.*, 1995), 5 cm-long sections of tail were removed from euthanized adult *Bmi1*$^{+/+}$ and *Bmi1*$^{-/-}$ mice. The skin was removed as a contiguous sheet, and floated dermis side down in a dish of 0.25% trypsin (Invitrogen) overnight at 4°C. The following morning, the skin was placed epidermis side down on a dry culture dish, and the dermis was carefully removed with forceps and discarded. The remaining epithelial portion was placed in a 15 mL conical tube containing growth medium, gently vortexed, then passed through a 40 μm cell strainer. The resulting cells were plated at multiple dilutions for low density primary colony formation assays, and at higher density for use in additional assays. All cells were plated overnight in plating medium: SMEM (Invitrogen) with 10% fetal calf serum at 0.3 mM Ca^{++}. The following morning, plates were rinsed with sterile phosphate buffered saline, and media was replaced with either Low Ca^{++} medium, identical to plating medium but containing 0.05 mM Ca^{++}, or Low Ca^{++} medium with 1 ng/ml keratinocyte growth factor. Subsequently, culture medium was aspirated and replaced with fresh medium every second day.

For first passage colony formation assays, cells were allowed to grow for 14 days, then were fixed and stained with crystal violet to visualize colonies. For second passage colony formation assays and total cell output experiments, high density plates were grown for two days, then treated with 0.025% trypsin with EDTA (Invitrogen), and the

resulting single cell suspension was counted using a Coulter Counter Z2 particle analyzer. 1 x 10^5, 1 x 10^4, or 1 x 10^3 cells were plated per well in 6-well culture plates. For second passage colony-formation assays, plates were grown and fixed as above. For total cell output experiments, triplicate wells in 6-well plates were plated with 2 x 10^5 cells. Cells were maintained in culture for up to 50 days. Each time plates were fed, the culture medium was collected and the number of suspended cells was counted.

Primary keratinocytes were prepared from newborn animals in the same manner as adult tail skin, with minor differences. Newborn animals were sacrificed by primary CO_2 narcosis followed by immersion in ice water for 20 minutes. Limbs and tails were removed, and the skin was cut longitudinally prior to floating on trypsin. Skins were removed and prepared as adult tail skins. Following vortexing, the cornified envelope was removed with a glass pipette, and the suspension was not filtered. Primary keratinocytes were plated as above.

To assess *in vitro* proliferation, newborn *Bmi1*$^{+/+}$ and *Bmi1*$^{-/-}$ keratinocytes were prepared as above and plated at medium density. 5 days after plating and 24 hours after the last medium change, 30 μM BrdU was added to the culture medium. 1 hour after BrdU addition, cells were fixed with 70% ethanol. After fixation, cells were permeabilized with 2N HCl, 0.5% Triton X-100. Cells were then washed, blocked with 0.5% BSA/PBS, and exposed to α-BrdU antibody diluted 1:100 (Zymed 03-3900). Primary antibody was visualized using Texas Red-conjugated anti-mouse secondary antibody (Jackson ImmunoResearch), and cells were mounted under VectaShield aqueous mounting medium with DAPI (Vector labs).

Immunohistochemistry

Tissue was fixed overnight in 10% neutral buffered formalin and processed as previously described. To definitively confirm the absence of tumor burden in *SmoA1*;*Bmi1*$^{-/-}$ mice, serial coronal sections were cut through the entire rostral-caudal length of the cerebella. All sections were cut at 5 μm thick. Prior to immunostaining for HA, NeuN, GFAP, Nestin or PCNA, tissues were subjected to antigen retrieval by boiling in sodium citrate buffer for 10 minutes. The antibodies used comprised HA (Roche 3F10, 1:100), NeuN (Chemicon MAB372, 1:200), GFAP (Neomarkers Ab-4, 1:200), Nestin (Developmental Studies Hybridoma Bank Rat-401, 1:4), PCNA (Neomarkers PC10, 1:200), and TUNEL (Chemicon ApopTag *in situ* peroxidase kit). Images were obtained on an Olympus BX51 microscope, using an Olympus DP71 digital camera. For immunostaining of Bmi1, Cyclin D1 and p19^{Arf}, microwave antigen retrieval was performed for 20 minutes. The following primary antibodies were used: Bmi1 (mouse monoclonal F6, 1:50), Cyclin D1 (Santa Cruz Sc-753, 1:100), and p19^{Arf} (Abcam R562, 1:150). Antibodies were detected by peroxidase staining using the Powervision system (Immunologics) followed by visualization on a Zeiss Axiovert microscope.

Tissue volume, PCNA, and TUNEL measurements

Approximate tissue volumes were calculated using a previously published protocol (Pogoriler *et al.*, 2006). Serial 5 μm-thick coronal sections were cut through the entire rostral-caudal length of P21 *SmoA1;Bmi1*$^{+/+}$ and S*moA1;Bmi1*$^{-/-}$ cerebella (N = 3 for each group), and every third or every fourth slide was stained with hematoxylin and eosin (H&E). In order to calculate the rostral-caudal extent of the lesions, I counted the total number of sections over which the lesions extended, measured the cross-sectional

surface area on each H&E-stained section for an individual lesion using ImageJ software, and averaged these values to obtain a mean cross-sectional lesion area. I multiplied this mean area by the total rostral-caudal length of the lesion to calculate approximate volume measurements. *P*-values were obtained using two-tailed t-test, assuming unequal variances.

The percentage of PCNA- or TUNEL-positive cells was determined on sections from P21 *SmoA1;Bmi1*$^{+/+}$ and *SmoA1;Bmi1*$^{-/-}$ mice (N = 3 for each group). After immunostaining tissue sections for PCNA or TUNEL as described, we photographed 10 random, non-overlapping high power fields of tumor or ectopic tissue for each animal. If there were fewer than 10 high power fields' worth of cells in a given *SmoA1;Bmi1*$^{-/-}$ lesion, we photographed all ectopic cells present in the section. We then counted both the number of PCNA or TUNEL positive nuclei per field and the total number of nuclei per field, and divided the number of positive nuclei by the total number of nuclei to obtain the percent positive nuclei. *P*-values were calculated as above.

Results and Discussion

Bmi1$^{-/-}$ keratinocytes have impaired colony forming ability and *in vitro* growth potential

When plated at successively increasing dilutions, *Bmi1*$^{-/-}$ primary adult tail keratinocytes displayed inhibited colony formation ability (Fig. 4-1 A), indicating a depletion or impaired performance of clonogenic stem or transient-amplifying cells in the absence of *Bmi1*. These results were consistent across three independent experiments. Similar inhibition of colony formation was observed in keratinocytes isolated from newborn *Bmi1*$^{-/-}$ pups (not shown).

To generate single-cell suspensions in order to count and plate equal numbers of cells, I seeded portions of the adult primary keratinocyte preparations at high density and maintained them for two days. Trypsinization of these cultures resulted in single cell suspensions, which were counted in order to plate equal numbers of cells per well for quantification experiments. 14 days after plating equal numbers of second passage tail keratinocytes, I fixed and stained culture dishes to count colony number and size. While cells from *Bmi1*$^{+/+}$ mice formed an average of 82 colonies per 1000 cells plated, *Bmi1*$^{-/-}$ cells formed only 15 colonies per 1000 cells plated ($P=5.6 \times 10^{-4}$, Fig. 4-1 B). Additionally, *Bmi1*$^{+/+}$ colonies were significantly larger than knockout colonies (106 vs. 17 cells per colony, $P=4.4 \times 10^{-4}$, Fig. 4-1 C).

A key feature of stem cells is their ability to self-renew. Bmi1 is known to be a key determinant of the long-term proliferative potential of both neural and hematopoietic stem cells (Molofsky *et al.*, 2003, Park *et al.*, 2003), and, presumably through its modulation of $p16^{INK4A}$, controls the replicative potential of fibroblasts (Itahana *et al.*, 2003). In order to assess whether Bmi1 plays a similar role in maintenance of keratinocyte proliferation, I tracked the long-term proliferative capacity of wild type and *Bmi1*$^{-/-}$ cells. I plated 2×10^5 second-passage adult tail keratinocytes in triplicate wells of 6-well culture plates and monitored cell production for up to 50 days by counting cells floating in the culture medium at each feeding. These cells represent either cells which have died and lifted off the dish or have recently divided and not yet reattached.

In two separate experiments, *Bmi1*$^{-/-}$ cultures displayed inhibited daily cell output and total output. While cell output was similar for the first few days in culture, the wild type plates began producing more cells per day than *Bmi1*$^{-/-}$ cells within one week (Fig.

4-2 A). The total number of cells produced per well throughout the course of the experiment was significantly higher in wild type cells than *Bmi1*$^{-/-}$ cells (Fig. 4-2 B, P=0.0054). When this experiment was repeated, similar initial results were observed. After approximately three weeks in culture, two wells from the wild type culture overcame crisis, and continued proliferating until the termination of the experiment (data not shown). No post-crisis outgrowth was evident in *Bmi1*$^{-/-}$ cells from either experiment.

In addition to colony formation and total cell output, we also assessed *in vitro* BrdU incorporation over the span of one hour. BrdU was added to culture medium of newborn keratinocytes after 5 days in culture, 24 hours after the last feeding. The BrdU incorporation rate of wild type keratinocytes was approximately two-fold greater than that of *Bmi1*$^{-/-}$ cells (36% vs. 18.7%, P= 2.7 x 10^{-5}, Fig. 4-2 C, D). Taken together, these data suggest an important role for *Bmi1* in colony forming ability and proliferation of both newborn and adult keratinocytes *in vitro*, suggesting a requirement for Bmi1 in epithelial stem cell function.

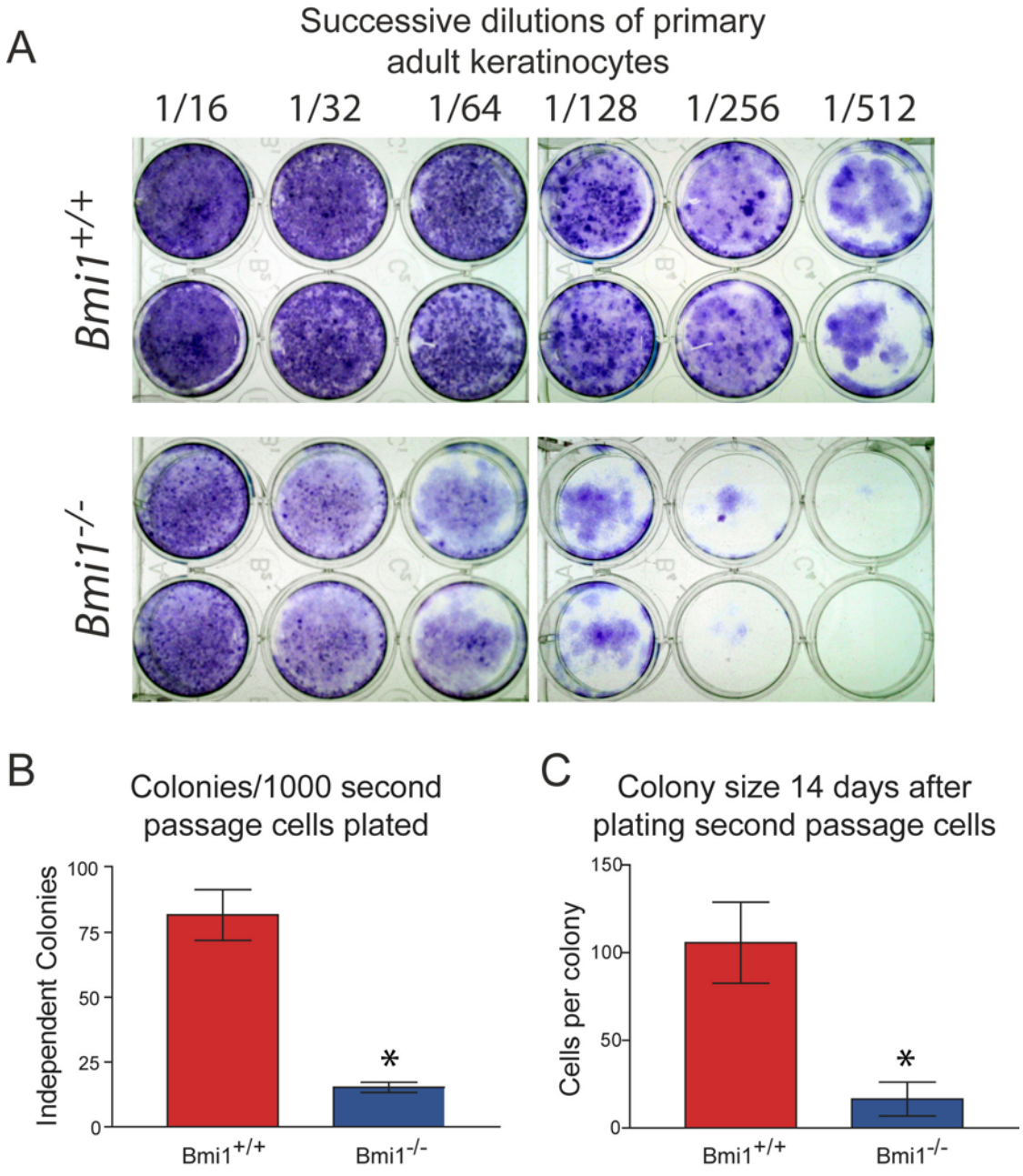

Figure 4-1. In vitro colony formation is dependent on *Bmi1*. (A) Successive dilutions of primary adult tail keratinocytes were plated as indicated. Fixation and crystal violet staining after two weeks of growth demonstrated impaired colony forming ability of *Bmi1*$^{-/-}$ keratinocytes compared with wild type controls. (B & C) 1000 second passage keratinocytes were plated per well in quadruplicate wells. 14 days after plating, cells were fixed and the number (B) and size (C) of colonies were measured. * indicates statistical significance (B: $P=5.6 \times 10^{-4}$; C: $P=4.4 \times 10^{-4}$).

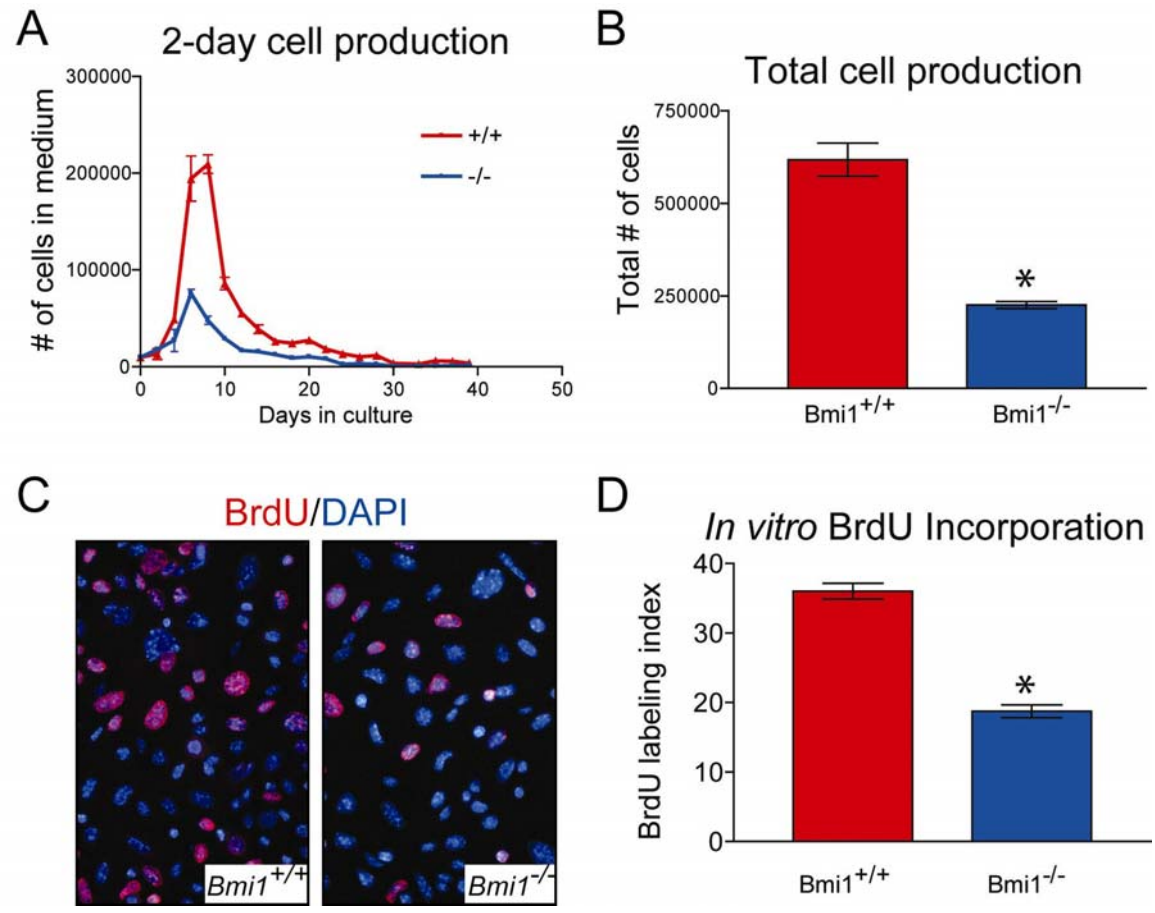

Figure 4-2. Loss of *Bmi1* inhibits proliferation rate and total proliferation potential of keratinocytes. (A & B) Equal numbers of cells were plated in triplicate, and total cell output was measured. Detached cells floating in the culture medium were counted every other day during cell feeding. Increased proliferation is evident in wild type cells (A). Total number of cells produced was significantly lower in *Bmi1*$^{-/-}$ cultures (P=0.01 (B). *In vitro* BrdU incorporation by keratinocytes isolated from newborn mice was assayed by immunostaining for BrdU after a 1 hour pulse (red). Nuclei are counterstained with DAPI (blue) (C). BrdU labeling index was twice as high in *Bmi1*$^{+/+}$ cells as in *Bmi1*$^{-/-}$ cells (36.0% vs. 18.7%, P=2.7 x 10^{-5} (D). * indicates statistical significance (P=2.7 x 10^{-5}).

Bmi1$^{-/-}$ mice exhibit delayed reactivation of hair cycling

To further probe the importance of Bmi1 in epithelial stem cell function in skin, I subjected *Bmi1*$^{+/+}$ and *Bmi1*$^{-/-}$ mice to repeated rounds of depilation. Depilation of mouse pelage skin, either mechanically or chemically with the over-the-counter hair removal cream Nair, induces resting, telogen hair follicles to re-enter anagen, the active growth phase of the hair cycle, a process known to be controlled by Hh signaling (Sato *et al.*, 1999, Paladini *et al.*, 2005). Cyclic reactivation of the hair cycle involves marked expansion of the follicular structures, and requires activation of hair follicle stem cells, which reside in the bulge region of the follicle (reviewed in (Tiede *et al.*, 2007)). Based on the proposed importance of Bmi1 in follicular stem cells, I hypothesized that *Bmi1*$^{-/-}$ mice would exhibit an alteration in the onset or magnitude of proliferative expansion of hair follicle epithelium during the anagen growth phase of the hair cycle, particularly as animals aged. To test this hypothesis, I subjected *Bmi1*$^{-/-}$ and wild type control mice to repeated rounds of depilation and observed the time until anagen induction.

In total, I depilated 10 *Bmi1*$^{-/-}$ mice and an equal number of age-matched controls during the first extended postnatal telogen period. Change in depilated skin color from pink to grey, indicative of anagen induction, was detected in all of the control mice and 5 of the *Bmi1*$^{-/-}$ mice within 7 days following depilation. The appearance of anagen in the remaining 5 *Bmi1*$^{-/-}$ mice was delayed between one and 21 days; one of the anagen-delayed mice was sacrificed 12 days after depilation for histological examination and had not yet re-entered anagen (Fig. 4-3 A). Representative images of a cohort of depilated animals exhibiting delayed anagen are shown (Fig. 4-3 B). Following a return of dorsal skin to telogen, 7 of the *Bmi1*$^{-/-}$ mice, together with wild-type controls, were depilated a

second time. The re-depilated mice included all 5 *Bmi1*$^{-/-}$ mice which did not exhibit delayed anagen following the first depilation. While anagen was detectable in wild-type mice within 7 days, all *Bmi1*$^{-/-}$ mice were delayed in their return to anagen. Two mice died spontaneously approximately two weeks after depilation without any evidence of a return to anagen. Two mice entered anagen 7 weeks after depilation, one after 8 weeks, and the final two mice died without reappearance of anagen approximately 9 weeks after depilation. The reason for this delayed return to anagen is not immediately clear. If *Bmi1* is important for self-renewal of follicular epithelial stem cells as is the case in nervous and hematopoietic stem cells, loss of *Bmi1* may impair the ability of these cells to reactivate following depilation, a required event in hair follicle reactivation (reviewed in (Tiede *et al.*, 2007)). Another possibility is raised by the observation that putative stem cells from a deeper structure known as the secondary hair germ are capable of repopulating the bulge region of follicles with stem cells following trauma such as mechanical depilation (Ito *et al.*, 2004). If, as I hypothesized, bulge cells are progressively lost in the absence of Bmi1, this phenomenon, combined with treatment with the depilatory cream Nair, may effectively de-populate the bulge region of *Bmi1*$^{-/-}$ hair follicles, requiring repopulation from the secondary hair germ prior to anagen reactivation. This repopulation could, in turn, be inhibited or slowed by loss of *Bmi1*, as well, compounding the progressive defect in hair cycling.

Figure 4-3. *Bmi1*$^{-/-}$ mice exhibit delayed depilation-induced anagen. (A) Gross photograph and hematoxylin and eosin stained histological images of wild type and *Bmi1*$^{-/-}$ animals sacrificed 12 days after depilation. The depilated region of wild type skin has returned to anagen, as evidenced by the darkening of the skin and full-depth hair follicles on histological examination. The *Bmi1*$^{-/-}$ mouse has not returned to anagen – its skin remains pink, and follicles are still in telogen histologically. (B) A series of gross photographs of two wild type and two *Bmi1*$^{-/-}$ mice 16, 31 and 50 days after a single depilation. While all mice do eventually enter anagen and regrow hair, varying degrees of delay before the *Bmi1*$^{-/-}$ animals enter anagen can be appreciated.

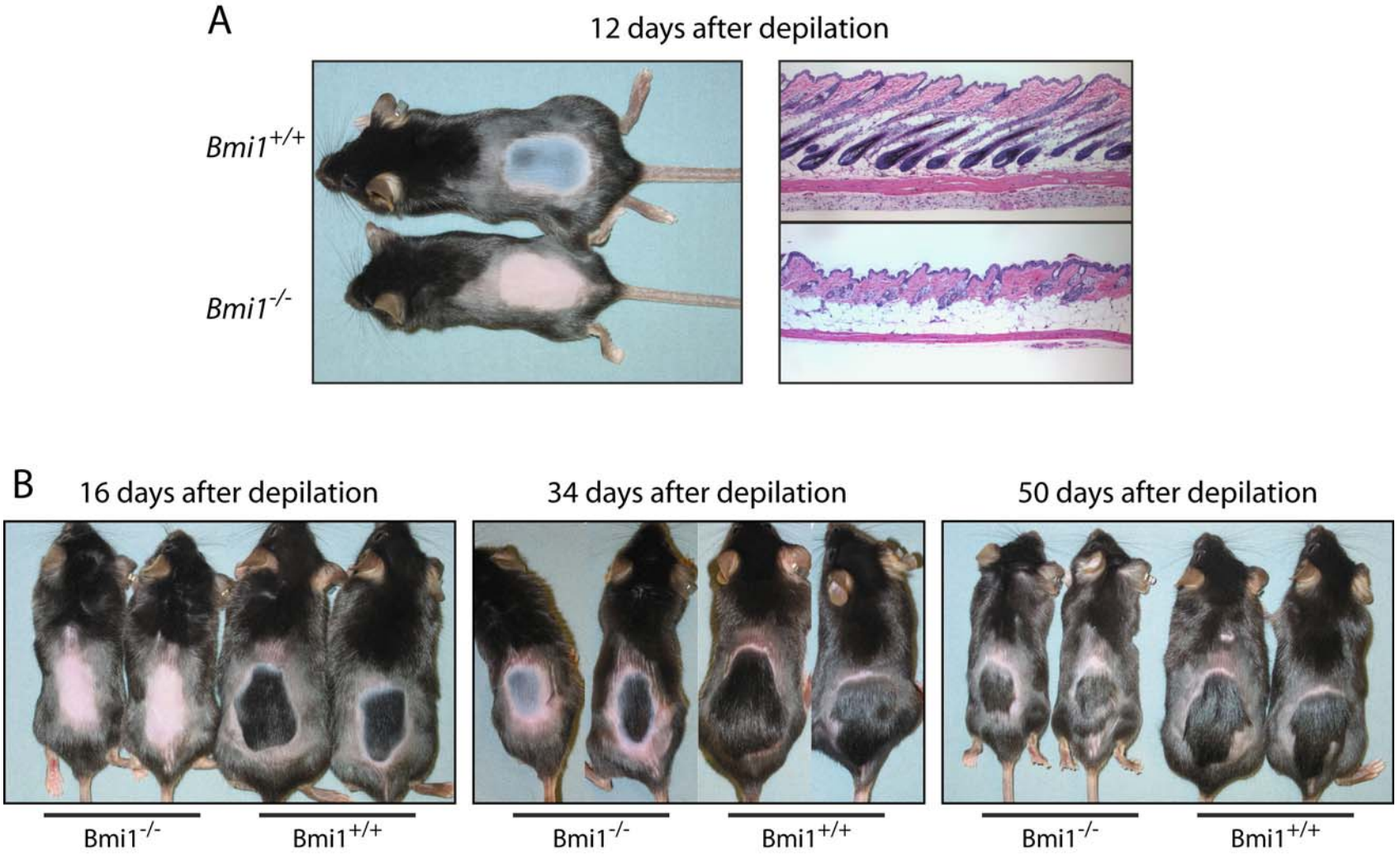
A
12 days after depilation
Bmi1+/+
Bmi1-/-
B
16 days after depilation
34 days after depilation
50 days after depilation
Bmi1-/-
Bmi1+/+
Bmi1-/-
Bmi1+/+
Bmi1-/-
Bmi1+/+

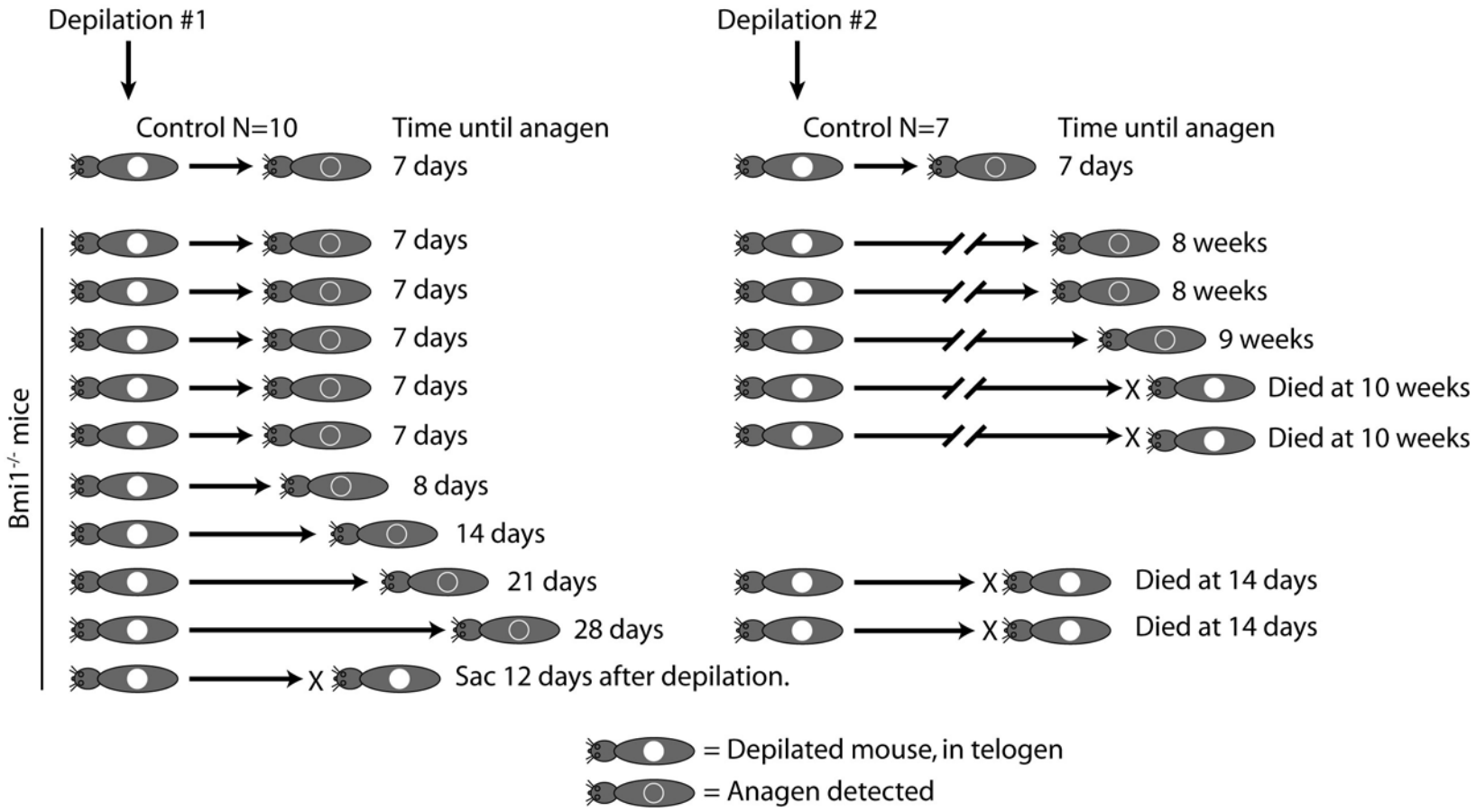

Figure 4-4. Illustration of anagen delay in wild type and *Bmi1*$^{-/-}$ mice. In three separate experiments, a total of 10 control and 10 *Bmi1*$^{-/-}$ mice were depilated, as shown above. Following an initial depilation (left panel), 5/10 *Bmi1*$^{-/-}$ mice re-entered anagen without delay, and the remainder exhibited varying delay in the inception of anagen. One anagen-delayed *Bmi1*$^{-/-}$ mouse was sacrificed for histology 12 days after initial depilation. 7 control and *Bmi1*$^{-/-}$ mice were depilated a second time (right panel). All *Bmi1*$^{-/-}$ mice exhibited a greatly prolonged delay before anagen reactivation, and four mice died without reactivating anagen.

Progressive pigmentation defect in *Bmi1*$^{-/-}$ mice

In addition to the delayed anagen seen in *Bmi1*$^{-/-}$ mice, we also observed an interesting pigmentation defect. *Bmi1*$^{-/-}$ mice have shortened lifespan, and generally do not survive past several months of age (van der Lugt *et al.*, 1994). However, in these experiments, several mice survived for almost 6 months. All mice from these experiments were on a pure C57BL/6 background, and had the expected dark black hair when young. By 6 months of age, wild-type mice exhibited minor lightening of hair color, particularly around the head and face, where the fur became slightly brown in color. *Bmi1*$^{-/-}$ mice, on the other hand, had lost all black color, and had become a light brown, although this was difficult to appreciate in photographs. More striking, however, was the loss of pigmentation in repeatedly depilated skin. New hair growth on wild type mice was dark black after both the first and second depilations, as expected. While hair which regrew following the initial depilation of *Bmi1*$^{-/-}$ mice was dark black, the hair induced by the second round of anagen had varying levels of pigmentation, with many hair shafts appearing to lack pigment altogether (Fig. 4-5, top). Imaging hair on a dissecting microscope confirmed loss of melanin in anagen-induced *Bmi1*$^{-/-}$ hair (Fig. 4-5, bottom), but additional studies are needed to ascertain whether this reflects a depletion of melanoblasts residing within the follicle stem cell niche, as has been described during the normal aging process and other settings where mice develop premature graying of hair (Lerner *et al.*, 1986, Nishimura *et al.*, 2005). This suggests an as yet undiscovered role for Bmi1 in melanocyte biology. Although the nature of this relationship is unclear, it is likely that *Bmi1* is required for maintenance of melanocyte stem cells, given its role in maintenance of neural and hematopoietic stem cells (Molofsky *et al.*, 2003, Park *et al.*, 2003, Bruggeman *et al.*, 2005).

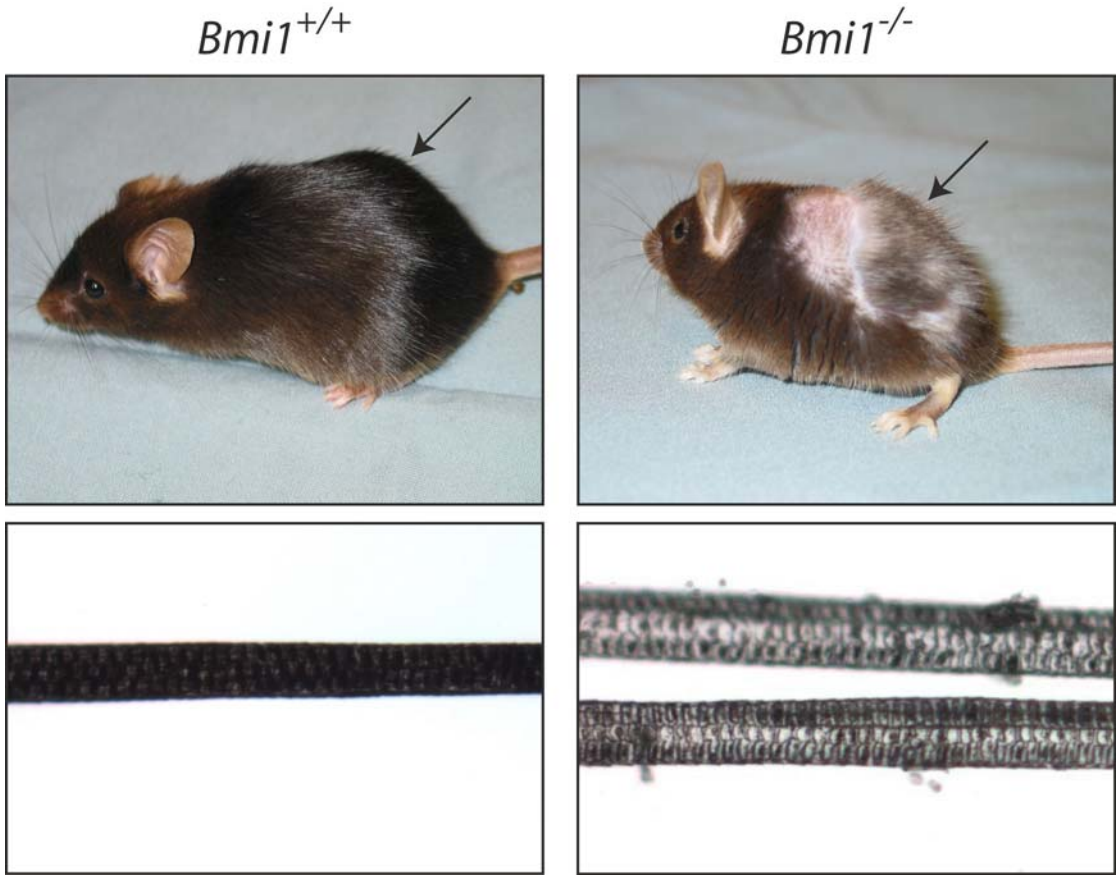

Figure 4-5. Aged and repeatedly depilated *Bmi1*$^{-/-}$ mice lose hair pigmentation. Gross photographs of 6 month-old repeatedly depilated mice (top) and transilluminated dissecting microscope images of hair shafts from depilated regions (bottom). Change of pelage fur color from the black of young animals to a faded brown color can be appreciated in the gross photograph of the *Bmi1*$^{-/-}$ mouse. A striking complete loss of pigment in much of the hair in the depilated region can also be appreciated, while the regrown hair of *Bmi1*$^{+/+}$ mice remains black. Arrows indicate regions of repeated depilation. Complete loss of melanin from the depilation-induced *Bmi1*$^{-/-}$ hair shafts can be appreciated microscopically.

***Bmi1*$^{-/-}$ mice do not develop full-blown medulloblastoma**

As discussed in Chapter 2, *GFAP-tTA;TRE-SmoA1* mice (referred to as *SmoA1* in this chapter for the sake of brevity) developed tumors resembling medulloblastoma as early as postnatal day 7 (P7), with 100% penetrance by P14. Early tumors were first detected as an expansion of EGL in a small ventrolateral region of the cerebellum. By P21, when the EGL was no longer detected in wild-type animals, tumors frequently extended along the entire rostral-caudal length of the cerebellum when examined in serial coronal sections (Fig. 4-6 Aa). Tumor-bearing *SmoA1* animals died within 10 to 12 weeks.

To generate *SmoA1* mice on a *Bmi1*-deficient background, I crossed *Bmi1*$^{+/-}$ mice with either *GFAP-tTA* or *TRE-SmoA1HA* mice, and then crossed the resulting *GFAP-tTA;Bmi1*$^{+/-}$ and *TRE-SmoA1HA;Bmi1*$^{+/-}$ progeny. I obtained *SmoA1* mice on wild-type (N=80), *Bmi1*$^{+/-}$ (N=17), and *Bmi1*$^{-/-}$ (N=6) backgrounds. In striking contrast to the complete tumor penetrance in *SmoA1* wild-type and *SmoA1;Bmi1*$^{+/-}$ mice, none of the six *SmoA1;Bmi1*$^{-/-}$ mice developed full-blown medulloblastomas when examined at P18-P26. One of two P18 *SmoA1;Bmi1*$^{-/-}$ mice contained a small focus of cells with some similarities to medulloblastoma, but with notable differences (see below). In the additional P18 *SmoA1;Bmi1*$^{-/-}$ mouse and three P21 *SmoA1;Bmi1*$^{-/-}$ mice, tumors were not detected. Instead, small ectopic foci of presumed abortive tumor cells were identified external to the molecular layer (Fig. 4-6 Ab), a region normally devoid of cells at this stage (Fig. 4-6 Ac, Ad). These cells were not detected at P26.

The presence of tumor-like cells in a P18 *SmoA1;Bmi1*$^{-/-}$ mouse, populations of residual ectopic cells in P18 and P21 mice, and the absence of these cells at P26 imply

that medulloblastoma formation is initiated in *Bmi1*$^{-/-}$ mice, but the subsequent expansion of tumors is blocked and residual tumor cells are ultimately eliminated (Fig. 4-6 B**)**. Our findings suggest a more stringent requirement for Bmi1 in medulloblastoma development than in leukemia, which is blocked by Bmi1 deficiency in secondary but not primary recipients (Lessard *et al.*, 2003). This may reflect differential requirements for Bmi1 in expansion of CGNPs versus hematopoietic stem cells.

Compared to age-matched wild-type medulloblastomas, ectopic cells in P21 *SmoA1*;*Bmi1*$^{-/-}$ mice had a lower nuclear to cytoplasmic ratio and pale eosinophilic cytoplasm, and the lesions occupied 1/140th the volume (Fig. 4-6 C): mean *SmoA1*;*Bmi1*$^{+/+}$ tumor volume was 2.69 mm^3, while mean *SmoA1*;*Bmi1*$^{-/-}$ lesion volume was 0.019 mm^3 (P=0.0044). Medulloblastoma cells in wild-type mice and cells in ectopic foci in *Bmi1*$^{-/-}$ mice both expressed *SmoA1* (Fig. 4-7 Aa), indicating that impaired tumor growth in *Bmi1*$^{-/-}$ mice cannot be attributed to lack of transgene expression. Apoptotic cells were 4.7-fold more abundant in ectopic cells than medulloblastoma (29.61% vs. 6.26% respectively, P = 0.028) (Fig. 4-7 Ab, C). Proliferation was also impaired in *SmoA1;Bmi1*$^{-/-}$ lesions; PCNA-positive cells were reduced 13.3-fold, from 81.93% in *SmoA1*;*Bmi1*$^{+/+}$ tumors to 6.18% in ectopic lesions (P=7.5 x 10^{-6}) (Fig. 4-7 Ac, D). These data suggest that both increased apoptosis and reduced proliferation contributed to the impaired outgrowth of putative medulloblastoma progenitors in the absence of *Bmi1*.

We next examined Bmi1 protein and cell cycle marker expression in P21 *Bmi1*$^{+/+}$ and *Bmi1*$^{-/-}$ lesions. *SmoA1*;*Bmi1*$^{+/+}$ tumors expressed Bmi1 in almost all cells, while no Bmi1 was detected in *SmoA1*;*Bmi1*$^{-/-}$ animals (Fig 4-7 Ba), as expected. Conversely,

nucleolar $p19^{Arf}$ was detected in cells scattered throughout the ectopic foci in *SmoA1;Bmi1*$^{-/-}$ cerebella, while it was weakly expressed in medulloblastomas (Fig. 4-7, Bb). This observation is consistent with an inhibitory role for $p19^{Arf}$ in CGNP proliferation and cerebellar development (Bruggeman *et al.*, 2005), and suggests that Bmi1 blocks $p19^{Arf}$ expression in Hh-induced medulloblastoma. $p19^{Arf}$ was also detected in scattered cells within the IGL of *Bmi1*$^{-/-}$, SmoA1-negative mice. However, it is difficult to determine from the current studies if SmoA1 induces increased $p19^{Arf}$ expression in the absence of *Bmi1*. Cyclin D1, a Hh target which acts downstream of $p16^{Ink4a}$ (Kenney *et al.*, 2000), was weakly expressed in a small fraction of ectopic cells in *SmoA1*;*Bmi1*$^{-/-}$ mice, but was strongly expressed in medulloblastomas (Fig. 4-7 Bc). Given that *Cyclin D1* is required for medulloblastoma development (Pogoriler *et al.*, 2006), its loss in *Bmi1*-deficient, SmoA1-expressing cerebellum may contribute to the failure to form tumors. Upregulation of the CDK inhibitor p21 was not detected in *Bmi1*-deficient ectopic lesions (not shown).

We also examined expression of differentiation markers and the stem and progenitor cell marker nestin. Compared to medulloblastomas, ectopic lesions in *SmoA1*;*Bmi1*$^{-/-}$ mice contained a predominance of cells intensely positive for GFAP, but essentially no NeuN positive neuronal cells (Fig. 4-8 A, B). This marker profile suggests that ectopic cells in *SmoA1*;*Bmi1*$^{-/-}$ mice are distinct from the pre-neoplastic lesions described in *Ptch*$^{lacZ/+}$ mice (Oliver *et al.*, 2005). In both *SmoA1*;*Bmi1*$^{+/+}$ and *SmoA1*;*Bmi1*$^{-/-}$ mice, clusters of post-mitotic, strongly NeuN-positive neuronal cells were detected in the outer molecular layer just deep to either tumors or ectopic regions, respectively (Fig. 4-8 B). The presence of these misplaced cell aggregates, never

detected in non-transgenic mice, is in keeping with the idea that there is similar initial tumorigenic response to SmoA1 in the EGL of *Bmi1*$^{-/-}$ and wild-type mice (see below), but it cannot be sustained in the absence of *Bmi1*. We also observed a striking reduction in nestin-positive cells in *SmoA1*;*Bmi1*$^{-/-}$ ectopic foci (Fig. 4-8 C), indicating a depletion of progenitor cells in these presumably abortive lesions. This loss of progenitor-like cells likely contributes to the failure of nascent medulloblastomas to progressively expand in the absence of *Bmi1*.

Figure 4-6. *Bmi1* is required for Hh-pathway driven medulloblastoma expansion. (A) Hematoxylin and eosin staining of coronal sections from cerebella of P21 mice. Tumors (a) or ectopic foci of presumed abortive tumor cells (b), both outlined with dotted black line, are evident external to the molecular (ML in c) in *SmoA1;Bmi1*$^{+/+}$ and *SmoA1;Bmi1*$^{-/-}$ animals, respectively. Areas of higher magnification are indicated by black boxes on low power images. (B) Schematic representation of proposed model showing cellular compartments in developing cerebellum and SmoA1-induced tumors. In transgenic mice expressing SmoA1, tumors arise within the EGL and undergo progressive expansion, leading to death within 10 to 12 weeks. The presence of a small focus of tumor-like cells in a P18 *SmoA1;Bmi1*$^{-/-}$ mouse, with ectopic cells observed in a similar location in P21 *SmoA1;Bmi1*$^{-/-}$ animals, argues that medulloblastoma formation is initiated in the absence of Bmi1, but subsequent tumor development is arrested. (C) Comparison of total volumes of medulloblastomas (*SmoA1;Bmi1*$^{+/+}$) and ectopic cells/abortive tumors (*SmoA1;Bmi1*$^{-/-}$) at P21 (N=3). Error bars indicate range; * indicates statistically significant difference (P=0.0044).

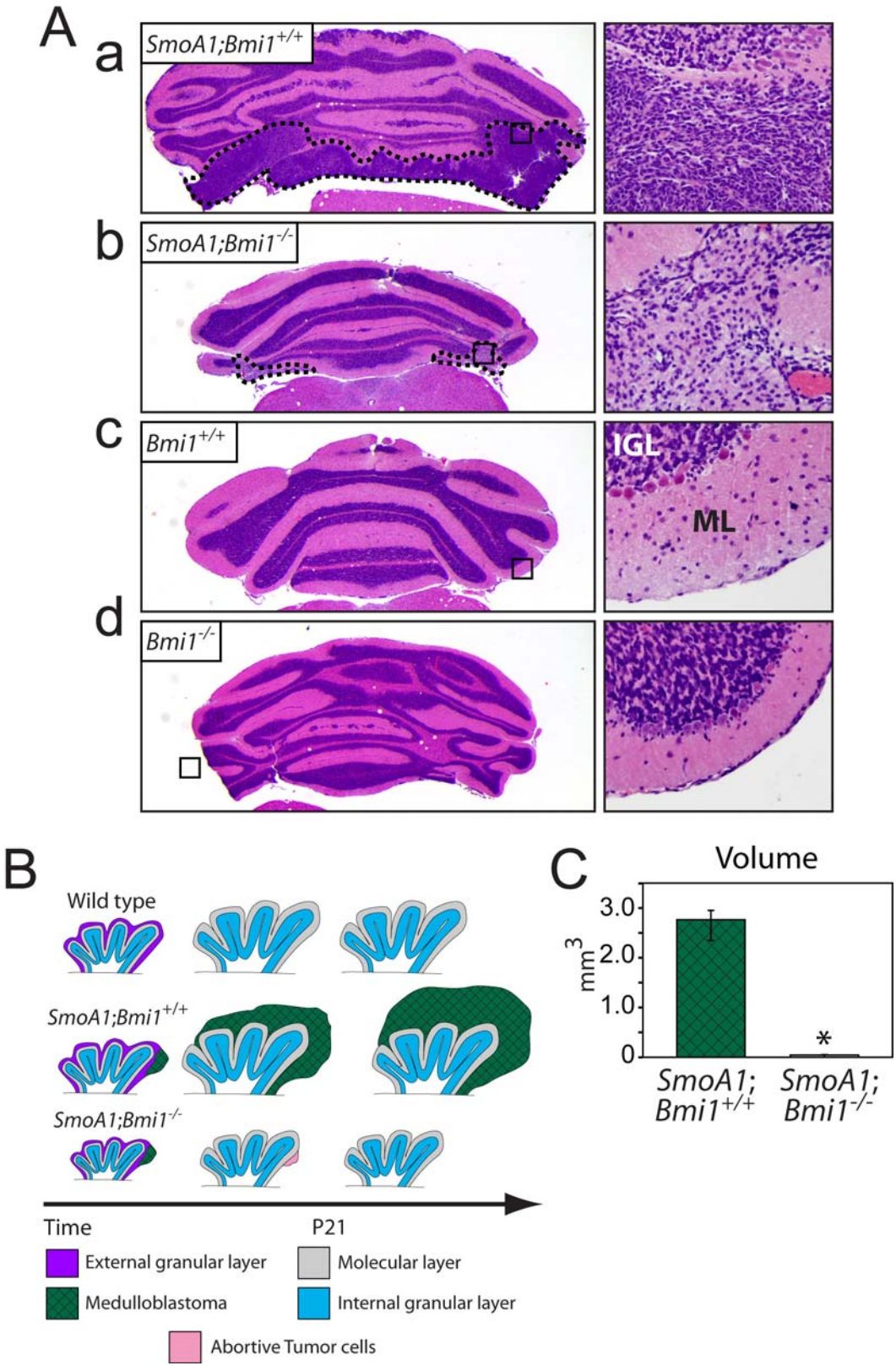
A
a
SmoA1;Bmi1+/+
b
SmoA1;Bmi1-/-
c
Bmi1+/+
IGL
ML
d
Bmi1-/-
B
Wild type
SmoA1;Bmi1+/+
SmoA1;Bmi1-/-
Time
P21
External granular layer
Molecular layer
Medulloblastoma
Internal granular layer
Abortive Tumor cells
C
Volume
mm3
3.0
2.0
1.0
0
*
SmoA1; Bmi1+/+
SmoA1; Bmi1-/-

Figure 4-7. Cell death and cell cycle marker expression in *SmoA1;Bmi1*$^{+/+}$ medulloblastomas and *SmoA1;Bmi1*$^{-/-}$ ectopic cells. (A) Immunohistochemical staining for transgene, apoptosis and proliferation in P21 mice, with outer edge of molecular layer, when visible, outlined with dotted black line. (a) HA-tagged SmoA1 is detected in *SmoA1* tumors and ectopic lesions in *SmoA1*;*Bmi1*$^{-/-}$ mice, as well as scattered cells in the molecular layer and internal granular later, but not in control (Wild Type) cerebellum. (b) TUNEL staining reveals apoptosis in both tumors and ectopic cells. (c) High proliferation rate of the tumors is evident from PCNA staining of the majority of tumor cells, while only a few cells stain in the lesions of *SmoA1*;*Bmi1*$^{-/-}$ mice. (B) Cell cycle marker expression in P21 mice, with outer edge of molecular layer, when visible, outlined with dotted black line. (a) Tumors express high levels of Bmi1 in nearly every cell. Bmi1 is also appreciable in cells of the molecular layer and internal granular layer of wild-type cerebellum. No Bmi1 is detected in tissue from *SmoA1*;*Bmi1*$^{-/-}$ mice. (b) p19^{Arf} is expressed in ectopic cells, and essentially undetectable within medulloblastomas. Higher magnification (inset) demonstrates nucleolar staining. (c) Cyclin D1 is broadly expressed in medulloblastomas, but is virtually absent from *Bmi1*-deficient lesions. (C) Apoptosis (% TUNEL-positive cells) is significantly higher in *SmoA1*;*Bmi1*$^{-/-}$ lesions and proliferation (% PCNA-positive cells) is significantly lower (D) (N=3). Error bars indicate range; * indicates significant differences at P = 0.028 (TUNEL) and P=7.5 x 10^{-6} (PCNA).

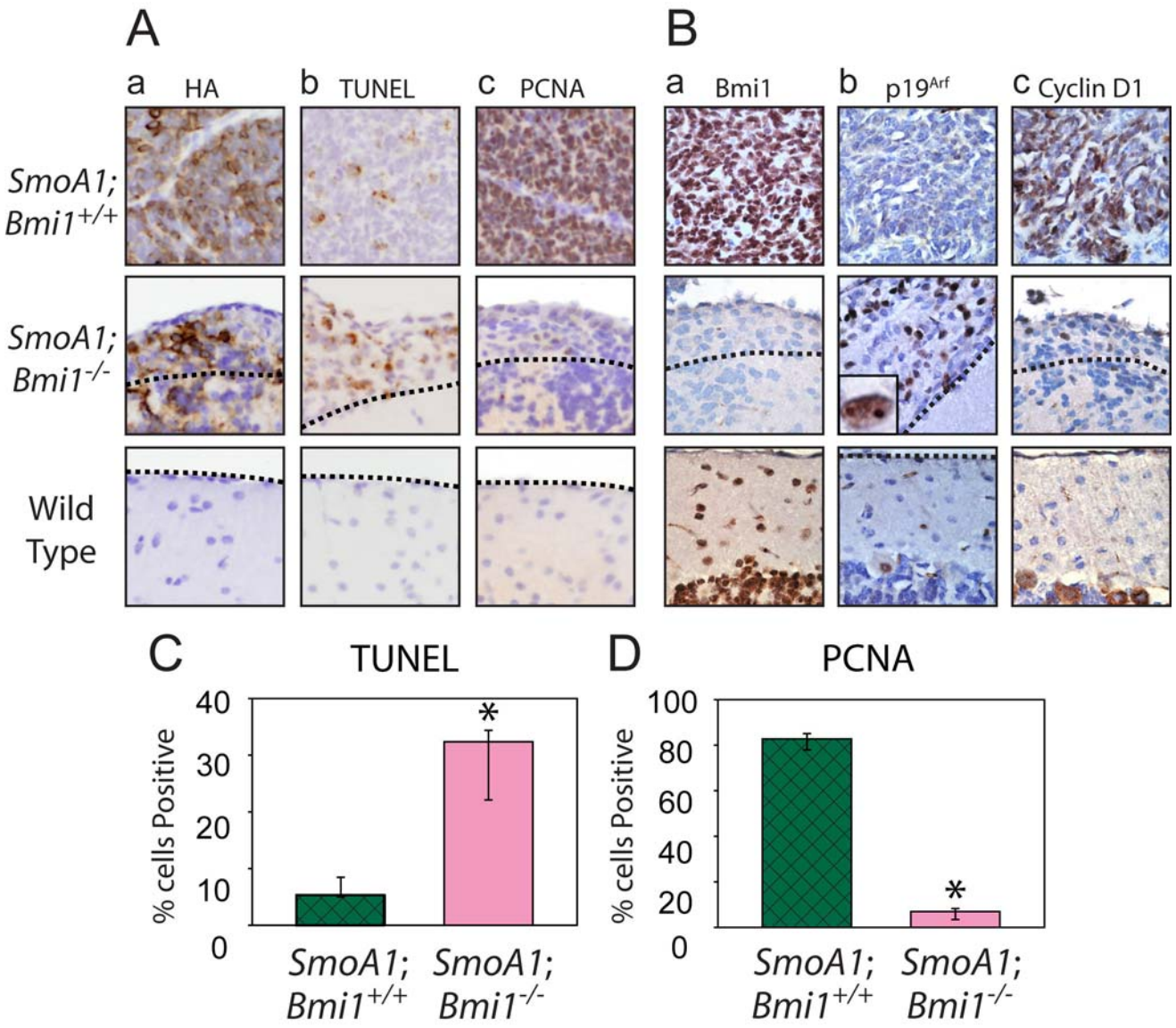
A
a HA
b TUNEL
c PCNA
B
a Bmi1
b p19Arf
c Cyclin D1
SmoA1; Bmi1+/+
SmoA1; Bmi1-/-
Wild Type
C
TUNEL
% cells Positive
40
30
20
10
0
*
SmoA1; Bmi1+/+
SmoA1; Bmi1-/-
D
PCNA
% cells Positive
100
80
60
40
20
0
*
SmoA1; Bmi1+/+
SmoA1; Bmi1-/-

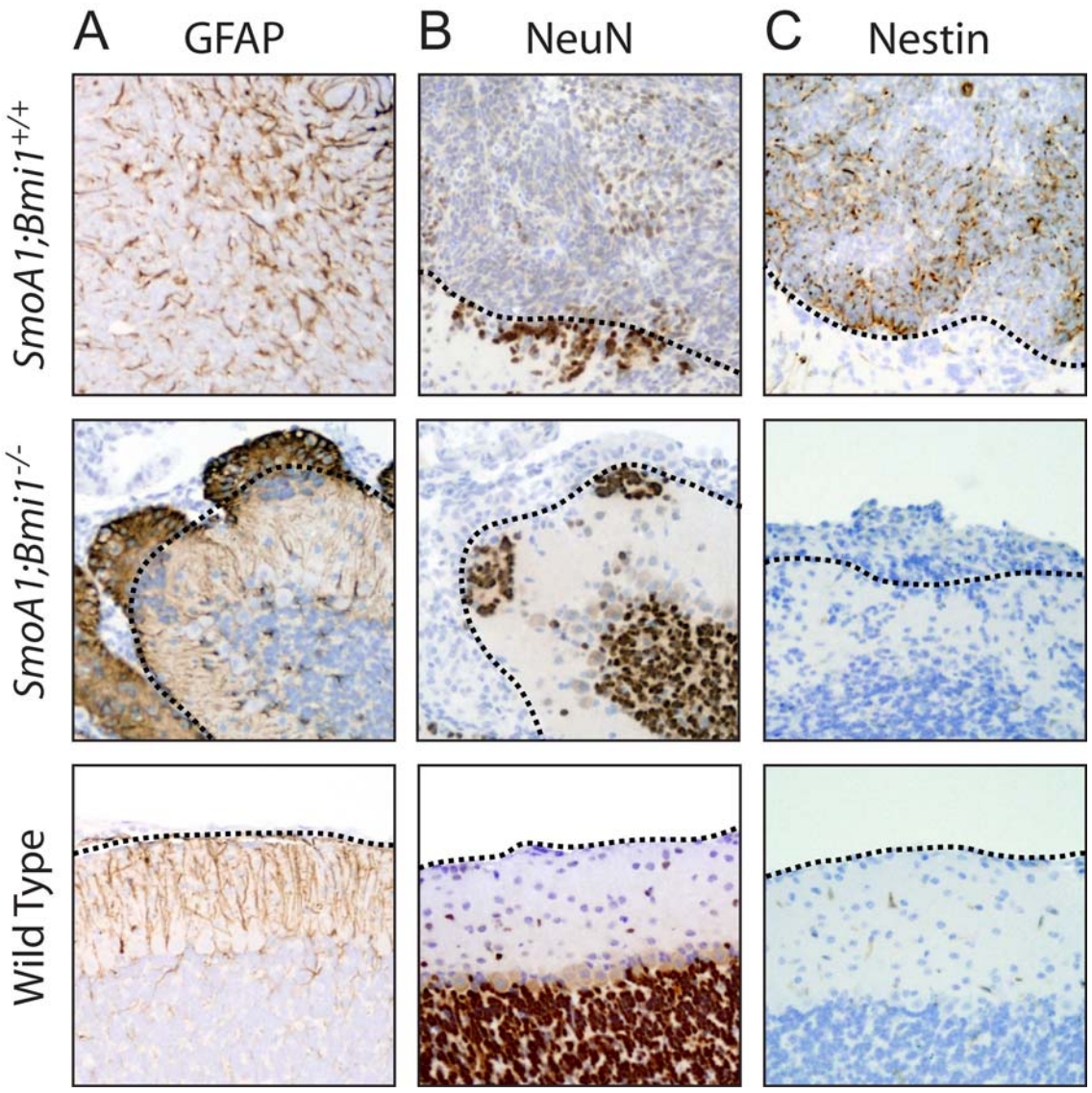

Figure 4-8. Differentiation marker expression in *SmoA1;Bmi1*$^{+/+}$ medulloblastomas and *SmoA1;Bmi1*$^{-/-}$ ectopic cells. (A-C) Immunohistochemical staining of tissue from P21 mice, with outer edge of molecular layer, when visible, outlined with dotted black line. (A) Intense immunostaining for the glial marker GFAP is seen in the ectopic cells of *SmoA1*;*Bmi1*$^{-/-}$ mice. Weaker GFAP immunostaining can be appreciated in cells scattered throughout the tumor of *SmoA1* mice, and in the molecular layer in all mice. (B) Weak expression of the neuronal marker NeuN is detected in scattered cells within medulloblastoma, but not abortive tumors. In addition, strongly NeuN positive clusters, representing aberrant collections of neurons, are evident within the outer molecular layers of both *SmoA1* and *SmoA1*;*Bmi1*$^{-/-}$ mice, but not control mice. NeuN-positive neurons are appreciable in the expected location in the internal granular layer of all mice. (C) Expression of the stem and progenitor cell marker nestin is appreciable in *SmoA1* tumors, but is largely undetectable in lesions in *SmoA1*;*Bmi1*$^{-/-}$ mice.

Tumor initiation, but not expansion, is evident in *SmoA1;Bmi1*$^{-/-}$ mice

In addition to our findings in P21 and P26 animals described above, we also examined *SmoA1*;*Bmi1*$^{-/-}$ mice at an earlier time point. While one of two P18 *SmoA1*;*Bmi1*$^{-/-}$ mice was similar to P21 mice, the other P18 *SmoA1*;*Bmi1*$^{-/-}$ mouse contained a small focus of cells with properties intermediate between medulloblastomas and ectopic foci seen in *SmoA1*;*Bmi1*$^{-/-}$ mice at P21. This intermediate lesion was much thinner than age-matched *SmoA1*;*Bmi1*$^{+/+}$ medulloblastoma (Fig. 4-9 A). While the abortive *SmoA1*;*Bmi1*$^{-/-}$ tumor-like lesion was proliferative, fewer cells stained for PCNA and Cyclin D1 than in *Bmi1*$^{+/+}$ tumor, and expression of p19^{Arf} was elevated (Fig. 4-9 B, C, D). Increased GFAP immunostaining was seen at the periphery of this lesion, as well (Fig. 4-10 A). In keeping with what is seen at P21, there is a marked reduction in nestin staining in the *Bmi1*-deficient lesion and an alteration in its subcellular distribution, including the appearance of large, round, nestin-positive cells (Fig. 4-10 B). These distinctive cells, which are never seen in wild-type control or *SmoA1*;*Bmi1*$^{+/+}$ mice, are detected both in regions of ectopic cells and in the molecular layer of 18-day-old and, to a lesser extent, 21-day-old animals, but are absent by postnatal day 26 (data not shown). Immunohistochemical data from all animals are summarized in Table 4-1.

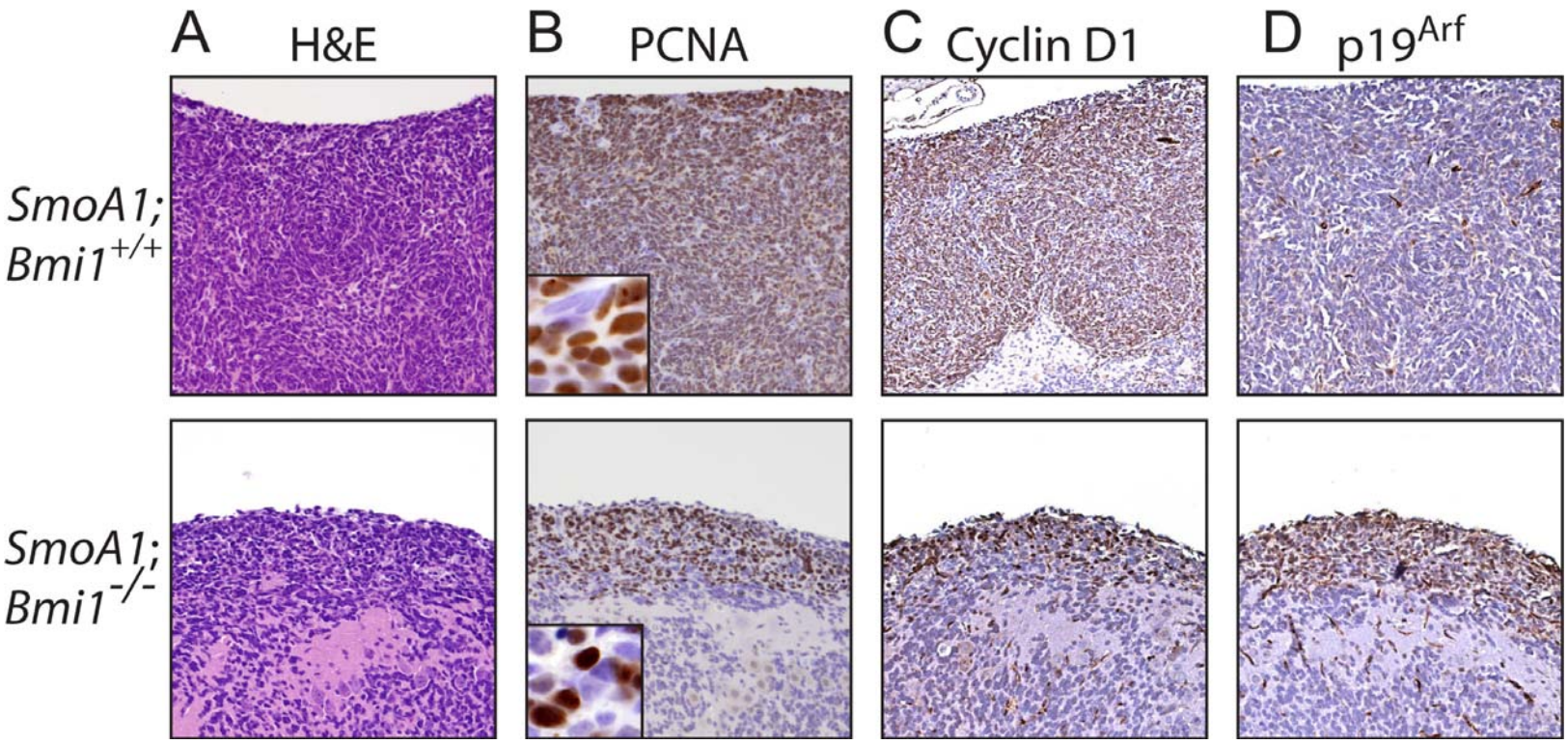

Figure 4-9. Cell cycle marker expression in tumor-like focus in P18 *SmoA1;Bmi1*$^{-/-}$ cerebellum versus medulloblastoma in *SmoA1;Bmi1*$^{+/+}$ mice. (A) Hematoxylin and eosin staining of medulloblastoma (P18 *SmoA1*) and intermediate lesion (P18 *SmoA1*;*Bmi1*$^{-/-}$). Histological appearance of intermediate tumor-like lesion is similar to full-blown tumor, but the lesion is notably smaller. Shown in this image is the ectopic region with the maximal cross-sectional area. (B) PCNA stains both tumor and intermediate *Bmi1*$^{-/-}$ tumor-like focus, but stains fewer cells in the *Bmi1*-deficient lesion. Insets show higher magnification. Cyclin D1 expression is reduced (C) and p19^{Arf} is elevated (D) in the *SmoA1*;*Bmi1*$^{-/-}$ lesion.

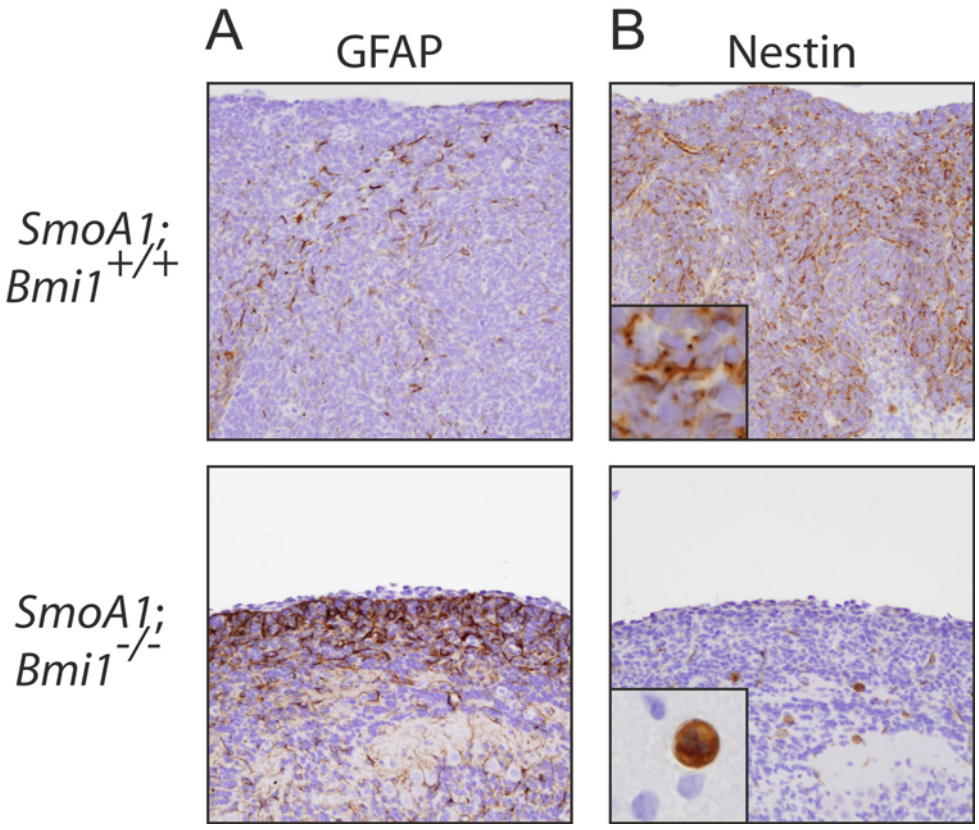

Figure 4-10. Increased GFAP expression and loss of nestin expression in P18 *SmoA1;Bmi1*$^{-/-}$ tumor-like lesion. (A) GFAP is detected in the outer region of the P18 *SmoA1*;*Bmi1*$^{-/-}$ tumor-like lesion, similar to the pattern seen in the ectopic regions of P21 animals. (B) Marked reduction of nestin positive cells and alteration of subcellular nestin distribution is appreciable in *SmoA1*;*Bmi1*$^{-/-}$ mice at P18. Insets show higher magnification of tumor (*SmoA1;Bmi1*$^{+/+}$) or molecular layer (*SmoA1*;*Bmi1*$^{-/-}$).

	***SmoA1;Bmi1*$^{+/+}$**	***SmoA1;Bmi1*$^{-/-}$**			
Age	**P14 and older**	**P18** (8940) *	**P18** (8941)	**P21** (8021, 132-3.2, 135-3.5)	**P26** (8221)
H&E †	Medulloblastoma	Medulloblastoma-like focus	Abortive tumor cells	Abortive tumor cells	Normal
PCNA	++++	+++	+	+	NA§
Cyclin D1	++++	+++	+	+	NA
Nestin	+++	+	-	-	NA
Nestin (large, round cells) ‡	-	++	++	+	-
NeuN (lesions)	+	+	-	-	NA
NeuN (clusters in molecular layer)	+	+	+	+	-
GFAP	+	++	++++	++++	NA
p19	+/-	+	++	++	NA

* Numbers in parentheses are animal identifiers.
† H&E histology refers specifically to any unexpected cell populations outside of the molecular layer.
‡ At P18, these distinctive cells were detected both in ectopic regions and molecular layer (Fig. 4-9); at P21, detected only in molecular layer.
§ NA = not analyzed, since ectopic cells were not detected at P26.

Table 4-1. Histology and immunophenotyping summary of cerebella from SmoA1-expressing wild-type and *Bmi1*$^{-/-}$ mice.

Summary

By exploring the consequences of *Bmi1* deficiency *in vitro* and *in vivo,* we tested the hypothesis that *Bmi1* is required for keratinocyte proliferation and repeated induction of hair cycling. Our results suggest a role for *Bmi1* in colony forming ability, proliferation rate and total proliferative potential of keratinocytes isolated from both newborn and adult animals. Furthermore, we observed a defect in hair follicle regeneration and pigmentation that worsens as animals age, suggesting a role for *Bmi1* not only in epithelial cell function, but also in the melanocyte lineage. Although additional studies will be needed to rigorously test whether there are alterations in epithelial and melanocyte stem cell number or function in *Bmi1*-deficient skin, the progressive nature of the follicular and pigmentation defects is in keeping with observations in other organ systems, where loss of *Bmi1* results in progressive post-natal deficits in both hematopoietic and neural stem cells. However, based on the methods employed, we cannot be certain if there is a progressive inhibition of *in vitro* keratinocyte proliferation, as well. This piece of information would be particularly useful in distinguishing between the importance of *Bmi1* in stem cell self renewal and transient amplifying cell proliferation, as *Bmi1* is required for both processes in the hematopoietic system (Lessard *et al.*, 1999, Lessard *et al.*, 2003), but appears to impact committed neural progenitor proliferation in the cerebellum, but not elsewhere in the central and peripheral nervous system (Molofsky *et al.*, 2003, Leung *et al.*, 2004).

By utilizing *Bmi1*$^{-/-}$ mice in concert with our robust, short-latency *SmoA1*-driven model, we were able to test the hypothesis that *Bmi1* is required for medulloblastoma development. While we detected small, relatively non-proliferative lesions, frank

medulloblastomas never developed in the context of disrupted *Bmi1*, indicating an absolute requirement for this polycomb gene in the pathogenesis of Hh-driven medulloblastoma. While we cannot formally exclude the possibility that failure of *SmoA1*;*Bmi1*$^{-/-}$ mice to develop full-blown medulloblastomas is due to a *Bmi1*-dependent loss of tumor progenitor cells, we do not believe this to be the case. *Bmi1* deficiency impairs Shh-driven proliferation of CGNPs, the likely cell of origin for the medulloblastomas in our model. However, the cerebella of *Bmi1*$^{-/-}$ mice develop relatively normally, despite their smaller size, with formation of the molecular, Purkinje, and internal granular layers, albeit with abnormal basket neuron arborization and reduced molecular layer cellularity (Leung *et al.*, 2004). Moreover, the presence of an intermediate tumor-like lesion in a *SmoA1*;*Bmi1*$^{-/-}$ mouse at P18 strongly argues that tumor initiation can occur.

Taken together, our data demonstrate involvement of Bmi1 in Hh-mediated epithelial stem cell function, establish an obligatory role for Bmi1 in Hh-driven medulloblastoma pathogenesis, provide the first demonstration that Bmi1 is required for *de novo* development of a spontaneously-arising solid tumor, and identify Bmi1 as a critical downstream effector in tumorigenesis driven by uncontrolled Hh-pathway activation. Progression of *SmoA1*-expressing CGNPs to medulloblastoma involves many of the same molecular pathways that regulate physiologic CGNP proliferation and growth arrest, and loss of *Bmi1*, by disrupting these signals, prevents expansion of Hh-driven medulloblastomas. These data raise the exciting possibility that Bmi1 may be required for other physiological or pathological responses to Hh signaling. Basal cell carcinomas, for example, display robust BMI1 expression (Reinisch *et al.*, 2007), suggesting potential

involvement in the development of these tumors. Additionally, further studies will be required to establish whether BMI1 will be a useful target for the prevention or treatment of human malignancy.

Chapter 5

Summary and Future Directions

The Hedgehog pathway is a major developmental regulatory pathway, controlling organogenesis or tissue maintenance in a wide range of tissues (Wicking *et al.*, 1999, Pasca di Magliano *et al.*, 2003). The darker side to the powerful mitogenic capacity of Hh signaling is its well-documented link to cancer development. Alterations in Hh signaling have been found in a variety of tumors in sites as disparate as the lung, pancreas, skin and brain (Pasca di Magliano *et al.*, 2003, Rubin *et al.*, 2006). In this thesis, I have addressed several questions in Hh-driven tumor biology using a novel mouse model that I developed for studying the oncogenic effects of Hh pathway activation via tissue-specific, inducible hyperactivation of Hh signaling. We achieved this by using the constitutively active *SmoA1* allele, mimicking a genetic aberration seen in human HH-driven neoplasia (Xie *et al.*, 1998, Taipale *et al.*, 2000). To generate our mouse model, we placed an HA epitope-tagged *SmoA1* allele under transcriptional control of the tetracycline response element (TRE). With assistance from the University of Michigan transgenic animal core, we generated three independent phenotype-producing lines of *TRE-SmoA1* mice.

Epithelial SmoA1 expression does not induce basal cell carcinomas or hair follicle growth reactivation (anagen)

We first utilized our *TRE-SmoA1* mice to assess the consequences of high-level, proximal activation of the Hh pathway in skin. Dysregulation of HH signaling is the

primary etiologic event in the majority of basal cell carcinomas (BCCs), the most common skin tumor (Bale *et al.*, 2001, Gorlin, 2004). Despite this well-established connection, previous attempts to model BCC development via upstream Hh activation have met with little success. While transgenic mice expressing the distal Hh effectors Gli1 and Gli2 in skin developed robust BCCs with striking similarities to human tumors (Grachtchouk *et al.*, 2000, Nilsson *et al.*, 2000, Hutchin *et al.*, 2005), mice overexpressing *SHH* or *M2SMO*, a mutant *SMO* allele cloned from a human BCC, developed only microscopic lesions at birth or slow-growing tumors that resembled basaloid follicular hamartomas (Oro *et al.*, 1997, Xie *et al.*, 1998, Grachtchouk *et al.*, 2003). Unfortunately, most of the mice from these models died at birth, making it difficult to follow tumor development postnatally. However, mice from the *ΔK5-M2SMO* model, which survived well into adulthood, developed slow-growing basaloid follicular hamartomas, but not BCCs, a phenomenon ascribed to insufficient activation of Hh signaling (Grachtchouk *et al.*, 2003). This raised both the possibility that the *ΔK5* promoter may not activate transgene expression to sufficient levels to induce tumorigenesis and the possibility that the human *M2SMO* allele may be insufficient to drive carcinogenesis in murine epithelium at all.

To address these questions, we crossed *TRE-SmoA1* mice with *K5-tTA* and *K5-rtTA* mice (Diamond *et al.*, 2000), which are known to be sufficient to drive BCC development via *Gli2* overexpression (Hutchin *et al.*, 2005). We observed that double transgenic *K5-tTA;TRE-SmoA1* mice maintained on doxycycline-free chow throughout gestation (SmoA1 transgene "on") were either stillborn or died in the first few hours after birth with significant developmental abnormalities, including distortions of the skin, gut

and limbs. Taking advantage of the conditional nature of our model system, we activated epithelial *SmoA1* expression postnatally in order to test they hypothesis that upstream dysregulation of Hh signaling by constitutively active murine SmoA1 can induce BCCs in adult mice. Following transgene activation, mice developed progressively worsening epithelial phenotype that began with a greasy appearance of the pelage fur and progressed to hair loss and thickening of the skin, with associated appearance of scale. Histological examination of skin from these animals revealed widespread distortion of both follicular structures and interfollicular epidermis, in a pattern quite similar to that seen in the previously characterized *ΔK5-M2SMO* mice. These data are in keeping with the previously described resistance of murine skin to BCC development (Dlugosz *et al.*, 2002), indicating a notable difference between proximal Hh-driven BCC susceptibility in mice and man.

It is somewhat difficult to speculate on the exact nature of this difference. Much of the mechanism involved in trafficking the signal between activated Smo and the Gli transcription factors remains incompletely understood. However, one intriguing possibility comes from the observation that the protein suppressor of fused (Sufu) is a key inhibitory factor in mammalian Hh signaling (Cheng *et al.*, 2002, Merchant *et al.*, 2004, Cooper *et al.*, 2005). Although the deposited sequences of murine and human Sufu proteins are 97% identical (Stone *et al.*, 1999), it is possible that there is differential activity or regulation of the protein in the two species, and that tight Hh pathway control by Sufu plays a role in mediating the resistance of mice to BCC development. Commercial antibodies are available that recognize both human and murine Sufu, and gene sequence data is readily available, facilitating investigation of relative Sufu levels in

human and mouse skin, both in physiologic and pathologic settings, by Western blot and qPCR.

Additionally, *Sufu* mutant mice have been generated, and while *Sufu*$^{-/-}$ mice died *in utero*, *Sufu*$^{+/-}$ mice survived, and developed very slow growing basaloid tumors well over a year after birth (Svärd *et al.*, 2006). When on a *p53*$^{-/-}$ background, however, *Sufu*$^{+/-}$ mice developed medulloblastomas and rhabdomyosarcomas, both of which are linked to Hh pathway dysregulation (Lee *et al.*, 2007). By selective breeding, it would be straightforward to generate *K5-tTA/rtTA;TRE-SmoA1* or even *ΔK5-M2SMO* mice on a *Sufu*$^{+/-}$ background. If these mice develop basal cell carcinomas instead of or in addition to the previously described hamartomas, this would suggest that differential function of *Sufu* at least partially explains the resistance of murine skin to proximal Hh-pathway mediated tumorigenesis.

Proximal and distal Hedgehog pathway activation in induction of brain tumors

I next turned my efforts towards examining the consequences of high level, proximal Hh activation in the brain, work described in Chapter 3. When directly driven by the *NeuroD2* promoter, *SmoA1* was sufficient to induce medulloblastoma formation in approximately 50% of *ND2:SmoA1* transgenic mice, and a higher percentage of homozygous transgenic *SmoA1/SmoA1* mice (Hallahan *et al.*, 2004, Hatton *et al.*, 2008). By employing the *GFAP-tTA* driver mouse, which is sufficient to drive *IFN-γ*-induced medulloblastomas (Lin *et al.*, 2004), I activated *SmoA1* expression in cerebellar granule neuron precursor cells of the developing EGL, resulting in robust, 100% penetrant medulloblastoma development, evident histologically within two weeks of birth. This represents a powerful model for Hh-driven medulloblastoma, allowing us to modulate

transgene expression (and potentially alter tumor development or maintenance) via selective doxycycline treatment.

In order to examine the consequences of complete transgene abrogation in established medulloblastoma, an rtTA ("Tet-on") was required, in order to globally inhibit transgene expression by withholding doxycycline. Because a *GFAP-rtTA* mouse was not available, I combined the rapid induction and de-induction of a *ROSA26*-driven rtTA/TRE system with the permanent, mitotically heritable activation of the Cre-loxP system. To achieve this, I performed multiple rounds of selective mouse breeding to obtain triple transgenic mice positive for *GFAP-Cre*, *R26-X-rtTA*, and *TRE-SmoA1* (Zhuo *et al.*, 2001, Belteki *et al.*, 2005). In these mice, the *GFAP* promoter induces expression of Cre recombinase, resulting in the excision of a strong stop sequence lying between the ubiquitously expressed *ROSA26* promoter and the reverse tetracycline transactivator. The excision is permanent, resulting in activation of *rtTA* expression from the *ROSA26* locus in the *GFAP*-positive cell and all of its progeny, and, in the presence of doxycycline, expression of *SmoA1* in these cells. These mice, when maintained on doxycycline throughout gestation, also developed completely penetrant medulloblastomas apparent within two weeks of birth.

I performed extensive characterization of SmoA1-induced tumors, including analysis of Hh pathway activation and key markers of human medulloblastomas, discovering that they exhibited many similarities to both human medulloblastomas and previously described mouse models. The doxycycline-regulated nature of this transgenic model provided us with a tool to assess the developmental window for medulloblastoma development, an important question in medulloblastoma pathogenesis, particularly with

respect to uncovering the identity of tumor precursor cells. The cell of origin for medulloblastoma has not yet been precisely defined, although many medulloblastomas, particularly those induced by Hh dysregulation, are believed to arise from the committed cerebellar granule neuron precursors of the EGL. The hypothesis that EGL cells serve as a pool of medulloblastoma precursors is supported by several observations. Medulloblastomas are pediatric cerebellar tumors with a bimodal distribution, usually occurring either between 3 and 4 years old or between 8 and 9 years old (Packer *et al.*, 1999). This narrow window of tumor susceptibility in early childhood suggests a transient precursor population, present only early in postnatal development. Both the location and developmental timing of many human medulloblastomas are consistent with a transient precursor cell population on the external surface of the cerebella, such as the EGL . Furthermore, cells within medulloblastomas often express NeuN, a marker for the mature cerebellar neurons which develop from the EGL (Min *et al.*, 2006). Lastly, some medulloblastomas express *Math1*, a key marker for cerebellar EGL cells (Ueba *et al.*, 2008). Work described in this thesis provides additional compelling evidence for the EGL as a pool of Hh-driven medulloblastoma progenitors.

As previously discussed, triple transgenic *GFAP-Cre;R26-X-rtTA;TRE-SmoA1* mice developed robust medulloblastomas when maintained on doxycycline throughout life. These mice also developed tumors when placed on doxycycline treatment at postnatal day 4 or 7. However, when doxycycline treatment is initiated at weaning, by which time the EGL has completely disappeared, animals never developed medulloblastomas, even after extensive duration of transgene expression. Additionally, medulloblastomas from both the double transgenic and triple transgenic models described

in this thesis expressed very high levels of the EGL marker *Math1*, when compared with control adult cerebellum. Furthermore, immunohistochemical examination of 7-day old *GFAP-tTA;TRE-SmoA1* mice revealed scattered expression of SmoA1 in individual cells throughout the EGL, and by postnatal day 14, obvious tumors were evident in the EGL, but only in regions of transgene expression. Taken together, these results provide very strong evidence that Hh-driven medulloblastomas can in fact arise from the EGL. More definitive proof of the EGL as a pool of potential precursors for medulloblastoma could be achieved by using the *tTA-SmoA1* model in concert with the *Math1-CreER*^{T2} (Machold *et al.*, 2005) mouse on a Cre-ROSA reporter background. Treating such mice with tamoxifen several days after birth, when Math1 is highly expressed in the EGL, would permanently activate the lacZ gene in CGNPs and all of their progeny. Demonstration of β-galactosidase activity by X-gal staining in medulloblastomas arising in these mice would lend additional strong support to this hypothesis.

Not all human medulloblastomas are thought to arise from cells of the EGL, however. Human medulloblastoma is a relatively heterogeneous disease, with variations in both histological and immunohistochemical subtype. It is likely that medulloblastomas can arise from several discrete cell types, including both the neuroepithelial cells lining the fourth ventricle, which give rise to the radial glia and stellate, basket, Golgi and Purkinje neurons of the molecular layer, and the CGNPs of the EGL (Marino, 2005, Eberhart, 2007). However, tumors did not appear to arise in any location other than the EGL in our model system. This argues against a causal role for deregulated Hh signaling in the pathogenesis of medulloblastomas arising in adults, and is consistent with the observations that HH pathway-driven medulloblastomas in human patients comprise the

tumors most consistent with having arisen from the EGL (Eberhart, 2007, Packer *et al.*, 2008).

When considering the question of medulloblastoma precursors, an additional potential cell of origin must be considered, as well – the postnatal cerebellar stem cell. The existence of uncommitted, neurosphere-producing stem cells in the cerebellar white matter is a relatively recent discovery (Lee *et al.*, 2005). These CD133+ cells do not express lineage markers, although a subset of them does co-express the stem cell marker nestin. The discovery of CD133+ stem cells in human medulloblastomas (Hemmati *et al.*, 2003, Singh *et al.*, 2003) bolstered the idea that some of these tumors may originate from postnatal cerebellar white matter stem cells, although these CD133+ cells may also arise from de-differentiation of more committed cells.

While the majority of cells within cerebellum-derived neurospheres were GFAP positive (Lee *et al.*, 2005), it is not known if the CD133+ stem cells in our *GFAP*-driven transgenic mice express SmoA1. It would be enlightening to purify CD133+ cerebellar stem cells from our postnatally-activated, non medulloblastoma-bearing transgenic mice via flow cytometry and examine them for SmoA1 expression. If these cells do express SmoA1, the absence of tumor development in postnatally activated *GFAP-tTA;TRE-SmoA1* and *GFAP-Cre;R26-X-rtTA;TRE-SmoA1* mice would indicate that proximal dysregulation of the Hh pathway in cerebellar stem cells is not sufficient to drive medulloblastoma formation. Failure of tumor formation secondary to SmoA1 expression in cerebellar stem cells would be consistent with the observation that CD133+ stem cells are unresponsive to Shh in culture (Lee *et al.*, 2005). This would not, of course, rule out the possibility of these cells serving as precursors to medulloblastoma

secondary to alternate oncogenic insults, such as overexpression of basic fibroblast growth factor, which induces proliferation of these cells (Lee *et al.*, 2005).

When I analyzed the *tTA-SmoA1* transgenic mice, I observed that using the *GFAP* promoter to drive transgene expression resulted in widespread transgene activation. As expected based on the known expression of GFAP in stem cells of the sub-ventricular zone (SVZ) (Zhu *et al.*, 2007), SmoA1 expression was detected in cells in this region. Despite this broad expression of transgene, tumors failed to develop in any locations other than the EGL. I also used the *TRE-Gli2* mouse model, which induces development of BCCs when activated in skin (Hutchin *et al.*, 2005), to activate pathway activity in a distal manner. Somewhat surprisingly, *tTA-Gli2* mice appeared completely normal, with no evidence of tumor development either in the cerebellum or the forebrain, even in mice over one year old. Likewise, postnatally activated *tTA-GLI2** mice, which express an active, repressor domain-deleted form of human GLI2, did not develop histologically detectable tumors arising from the SVZ.

These data are in keeping with a recent report from Galvin *et al.* that demonstrated that high level activation of the Hh pathway resulted in cell cycle arrest or apoptosis in neural stem cells (Galvin *et al.*, 2008). Further analysis will be required to determine whether increased apoptosis and decreased proliferation play a role in the failure of our *SmoA1*-, *Gli2*- or *GLI2**- expressing mice to develop SVZ-derived tumors. These experiments would likely include examination of a larger number of animals and careful quantitative measurement of transgene expression, Hh pathway activation, proliferation and apoptosis in cells of the SVZ. Ideally, these experiments would be performed as time-course experiments, quantifying the above criteria at multiple time

points following transgene activation. The study of transgene expression in *GFAP-tTA;TRE-Gli2* mice, however, would be complicated by the absence of an epitope tag.

In addition to expression of SmoA1 and GLI2* in the EGL and SVZ of our mice, I also observed the expected transgene expression in glial cells throughout the cerebellum and cerebrum. As discussed above, SmoA1 failed to induce tumors from any of these glial cells. Comparative immunostaining and *in situ* hybridization revealed that while SmoA1 expression was widespread in the forebrain, expression of *Ptch1* and *Gli1*, indicating activation of the Hh pathway, was detected only in cells along the SVZ. A clue as to the striking disparity in Hh pathway activation in response to SmoA1 may come from the observation that endogenous Hh pathway activity in the mature forebrain is essentially limited to the cells of the SVZ and SGZ (Ahn *et al.*, 2005, Becher *et al.*, 2008). Hh pathway activation in these regions may reflect endogenous signaling, or may be the result of SmoA1 expression. This raises the possibility that cells which normally respond to Shh express the appropriate intracellular components to transduce the signal, whereas normally non-Shh regulated cells do not. Given that *Ptch1* was not up-regulated in glia response to SmoA1 expression, it appears that any difference in Hh regulatory machinery must lie downstream of Ptch1 and Smo.

The above hypothesis was supported by the development of large numbers of small, proliferative, undifferentiated tumors scattered throughout both the cerebellum and cerebrum of post-natally activated *GFAP-tTA;TRE-GLI2** mice. In these mice, the normal regulatory mechanisms in place between Smo and activated Gli2 are bypassed. Development of these "progenitoromas" driven by GLI2* indicated that high level

activation of the Hh pathway at the most distal level is sufficient to induce a de-differentiation of mature glial cells to a progenitor cell-like phenotype. Conversely, full-length murine Gli2 was not sufficient to induce similar tumors. This raises the possibilities that glial cells either are less well equipped to process full-length Gli2 to its active form or more rapidly degrade full-length Gli2 than Shh-responsive EGL cells. This is consistent with that observation that, in skin, exogenously expressed full-length Gli2 is functionally inactive in the absence of Shh signal (Mill *et al.*, 2003). Experiments designed to address these possibilities may provide us with a deeper understanding of normal Hh regulation, and help clarify the differences between Hh regulation in disparate organs.

Hh signaling in tumor maintenance

Having established a powerful conditional model for robust Hh-driven medulloblastoma development, we were able to ask an important question in tumor biology with potential clinical impact: do Hh-induced medulloblastomas remain "addicted" to the oncogenic Hh stimulus? The translational extension of this question is whether treating medulloblastoma patients with HH antagonists can provide the basis for rational tumor-directed therapy. This is a particularly attractive notion when considering Gorlin syndrome patients, who are unable to tolerate the traditional craniospinal axis radiation therapy without development of massive numbers of BCCs, and would greatly benefit from alternative therapy.

My original efforts focused on the *GFAP-tTA;TRE-SmoA1* mice. I placed these mice on doxycycline treatment administered via chow and water to repress transgene expression at various ages ranging from three to 7 weeks old. In all doxycycline-treated

animals, focal transgene repression was observed. Although this regional blockade of transgene expression was somewhat unexpected, the results were quite encouraging since focal transgene inhibition correlated with focal repression of *Ptch1* and *Gli1* expression, indicating an inhibition of Hh signaling in these regions. Furthermore, this inhibition of Hh activity was linked to a regression of tumor burden in regions of transgene and Hh pathway shutdown. In regions where *SmoA1* expression persisted, tumor burden remained, and *Ptch1* and *Gli1* were detected. These observations support the hypothesis that these tumors remain dependent on Hh signaling for their continued survival. However, I was unable, based on these data, to conclude that Hh inhibition was sufficient to cause complete regression of tumors.

To more effectively address this question, I again exploited the triple transgenic *rtTA-SmoA1* model. The most likely explanation for incomplete *SmoA1* inhibition in *tTA-SmoA1* mice was insufficient delivery of doxycycline to tumor cells. One potential disadvantage of a tTA/TRE based system is the requirement for continued doxycycline delivery to every tTA-expressing cell to completely suppress transgene expression. As an alternate approach, I employed the reverse tetracycline transactivator (rtTA) to drive expression of SmoA1. To this end, we employed the previously established *GFAP-Cre* (Zhuo *et al.*, 2001) and *R26-X-rtTA* (Belteki *et al.*, 2005) mice, as described above.

Tumor regression studies in triple transgenic *rtTA-SmoA1* mice revealed a complete dependence of these tumors on continued Hh activation. Following cessation of doxycycline treatment, tumors completely disappeared within three weeks. Furthermore, this regression was permanent, as tumors never returned, following either long-term cessation of doxycycline treatment or brief periods of doxycycline

discontinuation followed by resumption of doxycycline treatment. Lack of tumor recurrence in this model suggests that all tumor cells either die or terminally differentiate following transgene inhibition, leaving behind no dormant tumor cells with tumorigenic potential. These results are in stark contrast to the persistence of dormant tumor initiating cells and tumor recurrence seen in regressed BCCs from *K5-tTA;TRE-Gli2* mice (Hutchin *et al.*, 2005) and other conditional models (Boxer *et al.*, 2004, Shachaf *et al.*, 2004).

The durable elimination of SmoA1-induced medulloblastomas strongly argues that anti-HH therapy may have an important place in the clinical management of a subset of medulloblastoma patients. Although only 20 – 30% of human medulloblastomas have identifiable mutations in Hh pathway components (Wetmore, 2003, Marino, 2005), a larger fraction demonstrate activation of the pathway, as measured by target gene expression (Hallahan *et al.*, 2004, Leung *et al.*, 2004). It is also known that Hh signaling is involved in murine medulloblastomas not directly driven by Hh dysregulation. For example, tumors induced by interferon-γ up-regulated Shh expression (Lin *et al.*, 2004), and medulloblastomas arising in *Cxcr6*$^{-/-}$ mice not only activated the Hh pathway, but in fact depended on it, responding to Hh antagonist therapy (Sasai *et al.*, 2007). Taken together with our data, these results suggest that anti-Hh therapy may be important in a greater proportion of patients than those with specifically identifiable Hh mutations. However, anti-Hh therapies may require refinement before they reach clinical utility, particularly in young patients, as a recent study demonstrated that even brief treatment of immature mice with the Smo inhibitor HhAntag resulted in permanent defects in bone structure (Kimura *et al.*, 2008).

The data from the regression experiments suggest that, following abrogation of Hh activation, tumors regress due to both decreased proliferation and increased apoptotic activity. One of the most striking changes that occur during regression is the complete loss of nestin-positive cells from regressing tumors. This loss is apparent in both *GFAP-tTA;TRE-SmoA1* and *GFAP-Cre;R26-X-rtTA;TRE*-SmoA1 mice, and in the triple transgenic system occurs within one week of transgene inhibition. Nestin is a marker for stem and progenitor cells (Lendahl *et al.*, 1990), and its expression in relatively few cells scattered throughout the tumors from our models raises the possibility that these cells are tumor stem cells. The fact that nestin-expressing cells are lost before the bulk of the tumor disappears supports this hypothesis. However, additional experiments are needed to confirm the importance of these nestin-positive cells to maintenance of tumors.

The most straightforward approach to directly assess the impact of these putative progenitor-like cells on tumor maintenance would be to specifically ablate nestin-expressing cells from SmoA1-driven tumors. This experiment would be possible to perform by taking advantage of the as-yet unpublished *nestin-tk* mice developed in the laboratory of Dr. Jack Parent here at the University of Michigan (personal communication). These mice express viral thymidine kinase from the *nestin* promoter, and as such, *nestin*-positive cells can be specifically ablated by treating mice with the antiviral drug gancyclovir. If, following gancyclovir treatment, medulloblastomas from SmoA1-expressing, *nestin-tk* mice gradually regress, that will provide confirmation that the crucial cells for maintenance of these tumors are in fact the nestin-positive progenitor cells. If tumors are not impacted by loss of *nestin*-positive cells in this experiment, this

would suggest that these cells do not represent tumor stem or progenitor cells, and would prompt a continued search for such a population.

Alternately, rather than ablating *nestin*+ cells, permanently labeling *nestin*+ cells and their progeny would facilitate tracking their behavior within tumors. By treating *tTA-SmoA1;nestin-CreER(T2);ROSA26R* mice (Lagace *et al.*, 2007) with tamoxifen after tumor formation, the behavior of *nestin*+ tumor cells could be followed over time. If these cells truly represent medulloblastoma stem or progenitor cells, a continually-increasing proportion of the tumors should stain with X-gal. Purification of *nestin*+ cells from *tTA-SmoA1;nestin-GFP* tumors (Mignone *et al.*, 2004) by flow cytometry would facilitate investigation of the tumor stem cell potential of these cells in grafting studies and *in vitro* tumor stem cell assays.

Bmi1 in epithelial maintenance and medulloblastoma progression

The final questions we asked in the course of this work involved the function of the polycomb group gene *Bmi1* in maintenance of normal epithelium and development of Hh-driven medulloblastoma. *Bmi1* mediates stem cell self renewal or committed progenitor proliferation in multiple tissues, and is required for development of full-blown, serially transplantable murine leukemia and maintenance of breast cancer stem cells and gliomas (Lessard *et al.*, 2003, Molofsky *et al.*, 2003, Park *et al.*, 2003, Liu *et al.*, 2006b, Bruggeman *et al.*, 2007). Furthermore, RNAi-mediated knockdown of *BMI1* induced cell cycle arrest and death of numerous cancer cell lines, but not normal cell lines (Liu *et al.*, 2006a), suggesting a requirement for *BMI1* in a wide range of tumors.

Our *in vitro* assays suggested that appropriate expression of *Bmi1* is required for the maintenance of epithelial cells, and that *Bmi1* controls the replicative lifespan of

epithelial stem or transient amplifying cells. Repeated forced reactivation of hair cycling revealed a progressive defect in the capacity of *Bmi1*$^{-/-}$ follicles to re-enter the active anagen growth phase, a functional measure of follicular stem cell capacity. Additionally, aged *Bmi1*$^{-/-}$ mice displayed a general loss of pigmentation, as their coat color faded to a light brown, rather than the dark black color seen at birth. More impressive was the loss of pigmentation seen in regions of repeatedly depilated skin, in which many of the individual hair shafts were entirely amelanotic following two rounds of depilation. One interpretation of these results suggests a heretofore unknown role for *Bmi1* in melanocyte stem cell maintenance, which could be confirmed both by *in vitro* analysis of *Bmi1*$^{-/-}$ melanocyte stem cell self-renewal and by careful analysis of melanocyte numbers in aging or depilated *Bmi1*$^{-/-}$*;Dct-lacZ* melanocyte reporter mice (Mackenzie *et al.*, 1997). Given the early lethality of conventional *Bmi1*$^{-/-}$ mice, conditional deletion of *Bmi1* in the melanocyte lineage will be required to study this phenotype further and determine whether it reflects a cell-autonomous requirement for Bmi1 in melanoblasts, and examine the interaction between *Bmi1* and other key molecules involved in melanogenesis (reviewed in (Lin *et al.*, 2007)). Targeted deletion or knock-down of Bmi1 in cutaneous keratinocytes will similarly be important in examining the function of Bmi1 in epidermal and hair follicle homeostasis, and tumorigenesis (see below).

While our understanding of the requirement for *Bmi1* in epithelial and melanocyte lineages in skin is still in its early stages, its role in the developing cerebellum has been more thoroughly defined. In the absence of *Bmi1*, cerebellar granule neuron precursors of the EGL, the proposed cell of origin for medulloblastomas in our model, exhibit impaired proliferation in response to Shh stimulation, giving rise to

hypomorphic cerebella with decreased IGL area (Leung *et al.*, 2004). *Bmi1* itself is a downstream target of Hh signaling in the normal developing cerebellum, and BMI1 expression in medulloblastomas appears to be correlated with activation of the HH pathway (Leung *et al.*, 2004). Taken together, these data suggest an important role for Bmi1 in Hh-mediated medulloblastoma development.

To test this hypothesis, I performed selective breeding experiments to generate *GFAP-tTA;TRE-SmoA1* mice on a *Bmi1*-null background (designated *SmoA1;Bmi1*$^{-/-}$). In striking contrast to the complete tumor penetrance in *SmoA1;Bmi1* wt mice, none of the SmoA1-expressing *Bmi1*$^{-/-}$ mice developed full-blown medulloblastoma. At 21 days old, *SmoA1;Bmi1*$^{-/-}$ mice harbored small, loosely packed presumptive abortive tumor lesions which were significantly more apoptotic and less proliferative than *Bmi1* wild-type tumors. An intermediate lesion was detected in a P18 *SmoA1;Bmi1*$^{-/-}$ mouse, displaying proliferative activity and cell cycle marker expression midway between tumors and P21 abortive lesions. The observation of an early intermediate tumor-like lesion, 21 day old abortive lesions, and a lack of detectable ectopic tissue in a 26 day old mouse strongly argues for medulloblastoma initiation, but not progression, in the absence of *Bmi1*.

These data provide the first demonstration of the importance of *Bmi1* in spontaneous solid tumor development. The link between the Hh pathway and *Bmi1* both in normal cerebellar development and in medulloblastoma pathogenesis suggest a role for *Bmi1* in other Hh-mediated malignancies, such as BCCs, which are known to express BMI1 (Reinisch *et al.*, 2007). To test this hypothesis, it would be necessary to generate BCC-susceptible mice on a *Bmi1*$^{-/-}$ background. As I observed during the course of the experiments discussed in Chapter 5, it can be very difficult to obtain *Bmi1*$^{-/-}$ mice on a

tumor-bearing background, particularly when four individual alleles must be coordinated. As such, for practical reasons, a single-transgenic BCC model such as the *K5-Gli2* mouse would be most appropriate to use. Any such experiments would be complicated by the shortened lifespan of *Bmi1*$^{-/-}$ mice, however, which rarely survive past several months of age. Although several animals in our repeated depilation experiments survived for significantly longer, this is uncommon, and cannot be relied upon for robust, reproducible tumor modeling experiments.

To overcome this obstacle, grafting studies could be employed. By grafting full-thickness epithelia from *K5-Gli2* and *K5-Gli2;Bmi1*$^{-/-}$ newborn pups onto the flanks of immune-deficient mice, it would be possible to bypass the early lethality of *Bmi1*$^{-/-}$ mice and observe the long-term tumor formation potential of epithelial Hh pathway activation in the absence of *Bmi1*. As an alternative to grafting studies, development of conditional, Cre-mediated *Bmi1* knockout mice would allow for skin-specific postnatal ablation of *Bmi1* using tamoxifen-inducible *K5-Cre-ER*^{T2} or *K14-Cre-ER*^{tam} mice (Vasioukhin *et al.*, 1999, Kataoka *et al.*, 2008). Because systemic *Bmi1* expression would be preserved in these mice, they may not exhibit the shortened lifespan characteristic of *Bmi1*$^{-/-}$ mice, allowing them to survive past the latency period for *in situ* development of BCCs driven by *K5-Gli2*. If *Bmi1*-null skin in either of these experiments were to exhibit impaired BCC development when compared to *K5-Gli2;Bmi1* wild type skin, this would imply a more general role of *Bmi1* in Hh-driven tumors, which includes malignancies in a broad variety of organs.

Summary

In this thesis, I have described the use of a novel mouse model to examine the consequences of proximal dysregulation of the Hh pathway in the epithelium and the brain. I observed that activation of SmoA1 in epithelial basal cells and hair follicles did not result in BCC development, whereas expression within the EGL of developing cerebella induced aggressive medulloblastoma formation with complete penetrance, revealing a striking disparity in tumorigenic response between these two populations. Furthermore, comparing the tumorigenic potential of proximal versus distal Hh pathway activation in the brain suggested the existence of a strong Hh-inhibitory signal in mature glia, somewhere between the level of Smo and the level of activated Gli2. While further experiments will be required to fully understand the implications of these results, they provide exciting glimpses into the biology of Hh signaling.

I also exploited the conditional nature of our medulloblastoma model to demonstrate a potential clinical application for Hh inhibition in medulloblastoma therapy. Our data revealed that brief interruption of pathologic levels of Hh signaling was sufficient to achieve complete, durable elimination of medulloblastomas, without evidence of dormant tumor initiating cells – in effect curing mice of this devastating disease, even after resumption of transgene expression. While murine models and human patients are of course different in many ways, the results presented herein paint a very encouraging picture of a potential therapeutic avenue for the most common pediatric brain malignancy.

Lastly, I explored the contribution of a known stem cell maintenance gene to epithelial maintenance and medulloblastoma development. Our data suggest an impact of *Bmi1* deficiency on keratinocyte stem cell function *in vitro* and *in vivo*, and point to a role

for *Bmi1* in melanocyte stem cells, as well. Furthermore, I demonstrated an absolute requirement for *Bmi1* in progression, but not initiation, of Hh-driven medulloblastomas. This requirement, together with the observation of nestin-positive cells throughout *Bmi1* wild-type tumors, suggested the existence of a tumor stem cell population within Hh-driven medulloblastomas. If, with additional experiments, *Bmi1* dependence can be generalized to other Hh-driven tumor types, this would provide an important insight into, and suggest an additional potential therapeutic target for, a wide range of human malignancies.

References

Adesina, A.M., J. Nalbantoglu and W.K. Cavenee. 1994. p53 gene mutation and mdm2 gene amplification are uncommon in medulloblastoma. *Cancer Res* **54:** 5649-5651.

Ahn, S. and A.L. Joyner. 2005. In vivo analysis of quiescent adult neural stem cells responding to Sonic hedgehog. *Nature* **437:** 894-897.

Allen, M., M. Grachtchouk, H. Sheng, V. Grachtchouk, A. Wang, L. Wei, J. Liu, A. Ramirez, D. Metzger, P. Chambon, J. Jorcano and A.A. Dlugosz. 2003. Hedgehog signaling regulates sebaceous gland development. *Am J Pathol* **163:** 2173-2178.

Apionishev, S., N.M. Katanayeva, S.A. Marks, D. Kalderon and A. Tomlinson. 2005. Drosophila Smoothened phosphorylation sites essential for Hedgehog signal transduction. *Nat Cell Biol* **7:** 86-92.

Argenti, B., R. Gallo, L. Di Marcotullio, E. Ferretti, M. Napolitano, S. Canterini, E. De Smaele, A. Greco, M.T. Fiorenza, M. Maroder, I. Screpanti, E. Alesse and A. Gulino. 2005. Hedgehog antagonist REN(KCTD11) regulates proliferation and apoptosis of developing granule cell progenitors. *J Neurosci* **25:** 8338-8346.

Aszterbaum, M., J. Epstein, A. Oro, V. Douglas, P.E. LeBoit, M.P. Scott and E.H. Epstein, Jr. 1999. Ultraviolet and ionizing radiation enhance the growth of BCCs and trichoblastomas in patched heterozygous knockout mice. *Nat Med* **5:** 1285-1291.

Athar, M., X. Tang, J.L. Lee, L. Kopelovich and A.L. Kim. 2006. Hedgehog signalling in skin development and cancer. *Exp Dermatol* **15:** 667-677.

Bai, C.B., W. Auerbach, J.S. Lee, D. Stephen and A.L. Joyner. 2002. Gli2, but not Gli1, is required for initial Shh signaling and ectopic activation of the Shh pathway. *Development* **129:** 4753-4761.

Bale, A.E. 2000. Cancer: Sheep, lilies and human genetics. *Nature* **406:** 944-945.

Bale, A.E. and K.P. Yu. 2001. The hedgehog pathway and basal cell carcinomas. *Hum Mol Genet* **10:** 757-762.

Becher, O.J., D. Hambardzumyan, E.I. Fomchenko, H. Momota, L. Mainwaring, A.M. Bleau, A.M. Katz, M. Edgar, A.M. Kenney, C. Cordon-Cardo, R.G. Blasberg and

E.C. Holland. 2008. Gli activity correlates with tumor grade in platelet-derived growth factor-induced gliomas. *Cancer Res* **68:** 2241-2249.

Belteki, G., J. Haigh, N. Kabacs, K. Haigh, K. Sison, F. Costantini, J. Whitsett, S.E. Quaggin and A. Nagy. 2005. Conditional and inducible transgene expression in mice through the combinatorial use of Cre-mediated recombination and tetracycline induction. *Nucleic Acids Res* **33:** e51.

Berman, D.M., S.S. Karhadkar, A.R. Hallahan, J.I. Pritchard, C.G. Eberhart, D.N. Watkins, J.K. Chen, M.K. Cooper, J. Taipale, J.M. Olson and P.A. Beachy. 2002. Medulloblastoma growth inhibition by hedgehog pathway blockade. *Science* **297:** 1559-1561.

Bhatia, N., S. Thiyagarajan, I. Elcheva, M. Saleem, A. Dlugosz, H. Mukhtar and V.S. Spiegelman. 2006. Gli2 Is Targeted for Ubiquitination and Degradation by beta-TrCP Ubiquitin Ligase. *J. Biol. Chem.* **281:** 19320-19326.

Booth, D.R. 1999. The hedgehog signalling pathway and its role in basal cell carcinoma. *Cancer Metastasis Rev* **18:** 261-284.

Boxer, R.B., J.W. Jang, L. Sintasath and L.A. Chodosh. 2004. Lack of sustained regression of c-MYC-induced mammary adenocarcinomas following brief or prolonged MYC inactivation. *Cancer Cell* **6:** 577-586.

Bruggeman, S.W., M.E. Valk-Lingbeek, P.P. van der Stoop, J.J. Jacobs, K. Kieboom, E. Tanger, D. Hulsman, C. Leung, Y. Arsenijevic, S. Marino and M. van Lohuizen. 2005. Ink4a and Arf differentially affect cell proliferation and neural stem cell self-renewal in Bmi1-deficient mice. *Genes Dev* **19:** 1438-1443.

Bruggeman, S.W., D. Hulsman, E. Tanger, T. Buckle, M. Blom, J. Zevenhoven, O. van Tellingen and M. van Lohuizen. 2007. Bmi1 controls tumor development in an ink4a/arf-independent manner in a mouse model for glioma. *Cancer Cell* **12:** 328-341.

Casey, B. and B.P. Hackett. 2000. Left-right axis malformations in man and mouse. *Curr Opin Genet Dev* **10:** 257-261.

Chen, W., X.R. Ren, C.D. Nelson, L.S. Barak, J.K. Chen, P.A. Beachy, F. de Sauvage and R.J. Lefkowitz. 2004. Activity-dependent internalization of smoothened mediated by beta-arrestin 2 and GRK2. *Science* **306:** 2257-2260.

Cheng, S.Y. and J.M. Bishop. 2002. Suppressor of Fused represses Gli-mediated transcription by recruiting the SAP18-mSin3 corepressor complex. *Proc Natl Acad Sci U S A* **99:** 5442-5447.

Chiang, C., Y. Litingtung, E. Lee, K.E. Young, J.L. Corden, H. Westphal and P.A. Beachy. 1996. Cyclopia and defective axial patterning in mice lacking Sonic hedgehog gene function. *Nature* **383:** 407-413.

Chiang, C., R.Z. Swan, M. Grachtchouk, M. Bolinger, Y. Litingtung, E.K. Robertson, M.K. Cooper, W. Gaffield, H. Westphal, P.A. Beachy and A.A. Dlugosz. 1999. Essential role for Sonic hedgehog during hair follicle morphogenesis. *Dev Biol* **205:** 1-9.

Chin, L., A. Tam, J. Pomerantz, M. Wong, J. Holash, N. Bardeesy, Q. Shen, R. O'Hagan, J. Pantginis, H. Zhou, J.W. Horner, 2nd, C. Cordon-Cardo, G.D. Yancopoulos and R.A. DePinho. 1999. Essential role for oncogenic Ras in tumour maintenance. *Nature* **400:** 468-472.

Chintagumpala, M., S. Berg and S.M. Blaney. 2001. Treatment controversies in medulloblastoma. *Curr Opin Oncol* **13:** 154-159.

Chuang, P.T. and T.B. Kornberg. 2000. On the range of hedgehog signaling. *Curr Opin Genet Dev* **10:** 515-522.

Claudinot, S., M. Nicolas, H. Oshima, A. Rochat and Y. Barrandon. 2005. Long-term renewal of hair follicles from clonogenic multipotent stem cells. *Proc Natl Acad Sci U S A* **102:** 14677-14682.

Clement, V., P. Sanchez, N. de Tribolet, I. Radovanovic and A. Ruiz i Altaba. 2007. HEDGEHOG-GLI1 signaling regulates human glioma growth, cancer stem cell self-renewal, and tumorigenicity. *Curr Biol* **17:** 165-172.

Cooper, A.F., K.P. Yu, M. Brueckner, L.L. Brailey, L. Johnson, J.M. McGrath and A.E. Bale. 2005. Cardiac and CNS defects in a mouse with targeted disruption of suppressor of fused. *Development* **132:** 4407-4417.

Corbit, K.C., P. Aanstad, V. Singla, A.R. Norman, D.Y. Stainier and J.F. Reiter. 2005. Vertebrate Smoothened functions at the primary cilium. *Nature* **437:** 1018-1021.

Corcoran, R.B. and M.P. Scott. 2001. A mouse model for medulloblastoma and basal cell nevus syndrome. *J Neurooncol* **53:** 307-318.

Corcoran, R.B. and M.P. Scott. 2006. Oxysterols stimulate Sonic hedgehog signal transduction and proliferation of medulloblastoma cells. *Proc Natl Acad Sci U S A* **103:** 8408-8413.

Corrales, J.D., S. Blaess, E.M. Mahoney and A.L. Joyner. 2006. The level of sonic hedgehog signaling regulates the complexity of cerebellar foliation. *Development* **133:** 1811-1821.

Cui, H., B. Hu, T. Li, J. Ma, G. Alam, W.T. Gunning and H.F. Ding. 2007. Bmi-1 is essential for the tumorigenicity of neuroblastoma cells. *Am J Pathol* **170:** 1370-1378.

D'Cruz, C.M., E.J. Gunther, R.B. Boxer, J.L. Hartman, L. Sintasath, S.E. Moody, J.D. Cox, S.I. Ha, G.K. Belka, A. Golant, R.D. Cardiff and L.A. Chodosh. 2001. c-MYC induces mammary tumorigenesis by means of a preferred pathway involving spontaneous Kras2 mutations. *Nat Med* **7:** 235-239.

Dahmane, N. and A. Ruiz i Altaba. 1999. Sonic hedgehog regulates the growth and patterning of the cerebellum. *Development* **126:** 3089-3100.

Dakubo, G.D., C.J. Mazerolle and V.A. Wallace. 2006. Expression of Notch and Wnt pathway components and activation of Notch signaling in medulloblastomas from heterozygous patched mice. *J Neurooncol* **79:** 221-227.

Di Marcotullio, L., E. Ferretti, E. De Smaele, B. Argenti, C. Mincione, F. Zazzeroni, R. Gallo, L. Masuelli, M. Napolitano, M. Maroder, A. Modesti, F. Giangaspero, I. Screpanti, E. Alesse and A. Gulino. 2004. REN(KCTD11) is a suppressor of Hedgehog signaling and is deleted in human medulloblastoma. *Proc Natl Acad Sci U S A* **101:** 10833-10838.

Diamond, I., T. Owolabi, M. Marco, C. Lam and A. Glick. 2000. Conditional gene expression in the epidermis of transgenic mice using the tetracycline-regulated transactivators tTA and rTA linked to the keratin 5 promoter. *J Invest Dermatol* **115:** 788-794.

Dlugosz, A. 1999. The Hedgehog and the hair follicle: a growing relationship. *J Clin Invest* **104:** 851-853.

Dlugosz, A., G. Merlino and S.H. Yuspa. 2002. Progress in cutaneous cancer research. *J Investig Dermatol Symp Proc* **7:** 17-26.

Dlugosz, A.A., A.B. Glick, T. Tennenbaum, W.C. Weinberg and S.H. Yuspa. 1995. Isolation and utilization of epidermal keratinocytes for oncogene research. *Methods Enzymol* **254:** 3-20.

Eberhart, C.G. 2007. In search of the medulloblast: neural stem cells and embryonal brain tumors. *Neurosurg Clin N Am* **18:** 59-69, viii-ix.

Evangelista, M., H. Tian and F.J. de Sauvage. 2006. The Hedgehog Signaling Pathway in Cancer. *Clin Cancer Res* **12:** 5924-5928.

Ewald, D., M. Li, S. Efrat, G. Auer, R.J. Wall, P.A. Furth and L. Hennighausen. 1996. Time-sensitive reversal of hyperplasia in transgenic mice expressing SV40 T antigen. *Science* **273:** 1384-1386.

Felsher, D.W. and J.M. Bishop. 1999. Reversible tumorigenesis by MYC in hematopoietic lineages. *Mol Cell* **4:** 199-207.

Frank-Kamenetsky, M., X.M. Zhang, S. Bottega, O. Guicherit, H. Wichterle, H. Dudek, D. Bumcrot, F.Y. Wang, S. Jones, J. Shulok, L.L. Rubin and J.A. Porter. 2002. Small-molecule modulators of Hedgehog signaling: identification and characterization of Smoothened agonists and antagonists. *J Biol* **1:** 10.

Galvin, K.E., H. Ye, D.J. Erstad, R. Feddersen and C. Wetmore. 2008. Gli1 Induces G2/M Arrest and Apoptosis in Hippocampal but not Tumor-Derived Neural Stem Cells. *Stem Cells*

Gerdes, M.J. and S.H. Yuspa. 2005. The contribution of epidermal stem cells to skin cancer. *Stem Cell Rev* **1:** 225-231.

Gilbertson, R.J. 2004. Medulloblastoma: signalling a change in treatment. *Lancet Oncol* **5:** 209-218.

Goodrich, L.V., L. Milenkovi, K.M. Higgins and M.P. Scott. 1997. Altered Neural Cell Fates and Medulloblastoma in Mouse patched Mutants. *Science* **277:** 1109-1113.

Gorlin, R.J. 1995. Nevoid basal cell carcinoma syndrome. *Dermatol Clin* **13:** 113-125.

Gorlin, R.J. 2004. Nevoid basal cell carcinoma (Gorlin) syndrome. *Genet Med* **6:** 530-539.

Grachtchouk, M., R. Mo, S. Yu, X. Zhang, H. Sasaki, C.C. Hui and A.A. Dlugosz. 2000. Basal cell carcinomas in mice overexpressing Gli2 in skin. *Nat Genet* **24:** 216-217.

Grachtchouk, V., M. Grachtchouk, L. Lowe, T. Johnson, L. Wei, A. Wang, F. de Sauvage and A.A. Dlugosz. 2003. The magnitude of hedgehog signaling activity defines skin tumor phenotype. *Embo J* **22:** 2741-2751.

Grimmer, M.R. and W.A. Weiss. 2008. BMPs oppose Math1 in cerebellar development and in medulloblastoma. *Genes Dev.* **22:** 693-699.

Gulino, A., L. Di Marcotullio, E. Ferretti, E. De Smaele and I. Screpanti. 2007. Hedgehog signaling pathway in neural development and disease. *Psychoneuroendocrinology* **32:** S52-S56.

Gunther, E.J., S.E. Moody, G.K. Belka, K.T. Hahn, N. Innocent, K.D. Dugan, R.D. Cardiff and L.A. Chodosh. 2003. Impact of p53 loss on reversal and recurrence of conditional Wnt-induced tumorigenesis. *Genes Dev* **17:** 488-501.

Hahn, H., L. Wojnowski, A.M. Zimmer, J. Hall, G. Miller and A. Zimmer. 1998. Rhabdomyosarcomas and radiation hypersensitivity in a mouse model of Gorlin syndrome. *Nat Med* **4:** 619-622.

Hallahan, A.R., J.I. Pritchard, S. Hansen, M. Benson, J. Stoeck, B.A. Hatton, T.L. Russell, R.G. Ellenbogen, I.D. Bernstein, P.A. Beachy and J.M. Olson. 2004. The SmoA1 mouse model reveals that notch signaling is critical for the growth and survival of sonic hedgehog-induced medulloblastomas. *Cancer Res* **64:** 7794-7800.

Hatsell, S. and A.R. Frost. 2007. Hedgehog signaling in mammary gland development and breast cancer. *J Mammary Gland Biol Neoplasia* **12:** 163-173.

Hatten, M.E. 1999. Central nervous system neuronal migration. *Annu Rev Neurosci* **22:** 511-539.

Hatton, B.A., P.S. Knoepfler, A.M. Kenney, D.H. Rowitch, I.M. de Alboran, J.M. Olson and R.N. Eisenman. 2006. N-myc is an essential downstream effector of Shh signaling during both normal and neoplastic cerebellar growth. *Cancer Res* **66:** 8655-8661.

Hatton, B.A., E.H. Villavicencio, K.D. Tsuchiya, J.I. Pritchard, S. Ditzler, B. Pullar, S. Hansen, S.E. Knoblaugh, D. Lee, C.G. Eberhart, A.R. Hallahan and J.M. Olson. 2008. The Smo/Smo model: hedgehog-induced medulloblastoma with 90% incidence and leptomeningeal spread. *Cancer Res* **68:** 1768-1776.

Hayry, V., O. Tynninen, H.K. Haapasalo, J. Wolfer, W. Paulus, M. Hasselblatt, H. Sariola, A. Paetau, S. Sarna, M. Niemela, K. Wartiovaara and N.N. Nupponen. 2008. Stem cell protein BMI-1 is an independent marker for poor prognosis in oligodendroglial tumours. *Neuropathol Appl Neurobiol*

Helms, A.W. and J.E. Johnson. 1998. Progenitors of dorsal commissural interneurons are defined by MATH1 expression. *Development* **125:** 919-928.

Hemmati, H.D., I. Nakano, J.A. Lazareff, M. Masterman-Smith, D.H. Geschwind, M. Bronner-Fraser and H.I. Kornblum. 2003. Cancerous stem cells can arise from pediatric brain tumors. *Proc Natl Acad Sci U S A* **100:** 15178-15183.

Huntzicker, E.G., I.S. Estay, H. Zhen, L.A. Lokteva, P.K. Jackson and A.E. Oro. 2006. Dual degradation signals control Gli protein stability and tumor formation. *Genes Dev.* **20:** 276-281.

Hutchin, M.E., M.S.T. Kariapper, M. Grachtchouk, A. Wang, L. Wei, D. Cummings, J. Liu, L.E. Michael, A. Glick and A.A. Dlugosz. 2005. Sustained Hedgehog signaling is required for basal cell carcinoma proliferation and survival: conditional skin tumorigenesis recapitulates the hair growth cycle. *Genes Dev.* **19:** 214-223.

Itahana, K., Y. Zou, Y. Itahana, J.-L. Martinez, C. Beausejour, J.J.L. Jacobs, M. van Lohuizen, V. Band, J. Campisi and G.P. Dimri. 2003. Control of the Replicative Life Span of Human Fibroblasts by p16 and the Polycomb Protein Bmi-1. *Mol. Cell. Biol.* **23:** 389-401.

Ito, M., K. Kizawa, K. Hamada and G. Cotsarelis. 2004. Hair follicle stem cells in the lower bulge form the secondary germ, a biochemically distinct but functionally equivalent progenitor cell population, at the termination of catagen. *Differentiation* **72:** 548-557.

Jackson, E.L., J.M. Garcia-Verdugo, S. Gil-Perotin, M. Roy, A. Quinones-Hinojosa, S. VandenBerg and A. Alvarez-Buylla. 2006. PDGFR[alpha]-Positive B Cells Are Neural Stem Cells in the Adult SVZ that Form Glioma-like Growths in Response to Increased PDGF Signaling. *Neuron* **51:** 187-199.

Jacobs, J.J., K. Kieboom, S. Marino, R.A. DePinho and M. van Lohuizen. 1999. The oncogene and Polycomb-group gene bmi-1 regulates cell proliferation and senescence through the ink4a locus. *Nature* **397:** 164-168.

Jia, J., C. Tong, B. Wang, L. Luo and J. Jiang. 2004. Hedgehog signalling activity of Smoothened requires phosphorylation by protein kinase A and casein kinase I. *Nature* **432:** 1045-1050.

Kasai, K., M. Takahashi, N. Osumi, S. Sinnarajah, T. Takeo, H. Ikeda, J.H. Kehrl, G. Itoh and H. Arnheiter. 2004. The G12 family of heterotrimeric G proteins and Rho GTPase mediate Sonic hedgehog signalling. *Genes Cells* **9:** 49-58.

Kataoka, K., D.J. Kim, S. Carbajal, J. Clifford and J. Digiovanni. 2008. Stage-specific disruption of Stat3 demonstrates a direct requirement during both the initiation and promotion stages of mouse skin tumorigenesis. *Carcinogenesis*

Kato, K. 1990. Novel GABAA receptor [alpha] subunit is expressed only in cerebellar granule cells. *J Mol Biol* **214:** 619-624.

Kenney, A.M. and D.H. Rowitch. 2000. Sonic hedgehog promotes G(1) cyclin expression and sustained cell cycle progression in mammalian neuronal precursors. *Mol Cell Biol* **20:** 9055-9067.

Kim, J.Y., A.L. Nelson, S.A. Algon, O. Graves, L.M. Sturla, L.C. Goumnerova, D.H. Rowitch, R.A. Segal and S.L. Pomeroy. 2003. Medulloblastoma tumorigenesis diverges from cerebellar granule cell differentiation in patched heterozygous mice. *Dev Biol* **263:** 50-66.

Kimonis, V.E., A.M. Goldstein, B. Pastakia, M.L. Yang, R. Kase, J.J. DiGiovanna, A.E. Bale and S.J. Bale. 1997. Clinical manifestations in 105 persons with nevoid basal cell carcinoma syndrome. *Am J Med Genet* **69:** 299-308.

Kimura, H., D. Stephen, A. Joyner and T. Curran. 2005. Gli1 is important for medulloblastoma formation in Ptc1+/- mice. *Oncogene* **24:** 4026-4036.

Kimura, H., J.M. Ng and T. Curran. 2008. Transient inhibition of the Hedgehog pathway in young mice causes permanent defects in bone structure. *Cancer Cell* **13:** 249-260.

Kinzler, K.W., S.H. Bigner, D.D. Bigner, J.M. Trent, M.L. Law, S.J. O'Brien, A.J. Wong and B. Vogelstein. 1987. Identification of an amplified, highly expressed gene in a human glioma. *Science* **236:** 70-73.

Kozmik, Z., U. Sure, D. Ruedi, M. Busslinger and A. Aguzzi. 1995. Deregulated expression of PAX5 in medulloblastoma. *Proc Natl Acad Sci U S A* **92:** 5709-5713.

Lagace, D.C., M.C. Whitman, M.A. Noonan, J.L. Ables, N.A. DeCarolis, A.A. Arguello, M.H. Donovan, S.J. Fischer, L.A. Farnbauch, R.D. Beech, R.J. DiLeone, C.A. Greer, C.D. Mandyam and A.J. Eisch. 2007. Dynamic Contribution of Nestin-Expressing Stem Cells to Adult Neurogenesis. *J. Neurosci.* **27:** 12623-12629.

Lau, J., H. Kawahira and M. Hebrok. 2006. Hedgehog signaling in pancreas development and disease. *Cell Mol Life Sci* **63:** 642-652.

Lee, A., J.D. Kessler, T.A. Read, C. Kaiser, D. Corbeil, W.B. Huttner, J.E. Johnson and R.J. Wechsler-Reya. 2005. Isolation of neural stem cells from the postnatal cerebellum. *Nat Neurosci* **8:** 723-729.

Lee, K., G. Adhikary, S. Balasubramanian, R. Gopalakrishnan, T. McCormick, G.P. Dimri, R.L. Eckert and E.A. Rorke. 2008. Expression of Bmi-1 in epidermis enhances cell survival by altering cell cycle regulatory protein expression and inhibiting apoptosis. *J Invest Dermatol* **128:** 9-17.

Lee, Y., R. Kawagoe, K. Sasai, Y. Li, H.R. Russell, T. Curran and P.J. McKinnon. 2007. Loss of suppressor-of-fused function promotes tumorigenesis. *Oncogene* **26:** 6442-6447.

Lendahl, U., L.B. Zimmerman and R.D.G. McKay. 1990. CNS stem cells express a new class of intermediate filament protein. *Cell* **60:** 585-595.

Lerner, A.B., T. Shiohara, R.E. Boissy, K.A. Jacobson, M.L. Lamoreux and G.E. Moellmann. 1986. A mouse model for vitiligo. *J Invest Dermatol* **87:** 299-304.

Lessard, J., A. Schumacher, U. Thorsteinsdottir, M. van Lohuizen, T. Magnuson and G. Sauvageau. 1999. Functional antagonism of the Polycomb-Group genes eed and Bmi1 in hemopoietic cell proliferation. *Genes Dev* **13:** 2691-2703.

Lessard, J. and G. Sauvageau. 2003. Bmi-1 determines the proliferative capacity of normal and leukaemic stem cells. *Nature* **423:** 255-260.

Leung, C., M. Lingbeek, O. Shakhova, J. Liu, E. Tanger, P. Saremaslani, M. Van Lohuizen and S. Marino. 2004. Bmi1 is essential for cerebellar development and is overexpressed in human medulloblastomas. *Nature* **428:** 337-341.

Lewis, P.M., A. Gritli-Linde, R. Smeyne, A. Kottmann and A.P. McMahon. 2004. Sonic hedgehog signaling is required for expansion of granule neuron precursors and patterning of the mouse cerebellum. *Dev Biol* **270:** 393-410.

Li, L., M.C. Connelly, C. Wetmore, T. Curran and J.I. Morgan. 2003. Mouse Embryos Cloned from Brain Tumors. *Cancer Res* **63:** 2733-2736.

Lin, J.Y. and D.E. Fisher. 2007. Melanocyte biology and skin pigmentation. *Nature* **445:** 843-850.

Lin, W., A. Kemper, K.D. McCarthy, P. Pytel, J.P. Wang, I.L. Campbell, M.F. Utset and B. Popko. 2004. Interferon-gamma induced medulloblastoma in the developing cerebellum. *J Neurosci* **24:** 10074-10083.

Litingtung, Y. and C. Chiang. 2000. Specification of ventral neuron types is mediated by an antagonistic interaction between Shh and Gli3. *Nat Neurosci* **3:** 979-985.

Liu, L., L.G. Andrews and T.O. Tollefsbol. 2006a. Loss of the human polycomb group protein BMI1 promotes cancer-specific cell death. *Oncogene* **25:** 4370-4375.

Liu, S., G. Dontu, I.D. Mantle, S. Patel, N.S. Ahn, K.W. Jackson, P. Suri and M.S. Wicha. 2006b. Hedgehog signaling and Bmi-1 regulate self-renewal of normal and malignant human mammary stem cells. *Cancer Res* **66:** 6063-6071.

Machold, R., S. Hayashi, M. Rutlin, M.D. Muzumdar, S. Nery, J.G. Corbin, A. Gritli-Linde, T. Dellovade, J.A. Porter, L.L. Rubin, H. Dudek, A.P. McMahon and G. Fishell. 2003. Sonic hedgehog is required for progenitor cell maintenance in telencephalic stem cell niches. *Neuron* **39:** 937-950.

Machold, R. and G. Fishell. 2005. Math1 Is Expressed in Temporally Discrete Pools of Cerebellar Rhombic-Lip Neural Progenitors. *Neuron* **48:** 17-24.

Mackenzie, M.A.F., S.A. Jordan, P.S. Budd and I.J. Jackson. 1997. Activation of the Receptor Tyrosine Kinase Kit Is Required for the Proliferation of Melanoblasts in the Mouse Embryo. *Dev Biol* **192:** 99-107.

Mancuso, M., S. Leonardi, M. Tanori, E. Pasquali, M. Pierdomenico, S. Rebessi, V. Di Majo, V. Covelli, S. Pazzaglia and A. Saran. 2006. Hair Cycle-Dependent Basal

Cell Carcinoma Tumorigenesis in Ptc1neo67/+ Mice Exposed to Radiation. *Cancer Res* **66:** 6606-6614.

Mao, J., K.L. Ligon, E.Y. Rakhlin, S.P. Thayer, R.T. Bronson, D. Rowitch and A.P. McMahon. 2006. A Novel Somatic Mouse Model to Survey Tumorigenic Potential Applied to the Hedgehog Pathway. *Cancer Res* **66:** 10171-10178.

Marcotullio, L.D., E. Ferretti, A. Greco, E. De Smaele, A. Po, M.A. Sico, M. Alimandi, G. Giannini, M. Maroder, I. Screpanti and A. Gulino. 2006. Numb is a suppressor of Hedgehog signalling and targets Gli1 for Itch-dependent ubiquitination. *Nat Cell Biol* **8:** 1415-1423.

Marino, S. 2005. Medulloblastoma: developmental mechanisms out of control. *Trends Mol Med* **11:** 17-22.

Masdeu, C., H. Faure, J. Coulombe, A. Schoenfelder, A. Mann, I. Brabet, J.P. Pin, E. Traiffort and M. Ruat. 2006. Identification and characterization of Hedgehog modulator properties after functional coupling of Smoothened to G15. *Biochem Biophys Res Commun* **349:** 471-479.

Matise, M.P., D.J. Epstein, H.L. Park, K.A. Platt and A.L. Joyner. 1998. Gli2 is required for induction of floor plate and adjacent cells, but not most ventral neurons in the mouse central nervous system. *Development* **125:** 2759-2770.

Meloni, A.R., G.B. Fralish, P. Kelly, A. Salahpour, J.K. Chen, R.J. Wechsler-Reya, R.J. Lefkowitz and M.G. Caron. 2006. Smoothened signal transduction is promoted by G protein-coupled receptor kinase 2. *Mol Cell Biol* **26:** 7550-7560.

Merchant, M., F.F. Vajdos, M. Ultsch, H.R. Maun, U. Wendt, J. Cannon, W. Desmarais, R.A. Lazarus, A.M. de Vos and F.J. de Sauvage. 2004. Suppressor of fused regulates Gli activity through a dual binding mechanism. *Mol Cell Biol* **24:** 8627-8641.

Mignone, J.L., V. Kukekov, A.S. Chiang, D. Steindler and G. Enikolopov. 2004. Neural stem and progenitor cells in nestin-GFP transgenic mice. *J Comp Neurol* **469:** 311-324.

Mill, P., R. Mo, H. Fu, M. Grachtchouk, P.C. Kim, A.A. Dlugosz and C.C. Hui. 2003. Sonic hedgehog-dependent activation of Gli2 is essential for embryonic hair follicle development. *Genes Dev* **17:** 282-294.

Min, H.S., Y.J. Lee, K. Park, B.K. Cho and S.H. Park. 2006. Medulloblastoma: histopathologic and molecular markers of anaplasia and biologic behavior. *Acta Neuropathol* **112:** 13-20.

Miura, G.I. and J.E. Treisman. 2006. Lipid modification of secreted signaling proteins. *Cell Cycle* **5:** 1184-1188.

Miyazawa, K., T. Himi, V. Garcia, H. Yamagishi, S. Sato and Y. Ishizaki. 2000. A role for p27/Kip1 in the control of cerebellar granule cell precursor proliferation. *J Neurosci* **20:** 5756-5763.

Mo, R., A.M. Freer, D.L. Zinyk, M.A. Crackower, J. Michaud, H.H. Heng, K.W. Chik, X.M. Shi, L.C. Tsui, S.H. Cheng, A.L. Joyner and C. Hui. 1997. Specific and redundant functions of Gli2 and Gli3 zinc finger genes in skeletal patterning and development. *Development* **124:** 113-123.

Molofsky, A.V., R. Pardal, T. Iwashita, I.K. Park, M.F. Clarke and S.J. Morrison. 2003. Bmi-1 dependence distinguishes neural stem cell self-renewal from progenitor proliferation. *Nature* **425:** 962-967.

Molofsky, A.V., S. He, M. Bydon, S.J. Morrison and R. Pardal. 2005. Bmi-1 promotes neural stem cell self-renewal and neural development but not mouse growth and survival by repressing the p16Ink4a and p19Arf senescence pathways. *Genes Dev* **19:** 1432-1437.

Moody, S.E., C.J. Sarkisian, K.T. Hahn, E.J. Gunther, S. Pickup, K.D. Dugan, N. Innocent, R.D. Cardiff, M.D. Schnall and L.A. Chodosh. 2002. Conditional activation of Neu in the mammary epithelium of transgenic mice results in reversible pulmonary metastasis. *Cancer Cell* **2:** 451-461.

Mulhern, R.K., T.E. Merchant, A. Gajjar, W.E. Reddick and L.E. Kun. 2004. Late neurocognitive sequelae in survivors of brain tumours in childhood. *Lancet Oncol* **5:** 399-408.

Nery, S., H. Wichterle and G. Fishell. 2001. Sonic hedgehog contributes to oligodendrocyte specification in the mammalian forebrain. *Development* **128:** 527-540.

Nilsson, M., A.B. Unden, D. Krause, U. Malmqwist, K. Raza, P.G. Zaphiropoulos and R. Toftgard. 2000. Induction of basal cell carcinomas and trichoepitheliomas in mice overexpressing GLI-1. *Proc Natl Acad Sci U S A* **97:** 3438-3443.

Nishimura, E.K., S.R. Granter and D.E. Fisher. 2005. Mechanisms of hair graying: incomplete melanocyte stem cell maintenance in the niche. *Science* **307:** 720-724.

Okano-Uchida, T., T. Himi, Y. Komiya and Y. Ishizaki. 2004. Cerebellar granule cell precursors can differentiate into astroglial cells. *Proc Natl Acad Sci U S A* **101:** 1211-1216.

Oliver, T.G., L.L. Grasfeder, A.L. Carroll, C. Kaiser, C.L. Gillingham, S.M. Lin, R. Wickramasinghe, M.P. Scott and R.J. Wechsler-Reya. 2003. Transcriptional profiling of the Sonic hedgehog response: a critical role for N-myc in proliferation of neuronal precursors. *Proc Natl Acad Sci U S A* **100:** 7331-7336.

Oliver, T.G., T.A. Read, J.D. Kessler, A. Mehmeti, J.F. Wells, T.T. Huynh, S.M. Lin and R.J. Wechsler-Reya. 2005. Loss of patched and disruption of granule cell development in a pre-neoplastic stage of medulloblastoma. *Development* **132:** 2425-2439.

Olson, J.M., A. Asakura, L. Snider, R. Hawkes, A. Strand, J. Stoeck, A. Hallahan, J. Pritchard and S.J. Tapscott. 2001. NeuroD2 is necessary for development and survival of central nervous system neurons. *Dev Biol* **234:** 174-187.

Oro, A.E., K.M. Higgins, Z. Hu, J.M. Bonifas, E.H. Epstein, Jr. and M.P. Scott. 1997. Basal Cell Carcinomas in Mice Overexpressing Sonic Hedgehog. *Science* **276:** 817-821.

Packer, R.J., P. Cogen, G. Vezina and L.B. Rorke. 1999. Medulloblastoma: clinical and biologic aspects. *Neuro-Oncology* **1:** 232-250.

Packer, R.J., T. MacDonald and G. Vezina. 2008. Central nervous system tumors. *Pediatr Clin North Am* **55:** 121-145, xi.

Paladini, R.D., J. Saleh, C. Qian, G.-X. Xu and L.L. Rubin. 2005. Modulation of Hair Growth with Small Molecule Agonists of the Hedgehog Signaling Pathway. *J Investig Dermatol* **125:** 638-646.

Palma, V., D.A. Lim, N. Dahmane, P. Sanchez, T.C. Brionne, C.D. Herzberg, Y. Gitton, A. Carleton, A. Alvarez-Buylla and A. Ruiz i Altaba. 2005. Sonic hedgehog controls stem cell behavior in the postnatal and adult brain. *Development* **132:** 335-344.

Pan, Y., C.B. Bai, A.L. Joyner and B. Wang. 2006. Sonic hedgehog signaling regulates Gli2 transcriptional activity by suppressing its processing and degradation. *Mol Cell Biol* **26:** 3365-3377.

Park, H.L., C. Bai, K.A. Platt, M.P. Matise, A. Beeghly, C.C. Hui, M. Nakashima and A.L. Joyner. 2000. Mouse Gli1 mutants are viable but have defects in SHH signaling in combination with a Gli2 mutation. *Development* **127:** 1593-1605.

Park, I.K., D. Qian, M. Kiel, M.W. Becker, M. Pihalja, I.L. Weissman, S.J. Morrison and M.F. Clarke. 2003. Bmi-1 is required for maintenance of adult self-renewing haematopoietic stem cells. *Nature* **423:** 302-305.

Park, I.K., S.J. Morrison and M.F. Clarke. 2004. Bmi1, stem cells, and senescence regulation. *J Clin Invest* **113:** 175-179.

Pasca di Magliano, M. and M. Hebrok. 2003. Hedgehog signalling in cancer formation and maintenance. *Nat Rev Cancer* **3:** 903-911.

Pogoriler, J., K. Millen, M. Utset and W. Du. 2006. Loss of cyclin D1 impairs cerebellar development and suppresses medulloblastoma formation. *Development* **133:** 3929-3937.

Raffel, C., R.B. Jenkins, L. Frederick, D. Hebrink, B. Alderete, D.W. Fults and C.D. James. 1997. Sporadic medulloblastomas contain PTCH mutations. *Cancer Res* **57:** 842-845.

Rallu, M., R. Machold, N. Gaiano, J.G. Corbin, A.P. McMahon and G. Fishell. 2002. Dorsoventral patterning is established in the telencephalon of mutants lacking both Gli3 and Hedgehog signaling. *Development* **129:** 4963-4974.

Rao, G., C.A. Pedone, C.M. Coffin, E.C. Holland and D.W. Fults. 2003. c-Myc enhances sonic hedgehog-induced medulloblastoma formation from nestin-expressing neural progenitors in mice. *Neoplasia* **5:** 198-204.

Rao, G., C.A. Pedone, L. Del Valle, K. Reiss, E.C. Holland and D.W. Fults. 2004. Sonic hedgehog and insulin-like growth factor signaling synergize to induce medulloblastoma formation from nestin-expressing neural progenitors in mice. *Oncogene* **23:** 6156-6162.

Reifenberger, J., M. Wolter, R.G. Weber, M. Megahed, T. Ruzicka, P. Lichter and G. Reifenberger. 1998. Missense mutations in SMOH in sporadic basal cell carcinomas of the skin and primitive neuroectodermal tumors of the central nervous system. *Cancer Res* **58:** 1798-1803.

Reifenberger, J., M. Wolter, C.B. Knobbe, B. Kohler, A. Schonicke, C. Scharwachter, K. Kumar, B. Blaschke, T. Ruzicka and G. Reifenberger. 2005. Somatic mutations in the PTCH, SMOH, SUFUH and TP53 genes in sporadic basal cell carcinomas. *British Journal of Dermatology* **152:** 43-51.

Reinisch, C.M., A. Uthman, B.M. Erovic and J. Pammer. 2007. Expression of BMI-1 in normal skin and inflammatory and neoplastic skin lesions. *J Cutan Pathol* **34:** 174-180.

Ressler, S., J. Bartkova, H. Niederegger, J. Bartek, K. Scharffetter-Kochanek, P. Jansen-Durr and M. Wlaschek. 2006. p16INK4A is a robust in vivo biomarker of cellular aging in human skin. *Aging Cell* **5:** 379-389.

Robertson, P.L., K.M. Muraszko, E.J. Holmes, R. Sposto, R.J. Packer, A. Gajjar, M.S. Dias and J.C. Allen. 2006. Incidence and severity of postoperative cerebellar mutism syndrome in children with medulloblastoma: a prospective study by the Children's Oncology Group. *J Neurosurg* **105:** 444-451.

Roessler, E., A.N. Ermilov, D.K. Grange, A. Wang, M. Grachtchouk, A.A. Dlugosz and M. Muenke. 2005. A previously unidentified amino-terminal domain regulates transcriptional activity of wild-type and disease-associated human GLI2. *Hum. Mol. Genet.* **14:** 2181-2188.

Romer, J.T., H. Kimura, S. Magdaleno, K. Sasai, C. Fuller, H. Baines, M. Connelly, C.F. Stewart, S. Gould, L.L. Rubin and T. Curran. 2004. Suppression of the Shh pathway using a small molecule inhibitor eliminates medulloblastoma in Ptc1+/-p53-/- mice. *Cancer Cell* **6:** 229-240.

Ross, J.S., D.P. Schenkein, R. Pietrusko, M. Rolfe, G.P. Linette, J. Stec, N.E. Stagliano, G.S. Ginsburg, W.F. Symmans, L. Pusztai and G.N. Hortobagyi. 2004. Targeted therapies for cancer 2004. *Am J Clin Pathol* **122:** 598-609.

Rubin, L.L. and F.J. de Sauvage. 2006. Targeting the Hedgehog pathway in cancer. *Nat Rev Drug Discov* **5:** 1026-1033.

Ruiz i Altaba, A., B. Stecca and P. Sanchez. 2004. Hedgehog--Gli signaling in brain tumors: stem cells and paradevelopmental programs in cancer. *Cancer Lett* **204:** 145-157.

Ruiz i Altaba, A., C. Mas and B. Stecca. 2007. The Gli code: an information nexus regulating cell fate, stemness and cancer. *Trends in Cell Biology* **17:** 438-447.

Sanai, N., A. Alvarez-Buylla and M.S. Berger. 2005. Neural stem cells and the origin of gliomas. *N Engl J Med* **353:** 811-822.

Sanchez, P., V. Clement and A. Ruiz i Altaba. 2005a. Therapeutic Targeting of the Hedgehog-GLI Pathway in Prostate Cancer. *Cancer Res* **65:** 2990-2992.

Sanchez, P. and A. Ruiz i Altaba. 2005b. In vivo inhibition of endogenous brain tumors through systemic interference of Hedgehog signaling in mice. *Mech Dev* **122:** 223-230.

Sasai, K., J.T. Romer, Y. Lee, D. Finkelstein, C. Fuller, P.J. McKinnon and T. Curran. 2006. Shh pathway activity is down-regulated in cultured medulloblastoma cells: implications for preclinical studies. *Cancer Res* **66:** 4215-4222.

Sasai, K., J.T. Romer, H. Kimura, D.E. Eberhart, D.S. Rice and T. Curran. 2007. Medulloblastomas derived from Cxcr6 mutant mice respond to treatment with a smoothened inhibitor. *Cancer Res* **67:** 3871-3877.

Sato, N., P.L. Leopold and R.G. Crystal. 1999. Induction of the hair growth phase in postnatal mice by localized transient expression of Sonic hedgehog. *J Clin Invest* **104:** 855-864.

Saylors, R.L., 3rd, D. Sidransky, H.S. Friedman, S.H. Bigner, D.D. Bigner, B. Vogelstein and G.M. Brodeur. 1991. Infrequent p53 gene mutations in medulloblastomas. *Cancer Res* **51:** 4721-4723.

Schell-Apacik, C., M. Rivero, J.L. Knepper, E. Roessler, M. Muenke and J.E. Ming. 2003. SONIC HEDGEHOG mutations causing human holoprosencephaly impair neural patterning activity. *Hum Genet* **113:** 170-177.

Schiffer, D., P. Cavalla, A. Migheli, A. Chio, M.T. Giordana, S. Marino and A. Attanasio. 1995. Apoptosis and cell proliferation in human neuroepithelial tumors. *Neurosci Lett* **195:** 81-84.

Shachaf, C.M., A.M. Kopelman, C. Arvanitis, A. Karlsson, S. Beer, S. Mandl, M.H. Bachmann, A.D. Borowsky, B. Ruebner, R.D. Cardiff, Q. Yang, J.M. Bishop, C.H. Contag and D.W. Felsher. 2004. MYC inactivation uncovers pluripotent differentiation and tumour dormancy in hepatocellular cancer. *Nature* **431:** 1112-1117.

Sheng, H., S. Goich, A. Wang, M. Grachtchouk, L. Lowe, R. Mo, K. Lin, F.J. de Sauvage, H. Sasaki, C.-c. Hui and A.A. Dlugosz. 2002. Dissecting the Oncogenic Potential of Gli2: Deletion of an NH2-Terminal Fragment Alters Skin Tumor Phenotype. *Cancer Res* **62:** 5308-5316.

Singh, S.K., I.D. Clarke, M. Terasaki, V.E. Bonn, C. Hawkins, J. Squire and P.B. Dirks. 2003. Identification of a cancer stem cell in human brain tumors. *Cancer Res* **63:** 5821-5828.

Sofroniew, M.V. 2005. Reactive astrocytes in neural repair and protection. *Neuroscientist* **11:** 400-407.

Stone, D.M., M. Hynes, M. Armanini, T.A. Swanson, Q. Gu, R.L. Johnson, M.P. Scott, D. Pennica, A. Goddard, H. Phillips, M. Noll, J.E. Hooper, F. de Sauvage and A. Rosenthal. 1996. The tumour-suppressor gene patched encodes a candidate receptor for Sonic hedgehog. *Nature* **384:** 129-134.

Stone, D.M., M. Murone, S. Luoh, W. Ye, M.P. Armanini, A. Gurney, H. Phillips, J. Brush, A. Goddard, F.J. de Sauvage and A. Rosenthal. 1999. Characterization of the human suppressor of fused, a negative regulator of the zinc-finger transcription factor Gli. *J Cell Sci* **112 (Pt 23):** 4437-4448.

Svärd, J., K.H. Henricson, M. Persson-Lek, B. Rozell, M. Lauth, Å. Bergström, J. Ericson, R. Toftgård and S. Teglund. 2006. Genetic Elimination of Suppressor of

Fused Reveals an Essential Repressor Function in the Mammalian Hedgehog Signaling Pathway. *Developmental Cell* **10:** 187-197.

Taipale, J., J.K. Chen, M.K. Cooper, B. Wang, R.K. Mann, L. Milenkovic, M.P. Scott and P.A. Beachy. 2000. Effects of oncogenic mutations in Smoothened and Patched can be reversed by cyclopamine. *Nature* **406:** 1005-1009.

Taipale, J., M.K. Cooper, T. Maiti and P.A. Beachy. 2002. Patched acts catalytically to suppress the activity of Smoothened. *Nature* **418:** 892-897.

Takabatake, T., M. Ogawa, T.C. Takahashi, M. Mizuno, M. Okamoto and K. Takeshima. 1997. Hedgehog and patched gene expression in adult ocular tissues. *FEBS Lett* **410:** 485-489.

Taupin, P. and F.H. Gage. 2002. Adult neurogenesis and neural stem cells of the central nervous system in mammals. *J Neurosci Res* **69:** 745-749.

te Welscher, P., A. Zuniga, S. Kuijper, T. Drenth, H.J. Goedemans, F. Meijlink and R. Zeller. 2002. Progression of vertebrate limb development through SHH-mediated counteraction of GLI3. *Science* **298:** 827-830.

Tiede, S., J.E. Kloepper, E. Bodo, S. Tiwari, C. Kruse and R. Paus. 2007. Hair follicle stem cells: walking the maze. *Eur J Cell Biol* **86:** 355-376.

Ueba, T., E. Kadota, H. Kano, K. Yamashita and N. Kageyama. 2008. MATH-1 production by an adult medulloblastoma suggestive of a cerebellar external granule cell precursor origin. *J Clin Neurosci* **15:** 84-87.

Unden, A.B., P.G. Zaphiropoulos, K. Bruce, R. Toftgard and M. Stahle-Backdahl. 1997. Human patched (PTCH) mRNA is overexpressed consistently in tumor cells of both familial and sporadic basal cell carcinoma. *Cancer Res* **57:** 2336-2340.

Uziel, T., F. Zindy, S. Xie, Y. Lee, A. Forget, S. Magdaleno, J.E. Rehg, C. Calabrese, D. Solecki, C.G. Eberhart, S.E. Sherr, S. Plimmer, S.C. Clifford, M.E. Hatten, P.J. McKinnon, R.J. Gilbertson, T. Curran, C.J. Sherr and M.F. Roussel. 2005. The tumor suppressors Ink4c and p53 collaborate independently with Patched to suppress medulloblastoma formation. *Genes Dev* **19:** 2656-2667.

Valk-Lingbeek, M.E., S.W. Bruggeman and M. van Lohuizen. 2004. Stem cells and cancer; the polycomb connection. *Cell* **118:** 409-418.

van der Lugt, N.M., J. Domen, K. Linders, M. van Roon, E. Robanus-Maandag, H. te Riele, M. van der Valk, J. Deschamps, M. Sofroniew and M. van Lohuizen. 1994. Posterior transformation, neurological abnormalities, and severe hematopoietic defects in mice with a targeted deletion of the bmi-1 proto-oncogene. *Genes Dev.* **8:** 757-769.

Varjosalo, M., S.P. Li and J. Taipale. 2006. Divergence of hedgehog signal transduction mechanism between Drosophila and mammals. *Dev Cell* **10:** 177-186.

Vasioukhin, V., L. Degenstein, B. Wise and E. Fuchs. 1999. The magical touch: Genome targeting in epidermal stem cells induced by tamoxifen application to mouse skin. *Proceedings of the National Academy of Sciences* **96:** 8551-8556.

Voogd, J. and M. Glickstein. 1998. The anatomy of the cerebellum. *Trends Neurosci* **21:** 370-375.

Wang, B., J.F. Fallon and P.A. Beachy. 2000. Hedgehog-Regulated Processing of Gli3 Produces an Anterior/Posterior Repressor Gradient in the Developing Vertebrate Limb. *Cell* **100:** 423-434.

Wang, C., U. Rüther and B. Wang. 2007. The Shh-independent activator function of the full-length Gli3 protein and its role in vertebrate limb digit patterning. *Dev Biol* **305:** 460-469.

Wang, J., W. Lin, B. Popko and I.L. Campbell. 2004. Inducible production of interferon-gamma in the developing brain causes cerebellar dysplasia with activation of the Sonic hedgehog pathway. *Mol Cell Neurosci* **27:** 489-496.

Wang, V.Y. and H.Y. Zoghbi. 2001. Genetic regulation of cerebellar development. *Nat Rev Neurosci* **2:** 484-491.

Watkins, D.N., D.M. Berman, S.G. Burkholder, B. Wang, P.A. Beachy and S.B. Baylin. 2003. Hedgehog signalling within airway epithelial progenitors and in small-cell lung cancer. *Nature* **422:** 313-317.

Wechsler-Reya, R.J. and M.P. Scott. 1999. Control of neuronal precursor proliferation in the cerebellum by Sonic Hedgehog. *Neuron* **22:** 103-114.

Weiner, H.L., R. Bakst, M.S. Hurlbert, J. Ruggiero, E. Ahn, W.S. Lee, D. Stephen, D. Zagzag, A.L. Joyner and D.H. Turnbull. 2002. Induction of Medulloblastomas in Mice by Sonic Hedgehog, Independent of Gli1. *Cancer Res* **62:** 6385-6389.

Weinstein, I.B. 2002. Cancer. Addiction to oncogenes--the Achilles heal of cancer. *Science* **297:** 63-64.

Wetmore, C., D.E. Eberhart and T. Curran. 2000. The normal patched allele is expressed in medulloblastomas from mice with heterozygous germ-line mutation of patched. *Cancer Res* **60:** 2239-2246.

Wetmore, C., D.E. Eberhart and T. Curran. 2001. Loss of p53 but not ARF accelerates medulloblastoma in mice heterozygous for patched. *Cancer Res* **61:** 513-516.

Wetmore, C. 2003. Sonic hedgehog in normal and neoplastic proliferation: insight gained from human tumors and animal models. *Curr Opin Genet Dev* **13:** 34-42.

Weyer, A. and K. Schilling. 2003. Developmental and cell type-specific expression of the neuronal marker NeuN in the murine cerebellum. *J Neurosci Res* **73:** 400-409.

Wicking, C., I. Smyth and A. Bale. 1999. The hedgehog signalling pathway in tumorigenesis and development. *Oncogene* **18:** 7844-7851.

Wiederschain, D., L. Chen, B. Johnson, K. Bettano, D. Jackson, J. Taraszka, Y.K. Wang, M.D. Jones, M. Morrissey, J. Deeds, R. Mosher, P. Fordjour, C. Lengauer and J.D. Benson. 2007. Contribution of polycomb homologues bmi-1 and mel-18 to medulloblastoma pathogenesis. *Mol Cell Biol* **27:** 4968-4979.

Xie, J., M. Murone, S.M. Luoh, A. Ryan, Q. Gu, C. Zhang, J.M. Bonifas, C.W. Lam, M. Hynes, A. Goddard, A. Rosenthal, E.H. Epstein, Jr. and F.J. de Sauvage. 1998. Activating Smoothened mutations in sporadic basal-cell carcinoma. *Nature* **391:** 90-92.

Xie, J., M. Aszterbaum, X. Zhang, J.M. Bonifas, C. Zachary, E. Epstein and F. McCormick. 2001. A role of PDGFRalpha in basal cell carcinoma proliferation. *Proc Natl Acad Sci U S A* **98:** 9255-9259.

Zhang, C., E.H. Williams, Y. Guo, L. Lum and P.A. Beachy. 2004. Extensive phosphorylation of Smoothened in Hedgehog pathway activation. *Proc Natl Acad Sci U S A* **101:** 17900-17907.

Zhou, Q., S. Apionishev and D. Kalderon. 2006. The contributions of protein kinase A and smoothened phosphorylation to hedgehog signal transduction in Drosophila melanogaster. *Genetics* **173:** 2049-2062.

Zhu, H. and A. Dahlstrom. 2007. Glial fibrillary acidic protein-expressing cells in the neurogenic regions in normal and injured adult brains. *J Neurosci Res* **85:** 2783-2792.

Zhuo, L., M. Theis, I. Alvarez-Maya, M. Brenner, K. Willecke and A. Messing. 2001. hGFAP-cre transgenic mice for manipulation of glial and neuronal function in vivo. *Genesis* **31:** 85-94.